NEW FERROCENE CHEMOTHERAPEUTIC DRUGS AND EARLY DETECTION OF BREAST CANCER USING A NANOSTRUCTURED GOLD BIOSENSOR

by

Wanda Ibelitz Pérez Mercado

A dissertation submitted in partial fulfillment of the requirements for the degree of

DOCTOR OF PHILOSOPHY
in
Applied Chemistry

UNIVERSITY OF PUERTO RICO
MAYAGÜEZ CAMPUS
2015

Approved by:

_____	_____
Enrique Meléndez, Ph.D. President, Graduate Committee	Date
_____	_____
Mayra E. Cádiz, Ph.D. Member, Graduate Committee	Date
_____	_____
Jessica Torres, Ph.D. Member, Graduate Committee	Date
_____	_____,
Bárbara Calcagno, Ph.D. Representative of Graduate Studies	Date
_____	_____
Aidalú de los A. Joubert, Ph.D. Member, Graduate Committee Chairperson of the Department	Date

Abstract

Three new ferrocene complexes were synthesized with 4-(1H-pyrrol-1-yl)phenol group appended to the cyclopentadienyl (Cp) rings. These are: 1,1'-4-(1H-pyrrol-1-yl)phenyl ferrocenedicarboxylate, ('Fc-$(CO_2$-Ph-4-Py$)_2$'), 1,4-(1H-pyrrol-1-yl)phenyl, 1'-carboxyl ferrocenecarboxylate ('Fc-$(CO_2$-Ph-4-Py$)CO_2$H') and 4-(1H-pyrrol-1-yl)phenyl ferroceneacetylate ('Fc-CH_2CO_2-Ph-4-Py'). The new species were full characterized by spectroscopic methods (FT-IR, ^{1}HNMR, ^{13}CNMR, and MS), and by electrochemistry. Additionally, the X-ray single crystal structure of Fc-$(CO_2$-Ph-4-Py$)_2$ was resolved. The Fc-$(CO_2$-Ph-4-Py$)_2$ crystallizes in the orthorhombic space group Pbca with the Fe^{2+} cation positioned on an inversion center and the Cp rings adopted an anti conformation. Cyclic voltammetry experiments showed that Fc-CH_2CO_2-Ph-4-Py has a redox potential very similar to the Fc/Fc^+ redox couple whereas Fc-$(CO_2$-Ph-4-Py$)_2$ and Fc-(CO2-Ph-4-Py$)CO_2$H have redox potentials of over 400 mV higher than Fc/Fc+ redox couple. The *in vitro* studies of Fc-$(CO_2$-Ph-4-Py$)_2$ and Fc-$(CO_2$-Ph-4-Py$)CO_2$H revealed that the latter two compounds have moderate antiproliferative activity on MCF-7 breast cancer cell line with a IC_{50} values of 45.5(6) and 57(7) µM respectively. In contrast with Fc-CH_2CO_2-Ph-4-Py which displayed low anti-proliferative activity with an IC_{50} value of 103(6) µM. The genotoxic effects of the new synthesized ferrocenes were addressed with cytokinesis-block micronucleus assay (CBMN) and reactive oxygen species (ROS) induction assay. The Fc-$(CO_2$-Ph-4-Py$)_2$ showed with the higher genotoxic effects on the MCF-7 followed by Fc-$(CO_2$-Ph-4-Py$)CO_2$H, and Fc-CH_2CO_2-Ph-4-Py with the lower effects. There is a correlation between the IC_{50} values of the ferrocenes and the amount of micronucleus formation activity on binucleated cells and the reactive oxygen species (ROS) production on MCF-7 cell line. However, no correlation was found between the redox activity and the genotoxic effects.

A nanostructured gold dsDNA biosensor for early detection of breast cancer was designed and fabricated. The nanostructured gold dsDNA biosensor is based on the detection of the binding event of the beta protein 1 (BP_1) with dsDNA. A redox-active probe (methylene blue) was intercalated in dsDNA to monitor the electrochemical response of the binding event of BP_1. A linear correlation of the electrochemical response by

concentration of BP_1 was obtained (R^2 = 0.998) with a limit of detection of 1.2 nM. This nanostructured gold dsDNA sensor is shown to be sensitive, selective, stable, and reusable allowing for its potential clinical use.

Resumen

Tres nuevos complejos de ferroceno fueron sintetizados utilizando 4-(1H-pyrrol-1-yl)fenol como grupo funcional enlazado a los anillos de ciclopentadieno (Cp). Estos nuevos compuestos son: 1,1'-4-(1H-pyrrol-1-yl)fenol ferrocenodicarboxylato, ('Fc-(CO_2-Ph-4-Py)$_2$'), 1,4-(1H-pyrrol-1-yl)fenyl, 1'-carboxyl ferrocenocarboxylato ('Fc-(CO_2-Ph-4-Py)CO_2H') and 4-(1H-pyrrol-1-yl)fenyl ferrocenoacetylato ('Fc-CH_2CO_2-Ph-4-Py'). Estas nuevas especies fueron caracterizadas por métodos espectroscópicos (FT-IR, ^{1}HNMR, ^{13}CNMR, and MS) y electroquímicos. Además la estructura cristalina de Fc-(CO_2-Ph-4-Py)$_2$ fue resuelta por medio de rayos X. Fc-(CO_2-Ph-4-Py)$_2$ cristalizó en una celda ortorrómbica con grupo especial Pbca con los cations de Fe^{2+} posicionados en un punto de inversión y los anillos de Cp adoptando una conformación anti. Experimentos de voltametría cíclica demostraron que Fc-CH_2CO_2-Ph-4-Py posee un potencial redox similar al de Fc/Fc+ mientras que Fc-(CO_2-Ph-4-Py)$_2$ y Fc-(CO_2-Ph-4-Py)CO_2H tienen potenciales redox mayores a 400 mV. Estudios *in vitro* de Fc-(CO_2-Ph-4-Py)$_2$ y Fc-(CO_2-Ph-4-Py)CO_2H revelaron que estos compuestos poseen una actividad anti-proliferativa moderada en células de cáncer de seno, MCF-7, con un IC_{50} de 45.5(6) and 57(7) µM respectivamente. En cambio, Fc-CH_2CO_2-Ph-4-Py reflejó la menor actividad anti-proliferativa con un IC_{50} de 103(6) µM. Los efectos genotóxicos de los tres compuestos también fueron estudiados mediante el ensayo de bloqueo de citoquinesis (cytokinesis-block micronucleus assay, CBMN) y el ensayo de inducción de especies reactivas de oxígeno (ROS). El compuesto Fc-(CO_2-Ph-4-Py)$_2$ reflejó los efectos genotóxicos más altos en células MCF-7 seguido por Fc-(CO_2-Ph-4-Py)CO_2H, y Fc-CH_2CO_2-Ph-4-Py con efectos menores. Encontramos una correlación entre los valores de IC_{50} y la cantidad de formación de micro núcleos y la producción de especies reactivas de oxígeno. Mientras que no se pudo establecer una relación entre el efecto genotóxico y la actividad redox de los compuestos.

El problema de la detección temprana del cáncer de seno fue abordado mediante la elaboración de un biosensor basado en nanoestructuras de oro con DNA de doble hélice (dsDNA). El compuesto con actividad redox azul de metileno se utilizó como intercalador

para monitorear la respuesta electroquímica del evento de enlace de la beta proteína 1 (BP_1) con el dsDNA. Se obtuvo una relación lineal entre la respuesta del sensor con las concentraciones de BP_1 con un factor de correlación de $R^2 = 0.998$ y un límite de detección de 1.2 nM. Éste sensor nanoestructurado de oro demostró ser sensitivo, selectivo, estable y reusable teniendo así un potencial uso para la detección temprana del cáncer de seno a nivel clínico.

Quiero dedicar mi trabajo doctoral primeramente a Dios por haberme dado las fuerzas y la sabiduría para sobrellevar todos estos años.

Luego a mi esposo José A. Márquez por su apoyo incondicional.

A mis hijas Karen y Keren por siempre confiar en mí.

A mis padres Antonio Pérez y Margarita Mercado por siempre darme la mano, confiar en mí y brindarme todo su apoyo.

A mis suegros y familia en general que de una forma u otra me ayudaron a alcanzar ésta meta. Los amo.

A todos ellos les dedico mi doctorado.

Acknowledgements

I want to thank all the people who in one way or another helped me to reach my doctorate in philosophy.

I want to thank my graduate committee Dr. Mayra E. Cádiz, Dr. Aidalú de los A. Joubert, and Dr. Jessica Torres for their support and guidance to all years. Special thanks to my advisor, Dr. Enrique Meléndez for your patience, guidance and always being there for me whenever I needed. To Dr. Jaime Matta, Luisa Morales and Carmen Ortiz from Ponce School of Medicine and the Molecular and Genomics Core (NIMHD Grant MD007579) for their help with the practicum.

My most sincere thanks to all my friends that helped me, specially to José A. Carmona, Tamara Félix, Moralba Dominguez, Elena Flores, and my best friend since middle school Damaris Muñiz. Thanks to my lab partners José L. Vera, Xiomara Narvaez and the undergraduate students, Yarelys Soto, Alejandra Martinez, and Maria Pagán for your help and dedication during your research. I also want to thank Dr. José E. Cortés for inspiring me to begin in the PhD program. Special gratitude to the NIH-RISE 2 Best program (NIH-R25GM088023) and the Chemistry Department for the financial support.

Again I want to thank my beloved husband for your patience, support and help during this long process. To my twin daughters Karen and Keren, all this effort is for you. To my parents: Antonio and Margarita, thanks for your inspiration and help with my daughters. Special thanks to my in-laws Doris and Manuel for your help. I love you all.

List of Content

List of Tables

List of Figures

List of Appendixes

List of Symbols and Abbreviations

AFM	atomic force microscopy
Ag/AgCl	silver/silver chloride electrode
ATR	atenuated total reflectance
BP_1	beta protein 1
CaH_2	calcium hydride
CBMN	cytokinesis-block micronucleus assay
CH_2Cl_2	dichloromethane
CH_3CN	acetonitrile
Cp	cyclopentadiene
CT	charge transport
DCIS	ductal-carcinoma- *in situ*
DCM	dichloromethane
DCF	2’7’-dichlorofluorescein
DMSO	dimethyl sulfoxide
DMSO-d_6	dimethyl sulfoxide deuterated
D_2O	deuterated water
dsDNA	double stranded DNA
CV	cyclic voltammetry
EDTA	ethylenediaminetetraacetic acid
ERα	estrogen receptor alpha
ER_β	estrogen receptor beta
ER+	estrogen receptor-positive
ER-	estrogen receptor-negative

E_{pa}	anodic potential
E_{pc}	catodic potential
FBS	fetal bovine serum
Fc	ferrocene
Fc^{+}	ferrocenium
Fc-CH_2CO_2-Ph-4-Py	4-(1H-pyrrol-1-yl)phenyl ferroceneacetylate
Fc-CO_2-Ph-4-Br	4-bromophenyl ferrocenecarboxylate
Fc-CO_2-estradiol	ferrocenoyl 3b-estra1,3,5(10)-trien-17-one-3-olate or estradiol-3-(ferrocenecarboxylate)
Fc-(CO_2-Ph-4-Py)$_2$	1'-4-(1H-pyrrol-1-yl)phenyl ferrocenedicarboxylate
Fc-(CO_2-Ph-4-Py)CO_2H	1-4-(1H-pyrrol-1-yl)phenyl, 1'-carboxyl ferrocenecarboxylate
$FeCp_2$	ferrocene
$[FeCp_2]BF_4$	ferrocenium tetrafluoroborate
HCl	hydrochloric acid
H_2DCF-DA	2′,7′-dichlorodihydrofluoresceindiacetate
HT-29	colorectal adenocarcinoma cell line
HOMO	highest occupied molecular orbital
IC_{50}	half maximal inhibitory concentration
NaCl	sodium chloride
NG	nanostructured gold
$[NBu^n_4]PF_6$	tetrabutylammonium hexafluorophosphate
NMR	nuclear magnetic resonance
MB	methylene blue
MCF-7	breast adenocarcinoma cell line
MCF-10A	non-tumorigenic human breast epithelial cell line

MCH	mercaptohexanol
MDA-MB-231	hormone-independent breast cancer cells
MNi	micronuclei
MMS	methyl methane sulphonate
MTT	3-(4,5-dimethylthiazol-2-yl)-2,5-diphenyltetrazolium bromide
PBS	phosphate buffered saline
P	probability
POC	point-of-care
Pt	platinum
RBA	receptor binging affinity
ROS	reactive oxygenated species
SEM	scanning electron microscopy
SERMs	selective estrogen receptor modulator
SD	standard deviation
SWV	square-wave voltammetry

Chapter I

Introduction

1.1 Ferrocene Background

Ferrocene was first reported in 1951 by Pauson and Kealy[1,2]. They used $FeCl_3$ as a catalytist to synthesize fulvalene ($C_{10}H_8$) by the oxidation of cyclopentadienyl, and as a result the outcome was the bis(η^5-cyclopentadienyl)iron(II) compound[1]. A year later its chemical structure was then reported by Wilkinson et al. and Fischer and Pfab[3,4]. The bis(η^5-cyclopentadienyl)iron(II) complex is crystalline orange solid, with a melting point of 173 ^oC and a boiling point of 249 ^oC. Ferrocene is stable to air, water, acids and bases being soluble in most organic solvents and insoluble to water. The ferrocene structure (**Figure 1.1)** has a staggered configuration of the Cp rings with molecular center symmetry (D_{5d}). In 1979, Haaland discovered the eclipsed configuration of ferrocene by gas electron diffraction with a projected symmetry of D_{5h}[5].

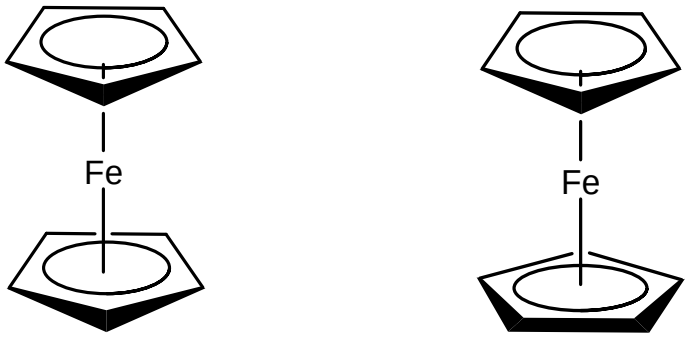

Figure 1. 1. Chemical structure of ferrocene.

Ferrocene has been studied for many years due to its properties and applications in material sciences like sensors[6–11], organic synthesis[12–14], and catalysis[15–18]. Two of the most important properties of ferrocene are its electrochemical properties and its stability. Ferrocene complex follow the 18 electron rule and have pared electrons localized at the nonbonding a'_{1g} which is the highest occupied molecular orbital (HOMO) represented on **Figure 1.2**. Due to its electronic configuration ferrocene undergoes an one-electron oxidation, a perfect electrochemistry, producing the dicyclopentadienyliron(III) cation, called ferrocenium, Fc^{+}. The ferrocenium ion has an unpaired electron in the non-bonding a'_{1g} orbital, and as a result it is a radical species with high stability. The oxidized ferrocene exhibit a blue color when it is diluted or blood red when it is concentrated[19].

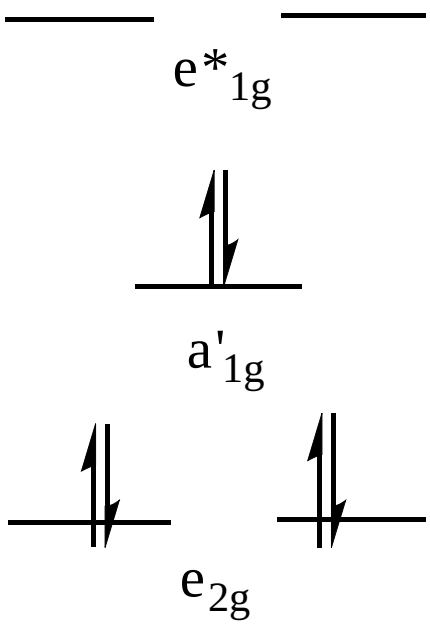

Figure 1. 2: Molecular orbital diagram of iron 3d-orbitas in ferrocene.

In 1984, Köpf-Maier and co-workers discovered the antitumoral properties of ferrocene complexes[22]. Those antitumoral properties are well studied and opened a new area of research during the past decades[22–25]. Many researchers have driven their attention to the synthesis of functionalized ferrocenes to increase their antitumoral activity[23,24,26–29]. Among all these ferrocene derivatives, the use of the anti-cancer drug, tamoxifen[30,31], was employed to improve the antitumoral properties of ferrocenes. Tamoxifen is an anti-cancer compound which acts as an estrogen receptor (ER) antagonist in endocrine therapy[32].

The tamoxifen anti-cancer drug was first coupled to ferrocene by Jaouen and coworkers[30,31] using its active metabolite, hydroxytamoxifen. As a result, these ferrocenyl derivatives combined the anti-estrogenic effect of tamoxifen and the cytotoxic properties of ferrocene. The tamoxifen coupled to the ferrocene acts as a vector carrying the drug inside the cell. Once the drug is inside the cell, the ferrocene produces the ferrocenium cations which lead to the formation of reactive oxygen species (ROS) causing cell death[33].

The new ferrocifens and hydroxyferrocyfens were synthesized using a McMurry coupling reaction. The synthesis results in a product mixture of Z and E isomeric forms. **Figure 1.3** shows the ferrocifen Z and E structural isomers. The Z and E isomers can be separated by HPLC, fractional crystallization or plate chromatography[30,31]. However, the Z isomer reisomerized to the E isomer leading to a racemic mixture (50:50/Z:E). In spite of this limitation, the receptor binding affinity (RBA) was determined for both isomers. The Z isomer has higher RBA to the estrogen receptor alpha (ER_α) and estrogen receptor beta (ER_β) than the E isomer. Given that the Z undergoes isomerization leads to a racemic mixture, the cytotoxic activity of these ferrocifens complexes were determined using mixture of isomers in hormone-dependent breast cancer cells (MCF-7) and hormone-independent breast cancer cells (MDA-MB-231)

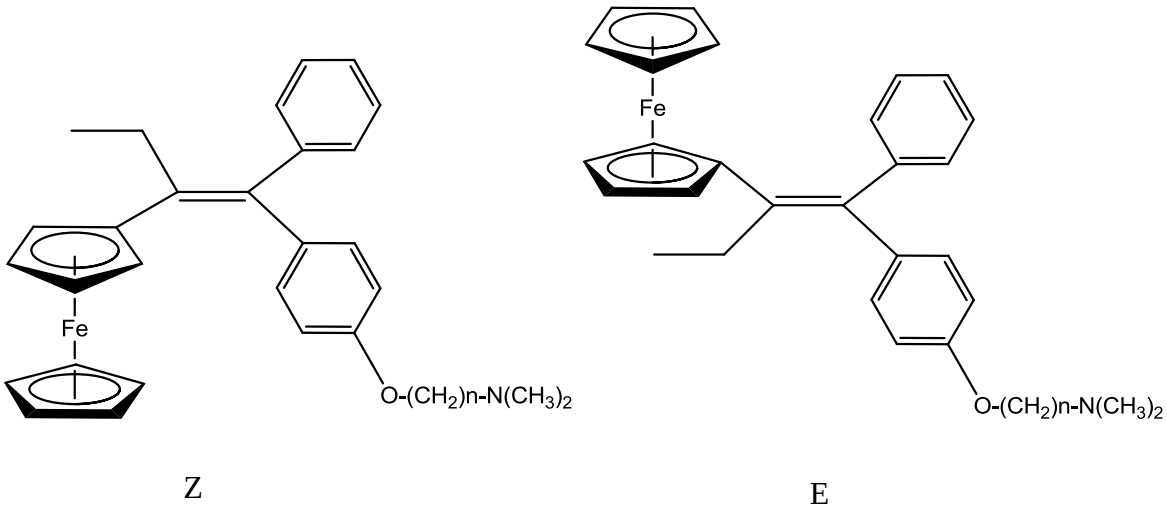

Z E

Figure 1. 3. Ferrocifen structures in the Z and E configurations.

Our research group has been working for many years on the ferrocene functionalization with different pendant groups to enhance their cytotoxic activity on breast cancer cells[28,34,35]. The synthesis of three vectorized ferrocenes modified with (3b,5*Z*,7*E*,22*E*)-9,10-secoergosta-5,7,10(19),22-tetraen-3-ol, (ergocalciferol, vitamin D), 17β-hydroxyestra-1,3,5(10)-trien-3-diol (estradiol), and 3β-estra-1,3,5(10)-trien-17-one-3-ol (estrone) showed important results on2 the synthesis of target specific drugs. The major success in this research area is ferrocenoyl 17β-hydroxy-estra-1,3,5(10)-trien-3-olate complex ("Fc-CO_2-estradiol"), which exhibited enhanced anti-proliferative activity on hormone-dependent breast epithelial adenocarcinoma cell line MCF-7[34]. Docking studies of this species into the alpha estrogen receptor (ERα) revealed that the ferrocene docks partially in the estrogen binding pocket, impairing the protein function[34].

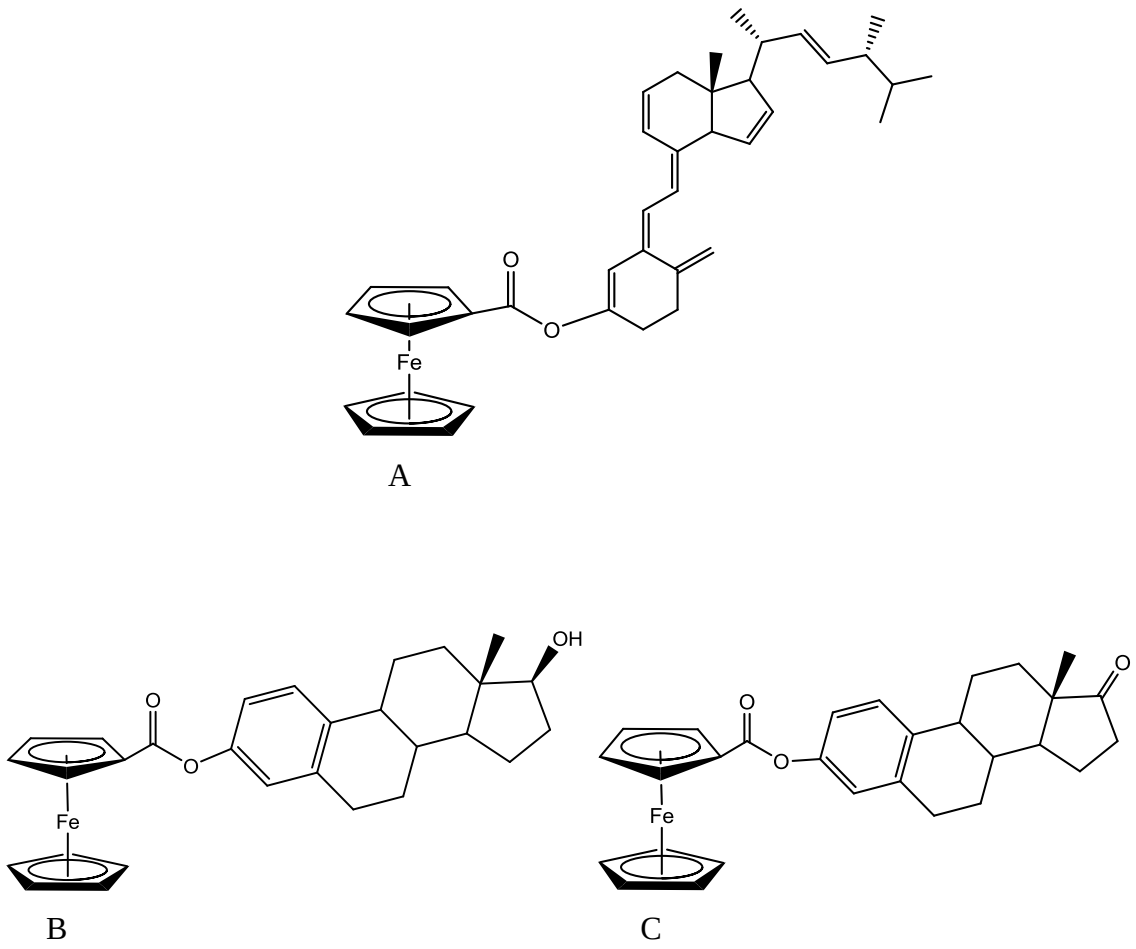

Figure 1. 4: Structures of A) (3b,5*Z*,7*E*,22*E*)-9,10-secoergosta-5,7,10(19),22-tetraen-3-olate, B) ferrocenoyl 17b-hydroxyestra-1,3,5(10)-trien-3-olate, and C) ferrocenoyl 3b-estra 1,3,5(10)-trien-17-one-3-olate.

Recently, our research group published a series of ferrocenoyl esters which have anti-proliferative activities depending on the pendant group attached to the Cp ring (**Figure 1.4 and 1.5**)[28]. The 4-bromophenyl ferrocenecarboxylate (Fc-CO_2-Ph-4-Br) displayed good anti-proliferative activity on breast cancer cell line MCF-7 and low anti-proliferative activity on non-tumorigenic human breast epithelial cell line MCF-10A[28]. In contrast to Fc-CO_2-estradiol, the Fc-CO_2-Ph-4-Br anti-proliferative activity does not correspond to the anti-estrogenic properties and it is correlated to the cytotoxic effects of the ferrocene

moiety. Also on the same publication, a ferrocenecarboxylate modified with a pyrrole group, 4-(1H-pyrrol-1-yl)phenyl ferrocenecarboxylate, (Fc-CO_2-Ph-4-Py), was reported showing good anti-proliferative activity on MCF-7[28]. However, also it has high anti-proliferative activity on non-tumorigenic human breast epithelial cell line MCF-10A, ruling out the use of this ferrocene in breast cancer treatment[28] .

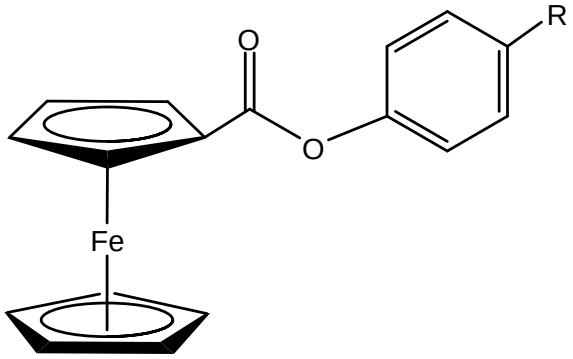

1: R = H, Fc-CO_2-Ph

2: R = F, Fc-CO_2-Ph-4-F

3: R = Cl, Fc-CO_2-Ph-4-Cl

4: R = Br, Fc-CO_2-Ph-4-Br

5: R = I, Fc-CO_2-Ph-4-I

6. R = Pyrrole, Fc-CO_2-Ph-4-Py

Figure 1. 5 General structure of ferrocenoyl phenyl derivatives.

1.2 Breast Cancer

1.2.1 Breast cancer statistics

Cancer is one of the major cause deaths in the United States. Statistically, one of four deaths in the United States is caused by cancer. The most common diagnosed cancer in woman is breast cancer. It is also the second leading cause of cancer death among women around the world[36]. During 2014, around 29% of the new cases of cancer in women were diagnosed to be breast cancer (Figure 1.6) [37]. According to the American Cancer Society, over 231,840 new cases of invasive breast cancer are expected to be diagnosed in the United States in 2015. Additionally, 60,290 new cases of carcinoma *in situ* breast cancer, which is the earliest form of breast cancer and it is also non-invasive, will be diagnosed in 2015. Unfortunately, about 40,290 diagnosed women will die of this condition.

	Males			Females	
Prostate	233,000	27%		Breast	232,670	29%
Lung & bronchus	116,000	14%		Lung & bronchus	108,210	13%
Colorectum	71,830	8%		Colorectum	65,000	8%
Urinary bladder	56,390	7%		Uterine corpus	52,630	6%
Melanoma of the skin	43,890	5%		Thyroid	47,790	6%
Kidney & renal pelvis	39,140	5%		Non-Hodgkin lymphoma	32,530	4%
Non-Hodgkin lymphoma	38,270	4%		Melanoma of the skin	32,210	4%
Oral cavity & pharynx	30,220	4%		Kidney & renal pelvis	24,780	3%
Leukemia	30,100	4%		Pancreas	22,890	3%
Liver & intrahepatic bile duct	24,600	3%		Leukemia	22,280	3%
All Sites	**855,220**	**100%**		**All Sites**	**810,320**	**100%**

Figure 1. 6: Ten Leading Cancer Types for the Estimated New Cancer Cases and Deaths by Sex, United States, 2014[37].

Breast cancer can be detected on five different stages depending on the development of the disease. The earliest form of the disease diagnosed is stage 0. This stage is related to the abnormal growing of cells in the wall of the breast ducts, it is also called ductal-carcinoma- *in situ.* (DCIS)[38]. The second stage on breast cancer is the stage I in which the cancerous cells begins to spread to the breast tissue away from the ducts forming the tumor[38]. When those cancerous cells move towards the lymph nodes over the arms and the tumor growth about 2cm diameter the cancer is classified as stage II[38]. The more advanced stages of breast cancer are stage III, and IV. During stage III, the breast cancer is known as locally advanced cancer. The cancer in stage III is subdivided in IIIA, IIIB or IIIC depending of the tumor size and the spreading of the cancerous cells (Breast Cancer Survival Rates by Stage, 2011). The final stage of the breast cancer is the stage IV, known as metastatic breast cancer in which the cancer is spread to other organs.

The American Cancer Society in 2014 published an article to create consciousness about the importance of the early detection of breast cancer in women. All women have to do screening exams to detect breast cancer on an early stage. Those screening exams help to detect the breast cancer before the symptoms begins. When the breast cancer is detected by its symptoms probably it is in an advance stage. The **Figure 1.7** shows the 5-year survival rates among the various stages of breast cancer. In accordance to this statistical study (Breast Cancer Survival Rates by Stage, 2011), about 89% of the diagnosed woman during stage 0 or stage I will survive. The survival rate decrease dramatically when the breast cancer is diagnosed in advance stages like stage III or IV[38]. For those reasons is very important the early detection of breast cancer.

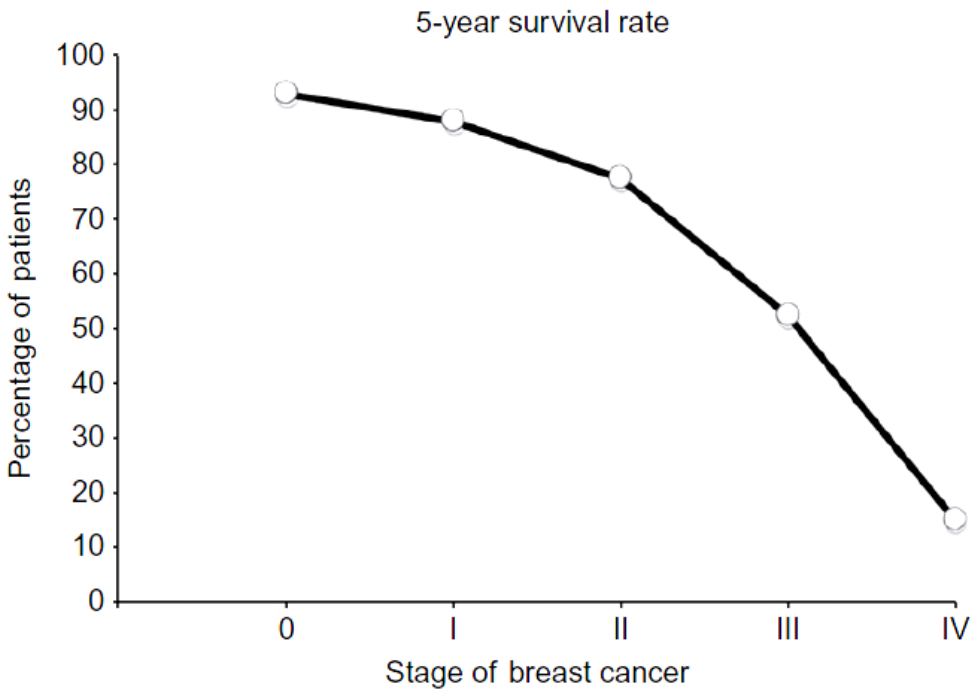

Figure 1. 7. Plot of the five-year survival rates among various stages of breast cancer published in Breast Cancer Survival Rates by Stage, 2011.

1.2.2 Breast cancer treatment

The invasive breast cancer is divided in three types of breast cancer such as: estrogen receptor-positive (ER+), estrogen receptor-negative (ER-), and triple negative. The principal incidence of breast cancer is related to estrogen receptor-positive (ER+) breast cancer while estrogen receptor-negative (ER-) breast cancer is less diagnosed[36]. Those type of breast cancers, ER+ and ER- are related to gene HER-2 or HER-2neu gene over expression[39]. The ER+ and ER- breast cancers can be sub-divided in four groups based on DNA microarrays experiments. The basal-like and HER2 positive are subtypes of the ER+ breast cancer whilst luminal A and B are subtypes of ER- breast cancer[40,41].

Meanwhile, the triple negative breast cancer is the one which is estrogen receptor negative, progesterone receptor negative, and HER2neu negative[39].

The most common methods of breast cancer treatment are: surgery, radiotherapy and chemotherapeutic treatments. The chemotherapeutic treatment has been of increased interest in the scientific community. One of the most known chemotherapeutic drug is cisplatin. Cisplatin was first described by Michele Peyrone in 1844 and known as Peyrone's salts[42]. Cisplatin is an antineoplastic drug which acts forming DNA adducts causing cell death[43,44]. Unfortunately, the patients who were treated with cisplatin showed different adverse side effects[45–47].

Today, the researchers have driven their attention to discover new chemotherapeutic drugs with the minimum adverse side effects. Therefore, as one of the potential alternatives, the design of target specific drugs has been pursued and has been of paramount importance in the cancer therapy. As mentioned previously, one of the most effective target specific drug is the tamoxifen which is a selective estrogen receptor modulator (SERMs)[48]. Tamoxifen acts as anti-estrogenic drug for ER+ breast cancer[49]. Recently other target specific drugs were synthesized including the ferrocenoyl group[23,26,30,31,48]. Therefore, we will present some of the modified ferrocenes with pendant groups that could behave as potential chemotherapeutic agents.

1.3 DNA Biosensors

The DNA double helical structure was elucidated around 1960 by Eley D and co-workers[50]. The double helical structure of DNA opened a new area of interest in research by the possibility that the π-stacked base pairs may promote the charge transport (CT)

through a surface[50–56]. The new concept and idea of DNA CT led to the development of a wide variety of biosensors [57–65]. The DNA-mediated CT provides the alternative to design high sensitive and simple assays; requires no labeling and it is also applicable to the detection of protein-DNA interactions[52,62,63,65–67]. The DNA CT is sensitive to perturbations causing interruptions of the CT process, including single base mismatch, lesions, or structural changes caused by protein interaction[57,68–70].

The DNA-mediated CT requires electronic coupling to the π-stacked base pairs. Therefore, a series of well conjugated charge donors or acceptors are employed to study the electrochemical properties of the DNA CT[59,70–73]. One of the most used intercalators to the DNA is the methylene blue (MB), represented on **Figure 1.8**. The MB is an organic molecule which interacts into the DNA through non-covalent or covalent interactions. The non-covalent interactions of the MB to the DNA is intercalation into the base stack of the DNA[66,70,74,75]. The non-covalent MB intercalation interaction with DNA is sensitive to the π-stack perturbations induced by the analyte and it undergoes electrocatalytic signal amplifications[76]. The MB was also studied using covalent interactions to the DNA[70]. The tethered MB demonstrated to be more strongly coupled to the π-stack[70] and more responsive to the π-stack perturbations induced by the analyte.

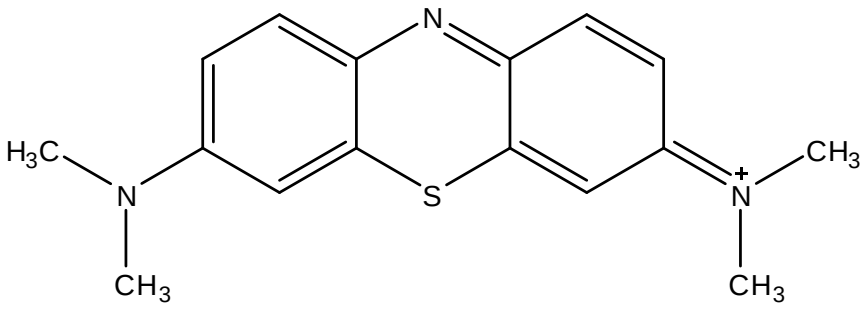

Figure 1. 8: Chemical structure of methylene blue.

The electrochemical assays based on DNA-mediated charge transport biosensors demonstrated to be more sensitive, specific, fast, simple, and low-cost, making them suitable for point-of-care (POC) diagnostics and multiplexed platforms[61]. This type of biosensors has been useful in assays to detect mutations and lesions as well as for the detection of protein binding at self-assembled DNA monolayers. However, its use for the detection of protein binding utilizing double-stranded (dsDNA) monolayers can be divided into electrodes modified with a hairpin oligonucleotide with conjugated redox-active probes[58,63,77–81], or with dsDNA that bends upon protein binding[67,82,83]. For the first type, the protein binding stabilizes an oligonucleotide conformation which brings the redox-active probe close to the electrode leading to a large increase in current signal. The second type, the protein binding bends the dsDNA limiting the flow of electrons.

Over the past years researchers have driven their attention to the use of nanotechnology to develop nanostructured materials as biomolecule immobilizing surfaces to improve electrochemical detection by their quantum confinement, high surface area to volume ratio, and macro quantum tunnel effects[84–87]. Nanostructured materials like nanostructured gold (NG) surfaces offer many unique features and have shown great

improvements in response time and sensitivity at the device interface. Their nanometer dimensions show an increased sensing surface and strong binding properties, allowing for more biomolecules to be immobilized, thus allowing a higher sensitivity[64,86–89]. The NG sensors modified with single-stranded DNA are mainly designed to characterize the hybridization event between the two complimentary strands which allows electrochemical charge transport[60,61,74,81,90]. The dsDNA biosensors conjugated with charge donors or acceptors are employed as redox active probes interacting by π-stacked base pairs in dsDNA to monitor the electrochemical binding event[58,63,67,70,73,91–94].

1.4 References

(1) Kealy, T. J.; Pauson, P. L. A New Type of Organo-Iron Compound. *Nature* **1951**, *168* (4285), 1039–1040.

(2) Miller, S. A.; Tebboth, J. A.; Tremaine, J. F. 114. Dicyclopentadienyliron. *J. Chem. Soc. Resumed* **1952**, 632.

(3) Wilkinson, G.; Rosenblum, M.; Whiting, M. C.; Woodward, R. B. THE STRUCTURE OF IRON BIS-CYCLOPENTADIENYL. *J. Am. Chem. Soc.* **1952**, *74* (8), 2125–2126.

(4) Pfab, W.; Fischer, E. O. Zur Kristallstruktur Der Di-Cyclopentadienyl-Verbindungen Des Zweiwertigen Eisens, Kobalts Und Nickels. *Z. Für Anorg. Allg. Chem.* **1953**, *274* (6), 316–322.

(5) Haaland, A. Molecular Structure and Bonding in the 3d Metallocenes. *Acc. Chem. Res.* **1979**, *12* (11), 415–422.

(6) Hendry, S. P.; Cardosi, M. F.; Turner, A. P. F.; Neuse, E. W. Polyferrocenes as Mediators in Amperometric Biosensors for Glucose. *Anal. Chim. Acta* **1993**, *281* (3), 453–459.

(7) Labande, A.; Astruc, D. Colloids as Redox Sensors: Recognition of H2PO4− and HSO4− by Amidoferrocenylalkylthiol–gold Nanoparticles. *Chem. Commun.* **2000**, No. 12, 1007–1008.

(8) Astruc, D. Ferrocenyl Dendrimers: Multi-Electron Redox Reagents and Their Applications. *New J. Chem.* **2011**, *35* (4), 764–772.

(9) Palomera, N.; Vera, J. L.; Meléndez, E.; Ramirez-Vick, J. E.; Tomar, M. S.; Arya, S. K.; Singh, S. P. Redox Active Poly(pyrrole-N-Ferrocene-Pyrrole) Copolymer Based Mediator-Less Biosensors. *J. Electroanal. Chem.* **2011**, *658* (1–2), 33–37.

(10) Astruc, D.; Ornelas, C.; Ruiz, J. Metallocenyl Dendrimers and Their Applications in Molecular Electronics, Sensing, and Catalysis. *Acc. Chem. Res.* **2008**, *41* (7), 841–856.

(11) Labande, A.; Ruiz, J.; Astruc, D. Supramolecular Gold Nanoparticles for the Redox Recognition of Oxoanions: Syntheses, Titrations, Stereoelectronic Effects, and Selectivity†. *J. Am. Chem. Soc.* **2002**, *124* (8), 1782–1789.

(12) Philipova, I.; Stavrakov, G.; Chimov, A.; Nikolova, R.; Shivachev, B.; Dimitrov, V. Synthesis of Ferrocene-Based Amido-Phosphine Ligands via Highly Diastereoselective Ortho-Lithiation and Their Application in Pd-Catalyzed Asymmetric Allylic Alkylations. *Tetrahedron Asymmetry* **2011**, *22* (9), 970–979.

(13) Watanabe, M.; Chang, Y. J.; Chou, P.-T.; Staykov, A.; Shibahara, M.; Sako, K.; Ishihara, T.; Chow, T. J. Synthesis and Electronic Properties of Ferrocene-Containing Organic Dyads. *Tetrahedron Lett.* **2015**.

(14) Sarhan, A. A. O.; Izumi, T. Design and Synthesis of New Functional Compounds Related to Ferrocene Bearing Heterocyclic Moieties. *J. Organomet. Chem.* **2003**, *675* (1-2), 1–12.

(15) Atkinson, R. C. J.; Gibson, V. C.; Long, N. J. The Syntheses and Catalytic Applications of Unsymmetrical Ferrocene Ligands. *Chem. Soc. Rev.* **2004**, *33* (5), 313.

(16) Gómez Arrayás, R.; Adrio, J.; Carretero, J. C. Recent Applications of Chiral Ferrocene Ligands in Asymmetric Catalysis. *Angew. Chem. Int. Ed.* **2006**, *45* (46), 7674–7715.

(17) Togni, A. *Ferrocenes: Homogeneous Catalysis, Organic Synthesis, Materials Science*; John Wiley & Sons, 2008.

(18) Frontmatter. In *Ferrocenes*; Togni, essor A., Hayashi, essor T., Eds.; Wiley-VCH Verlag GmbH, 1994; pp 1–23.

(19) On the Mechanism of the Antitumor Activity of Ferrocenium Derivatives* 1 http://www.academia.edu/295137/On_the_Mechanism_of_the_Antitumor_Activity_of_Ferrocenium_Derivatives_1 (accessed Feb 24, 2015).

(20) Tsierkezos, N. G. Cyclic Voltammetric Studies of Ferrocene in Nonaqueous Solvents in the Temperature Range from 248.15 to 298.15 K. *J. Solut. Chem.* **2007**, *36* (3), 289–302.

(21) Connelly, N. G.; Geiger, W. E. Chemical Redox Agents for Organometallic Chemistry. *Chem. Rev.* **1996**, *96* (2), 877–910.

(22) Köpf-Maier, P.; Köpf, H.; Neuse, E. W. Ferricenium Complexes: A New Type of Water-Soluble Antitumor Agent. *J. Cancer Res. Clin. Oncol.* **1984**, *108* (3), 336–340.

(23) Braga, S. S.; Silva, A. M. S. A New Age for Iron: Antitumoral Ferrocenes. *Organometallics* **2013**, *32* (20), 5626–5639.

(24) Gasser, G.; Ott, I.; Metzler-Nolte, N. Organometallic Anticancer Compounds. *J. Med. Chem.* **2011**, *54* (1), 3–25.

(25) Houlton, A.; Roberts, R. M. G.; Silver, J. Studies on the Anti-Tumour Activity of Some Iron Sandwich Compounds. *J. Organomet. Chem.* **1991**, *418* (1), 107–112.

(26) Fouda, M. F. R.; Abd-Elzaher, M. M.; Abdelsamaia, R. A.; Labib, A. A. On the Medicinal Chemistry of Ferrocene. *Appl. Organomet. Chem.* **2007**, *21* (8), 613–625.

(27) Meléndez, E. Metallocenes as Target Specific Drugs for Cancer Treatment. *Inorg. Chim. Acta* **2012**, *393*, 36–52.

(28) Vera, J. L.; Rullán, J.; Santos, N.; Jiménez, J.; Rivera, J.; Santana, A.; Briggs, J.; Rheingold, A. L.; Matta, J.; Meléndez, E. Functionalized Ferrocenes: The Role of the Para Substituent on the Phenoxy Pendant Group. *J. Organomet. Chem.* **2014**, *749*, 204–214.

(29) Ornelas, C. Application of Ferrocene and Its Derivatives in Cancer Research. *New J. Chem.* **2011**, *35* (10), 1973–1985.

(30) Top, S.; Dauer, B.; Vaissermann, J.; Jaouen, G. Facile Route to Ferrocifen, 1-[4-(2-Dimethylaminoethoxy)]-1-(phenyl-2-Ferrocenyl-but-1-Ene), First Organometallic Analogue of Tamoxifen, by the McMurry Reaction. *J. Organomet. Chem.* **1997**, *541* (1–2), 355–361.

(31) Top, S.; Tang, J.; Vessières, A.; Carrez, D.; Provot, C.; Jaouen, G. Ferrocenyl Hydroxytamoxifen: A Prototype for a New Range of Oestradiol Receptor Site-Directed Cytotoxics. *Chem. Commun.* **1996**, No. 8, 955–956.

(32) Giobbie-Hurder, A.; Price, K. N.; Gelber, R. D.; International Breast Cancer Study Group; BIG 1-98 Collaborative Group. Design, Conduct, and Analyses of Breast International Group (BIG) 1-98: A Randomized, Double-Blind, Phase-III Study Comparing Letrozole and Tamoxifen as Adjuvant Endocrine Therapy for Postmenopausal Women with Receptor-Positive, Early Breast Cancer. *Clin. Trials Lond. Engl.* **2009**, *6* (3), 272–287.

(33) Acevedo, C.Y.; Meléndez, E.; Singh, S.P.; Ramirez-Vick, J.E. Cytotoxicity and Reactive Oxygen Species Generated by Ferrocenium and Ferrocene on MCF7 and MCF10A Cell Lines. *J. Cancer Sci. Ther.* **2012**, *04* (09).

(34) Vera, J.; Gao, L. M.; Santana, A.; Matta, J.; Meléndez, E. Vectorized Ferrocenes with Estrogens and Vitamin D2: Synthesis, Cytotoxic Activity and Docking Studies. *Dalton Trans.* **2011**, *40* (37), 9557.

(35) Pérez, W. I.; Soto, Y.; Ortíz, C.; Matta, J.; Meléndez, E. Ferrocenes as Potential Chemotherapeutic Drugs: Synthesis, Cytotoxic Activity, Reactive Oxygen Species Production and Micronucleus Assay. *Bioorg. Med. Chem.* **2015**, *23* (3), 471–479.

(36) DeSantis, C.; Ma, J.; Bryan, L.; Jemal, A. Breast Cancer Statistics, 2013: Breast Cancer Statistics, 2013. *CA. Cancer J. Clin.* **2014**, *64* (1), 52–62.

(37) Siegel, R.; Ma, J.; Zou, Z.; Jemal, A. Cancer Statistics, 2014: Cancer Statistics, 2014. *CA. Cancer J. Clin.* **2014**, *64* (1), 9–29.

(38) McDaniel, R. E.; Maximov, P. Y.; Jordan, V. C. Estrogen-Mediated Mechanisms to Control the Growth and Apoptosis of Breast Cancer Cells. In *Vitamins & Hormones*; Elsevier, 2013; Vol. 93, pp 1–49.

(39) Dent, R.; Trudeau, M.; Pritchard, K. I.; Hanna, W. M.; Kahn, H. K.; Sawka, C. A.; Lickley, L. A.; Rawlinson, E.; Sun, P.; Narod, S. A. Triple-Negative Breast Cancer:

Clinical Features and Patterns of Recurrence. *Clin. Cancer Res.* **2007**, *13* (15), 4429–4434.

(40) Sørlie, T.; Perou, C. M.; Tibshirani, R.; Aas, T.; Geisler, S.; Johnsen, H.; Hastie, T.; Eisen, M. B.; Rijn, M. van de; Jeffrey, S. S.; et al. Gene Expression Patterns of Breast Carcinomas Distinguish Tumor Subclasses with Clinical Implications. *Proc. Natl. Acad. Sci.* **2001**, *98* (19), 10869–10874.

(41) Sørlie, T.; Tibshirani, R.; Parker, J.; Hastie, T.; Marron, J. S.; Nobel, A.; Deng, S.; Johnsen, H.; Pesich, R.; Geisler, S.; et al. Repeated Observation of Breast Tumor Subtypes in Independent Gene Expression Data Sets. *Proc. Natl. Acad. Sci.* **2003**, *100* (14), 8418–8423.

(42) Peyrone, M. Ueber Die Einwirkung Des Ammoniaks Auf Platinchlorür. *Justus Liebigs Ann. Chem.* **1844**, *51* (1), 1–29.

(43) Pinto, A. L.; Lippard, S. J. Binding of the Antitumor Drug Cis-diamminedichloroplatinum(II) (cisplatin) to DNA. *Biochim. Biophys. Acta BBA - Rev. Cancer* **1985**, *780* (3), 167–180.

(44) Prestayko, A. W.; D'Aoust, J. C.; Issell, B. F.; Crooke, S. T. Cisplatin (cis-Diamminedichloroplatinum II). *Cancer Treat. Rev.* **1979**, *6* (1), 17–39.

(45) Loehrer, P. J.; Einhorn, L. H. Drugs Five Years Later. Cisplatin. *Ann. Intern. Med.* **1984**, *100* (5), 704–713.

(46) Millá, A.; Grau, J. J.; Estapé, J. [Cisplatin]. *Med. Clínica* **1983**, *80* (6), 283–288.

(47) Milosavljevic, N.; Duranton, C.; Djerbi, N.; Puech, P. H.; Gounon, P.; Lagadic-Gossmann, D.; Dimanche-Boitrel, M. T.; Rauch, C.; Tauc, M.; Counillon, L.; et al. Nongenomic Effects of Cisplatin: Acute Inhibition of Mechanosensitive Transporters and Channels without Actin Remodeling. *Cancer Res.* **2010**, *70* (19), 7514–7522.

(48) Top, S.; Vessières, A.; Cabestaing, C.; Laios, I.; Leclercq, G.; Provot, C.; Jaouen, G. Studies on Organometallic Selective Estrogen Receptor Modulators. (SERMs) Dual Activity in the Hydroxy-Ferrocifen Series. *J. Organomet. Chem.* **2001**, *637-639*, 500–506.

(49) Nass, N.; Kalinski, T. Tamoxifen Resistance: From Cell Culture Experiments towards Novel Biomarkers. *Pathol. Res. Pract.* **2015**, *211* (3), 189–197.

(50) Eley, D. D.; Spivey, D. I. Semiconductivity of Organic Substances. Part 9.—Nucleic Acid in the Dry State. *Trans. Faraday Soc.* **1962**, *58* (0), 411–415.

(51) Szent-Györgyi, A.; Isenberg, I.; Baird, S. L. On the Electron Donating Properties of Carcinogens. *Proc. Natl. Acad. Sci. U. S. A.* **1960**, *46* (11), 1444–1449.

(52) Boon, E. M.; Barton, J. K. Charge Transport in DNA. *Curr. Opin. Struct. Biol.* **2002**, *12* (3), 320–329.

(53) Delaney, S.; Barton, J. K. Long-Range DNA Charge Transport. *J. Org. Chem.* **2003**, *68* (17), 6475–6483.

(54) Wagenknecht, H.-A. *Charge Transfer in DNA: From Mechanism to Application*; John Wiley & Sons, 2006.

(55) Giese, B. Long-Distance Charge Transport in DNA: The Hopping Mechanism. *Acc. Chem. Res.* **2000**, *33* (9), 631–636.

(56) Schuster, G. B. Long-Range Charge Transfer in DNA: Transient Structural Distortions Control the Distance Dependence. *Acc. Chem. Res.* **2000**, *33* (4), 253–260.

(57) Boon, E. M.; Ceres, D. M.; Drummond, T. G.; Hill, M. G.; Barton, J. K. Mutation Detection by Electrocatalysis at DNA-Modified Electrodes. *Nat. Biotechnol.* **2000**, *18* (10), 1096–1100.

(58) Cañete, S. J. P.; Yang, W.; Lai, R. Y. Folding-Based Electrochemical DNA Sensor Fabricated by “click” Chemistry. *Chem. Commun.* **2009**, No. 32, 4835–4837.

(59) Chen, Q.; Li, D.; Yang, H.; Zhu, Q.; Xu, J.; Zhao, Y. Interaction of a Novel Red-Region Fluorescent Probe, Nile Blue, with DNA and Its Application to Nucleic Acids Assay. *The Analyst* **1999**, *124* (6), 901–906.

(60) Kelley, S. O.; Jackson, N. M.; Hill, M. G.; Barton, J. K. Long-Range Electron Transfer through DNA Films. *Angew. Chem. Int. Ed.* **1999**, *38* (7), 941–945.

(61) Drummond, T. G.; Hill, M. G.; Barton, J. K. Electrochemical DNA Sensors. *Nat. Biotechnol.* **2003**, *21* (10), 1192–1199.

(62) Patel, M. K.; Solanki, P. R.; Kumar, A.; Khare, S.; Gupta, S.; Malhotra, B. D. Electrochemical DNA Sensor for Neisseria Meningitidis Detection. *Biosens. Bioelectron.* **2010**, *25* (12), 2586–2591.

(63) Rowe, A. A.; White, R. J.; Bonham, A. J.; Plaxco, K. W. Fabrication of Electrochemical-DNA Biosensors for the Reagentless Detection of Nucleic Acids, Proteins and Small Molecules. *J. Vis. Exp.* **2011**, No. 52.

(64) Zhong, G. Detection of Femtomolar Level Osteosarcoma-Related Gene via a Chronocoulometric DNA Biosensor Based on Nanostructure Gold Electrode. *Int. J. Nanomedicine* **2012**, 527.

(65) LUO, X.-W.; DU, F.-J.; WU, Y.; GAO, L.-J.; LI, X.-X. Electrochemical DNA Sensor for Determination of p53 Tumor Suppressor Gene Incorporating Gold Nanoparticles Modification. *Chin. J. Anal. Chem.* **2013**, *41* (11), 1664–1668.

(66) Kelley, S. O.; Barton, J. K.; Jackson, N. M.; Hill, M. G. Electrochemistry of Methylene Blue Bound to a DNA-Modified Electrode. *Bioconjug. Chem.* **1997**, *8* (1), 31–37.

(67) Gorodetsky, A. A.; Ebrahim, A.; Barton, J. K. Electrical Detection of TATA Binding Protein at DNA-Modified Microelectrodes. *J. Am. Chem. Soc.* **2008**, *130* (10), 2924–2925.

(68) Boon, E. M.; Salas, J. E.; Barton, J. K. An Electrical Probe of protein–DNA Interactions on DNA-Modified Surfaces. *Nat. Biotechnol.* **2002**, *20* (3), 282–286.

(69) Kelley, S. Single-Base Mismatch Detection Based on Charge Transduction through DNA. *Nucleic Acids Res.* **1999**, *27* (24), 4830–4837.

(70) Pheeney, C. G.; Barton, J. K. DNA Electrochemistry with Tethered Methylene Blue. *Langmuir* **2012**, *28* (17), 7063–7070.

(71) Bradley, D. F.; Stellwagen, N. C.; O'konski, C. T.; Paulson, C. M. Electric Birefringence and Dichroism of Acridine Orange and Methylene Blue Complexes with Polynucleotides. *Biopolymers* **1972**, *11* (3), 645–652.

(72) Nordén, B.; Tjerneld, F. Structure of Methylene blue–DNA Complexes Studied by Linear and Circular Dichroism Spectroscopy. *Biopolymers* **1982**, *21* (9), 1713–1734.

(73) Rohs, R.; Sklenar, H. Methylene Blue Binding to DNA with Alternating AT Base Sequence: Minor Groove Binding Is Favored over Intercalation. *J. Biomol. Struct. Dyn.* **2004**, *21* (5), 699–711.

(74) Gorodetsky, A. A.; Buzzeo, M. C.; Barton, J. K. DNA-Mediated Electrochemistry. *Bioconjug. Chem.* **2008**, *19* (12), 2285–2296.

(75) Slinker, J. D.; Muren, N. B.; Renfrew, S. E.; Barton, J. K. DNA Charge Transport over 34 Nm. *Nat. Chem.* **2011**, *3* (3), 228–233.

(76) Boon, E. M.; Barton, J. K.; Bhagat, V.; Nersissian, M.; Wang, W.; Hill, M. G. Reduction of Ferricyanide by Methylene Blue at a DNA-Modified Rotating-Disk Electrode. *Langmuir* **2003**, *19* (22), 9255–9259.

(77) Galas, D. J.; Schmitz, A. DNAse Footprinting: A Simple Method for the Detection of Protein-DNA Binding Specificity. *Nucleic Acids Res.* **1978**, *5* (9), 3157–3170.

(78) Ricci, F.; Bonham, A. J.; Mason, A. C.; Reich, N. O.; Plaxco, K. W. Reagentless, Electrochemical Approach for the Specific Detection of Double- and Single-Stranded DNA Binding Proteins. *Anal. Chem.* **2009**, *81* (4), 1608–1614.

(79) Vallée-Bélisle, A.; Bonham, A. J.; Reich, N. O.; Ricci, F.; Plaxco, K. W. Transcription Factor Beacons for the Quantitative Detection of DNA Binding Activity. *J. Am. Chem. Soc.* **2011**, *133* (35), 13836–13839.

(80) Zhiqiang Liang, A. D. Determination of Transcription Nuclear Factor-Kappa B Using an Electrochemical, DNA-Based Nanoswitch. *Anal. Lett.* **2014**, *47* (16), 2691–2698.

(81) Bonham, A. J.; Hsieh, K.; Ferguson, B. S.; Vallée-Bélisle, A.; Ricci, F.; Soh, H. T.; Plaxco, K. W. Quantification of Transcription Factor Binding in Cell Extracts Using an Electrochemical, Structure-Switching Biosensor. *J. Am. Chem. Soc.* **2012**, *134* (7), 3346–3348.

(82) Gorodetsky, A. A.; Dietrich, L. E. P.; Lee, P. E.; Demple, B.; Newman, D. K.; Barton, J. K. DNA Binding Shifts the Redox Potential of the Transcription Factor SoxR. *Proc. Natl. Acad. Sci.* **2008**, *105* (10), 3684–3689.

(83) Williams, K.; Kim, C.-S.; Kim, J. R.; Levicky, R. Multimodal Electrochemical Sensing of Transcription Factor–operator Complexes. *Analyst* **2014**, *139* (6), 1463–1471.

(84) H. Asif, M. Electrochemical Biosensors Based on ZnO Nanostructures to Measure Intracellular Metal Ions and Glucose. *J. Anal. Bioanal. Tech.* **2013**, *S7*.

(85) Arya, S. K.; Saha, S.; Ramirez-Vick, J. E.; Gupta, V.; Bhansali, S.; Singh, S. P. Recent Advances in ZnO Nanostructures and Thin Films for Biosensor Applications: Review. *Anal. Chim. Acta* **2012**, *737*, 1–21.

(86) Alubaidy, M.; Soleymani, L.; Venkatakrishnan, K.; Tan, B. Femtosecond Laser Nanostructuring for Femtosensitive DNA Detection. *Biosens. Bioelectron.* **2012**, *33* (1), 82–87.

(87) García-Mendiola, T.; Gamero, M.; Campuzano, S.; Revenga-Parra, M.; Alonso, C.; Pedrero, M.; Pariente, F.; Pingarrón, J. M.; Lorenzo, E. Nanostructured Rough Gold Electrodes as Platforms to Enhance the Sensitivity of Electrochemical Genosensors. *Anal. Chim. Acta* **2013**, *788*, 141–147.

(88) Wang, W.; Chen, C.; Qian, M.; Zhao, X. S. Aptamer Biosensor for Protein Detection Using Gold Nanoparticles. *Anal. Biochem.* **2008**, *373* (2), 213–219.

(89) Tansil, N. C.; Gao, Z. Nanoparticles in Biomolecular Detection. *Nano Today* **2006**, *1* (1), 28–37.

(90) Genereux, J. C.; Barton, J. K. Mechanisms for DNA Charge Transport. *Chem. Rev.* **2010**, *110* (3), 1642–1662.

(91) Pan, D.; Zuo, X.; Wan, Y.; Wang, L.; Zhang, J.; Song, S.; Fan, C. Electrochemical Interrogation of Interactions between Surface-Confined DNA and Methylene Blue. *Sensors* **2007**, *7* (11), 2671–2680.

(92) Zhong, G.; Liu, A.; Chen, X.; Wang, K.; Lian, Z.; Liu, Q.; Chen, Y.; Du, M.; Lin, X. Electrochemical Biosensor Based on Nanoporous Gold Electrode for Detection of PML/RARα Fusion Gene. *Biosens. Bioelectron.* **2011**, *26* (9), 3812–3817.

(93) Tuite, E.; Kelly, J. M. The Interaction of Methylene Blue, Azure B, and Thionine with DNA: Formation of Complexes with Polynucleotides and Mononucleotides as Model Systems. *Biopolymers* **1995**, *35* (5), 419–433.

(94) Zhao, G.-C.; Zhu, J.-J.; Zhang, J.-J.; Chen, H.-Y. Voltammetric Studies of the Interaction of Methylene Blue with DNA by Means of B-Cyclodextrin. *Anal. Chim. Acta* **1999**, *394* (2–3), 337–344.

Chapter II

Synthesis, characterization, cytotoxic and genotoxic activity of functionalized ferrocenes with 4-(1H-pyrrol-1-yl) phenolate

2.1. Introduction

During the past decades researchers have driven their interests into the development of metallic drugs, other than platinum compounds, for cancer treatment. One of the most studied organometallic compounds is based on ferrocene ($FeCp_2$). Ferrocene has been well studied due to its properties, applications in organic synthesis, catalysis and material science as well as its anticancer properties [1–7]. Among them, ferrocenium and ferrocene derivatives opened a new ground in the discovery of new chemotherapeutic agents [8]. The versatility and ease of ferrocene functionalization has allowed the design and synthesis of a wide variety of ferrocene derivatives with biological activity[4,9–20]. Numerous pendant (functional) groups have been attached or linked to the Cp ring to tailor the anti-proliferative properties of ferrocene, many of them with great success [4,9–20]. Recently, Ghorab M.M. et al[21] reported a new range of pyrrole derivatives which had effective cytotoxic activity on breast cancer cell line (MCF-7). Those pyrrole derivatives have opened a new research area due to its good anti-proliferative activity and increase in membrane permeability allowing the compounds to reach the nucleus[21–28].

Our research group has been working for many years in the structure modification of the Cp ring with different pendant groups aimed to enhance the cytotoxic activity of the corresponding functionalized ferrocene[19,20]. One of the most successful compounds is a functionalized ferrocenoyl complex with estradiol[19]. This complex have a IC_{50} of 9(2) μM on hormone-dependent breast epithelial adenocarcinoma cell line MCF-7. Docking studies

of ferrocenoyl 17β-hydroxy-estra-1,3,5(10)-trien-3-olate complex ("Fc-CO_2-estradiol"), **Figure 2.1** into the alpha estrogen receptor (ERα), **Figure 2.1,** revealed that the ferrocene docks partially in the estrogen binding pocket impairing the protein function[19]. Additionally, confocal microscopy studies of Fc-CO_2-estradiol on MCF-7 show that this complex reached the nucleus after 2h of drug exposure[18]. Other successful ferrocenoyl esters were recently published by our research group which have anti-proliferative activities depending on the pendant group attached to the Cp ring[20]. Of particular interest is 4-bromophenyl ferrocenecarboxylate (Fc-CO_2-Ph-4-Br) which also displayed good anti-proliferative activity on breast cancer cell line MCF-7 and low anti-proliferative activity on non-tumorigenic human breast epithelial cell line MCF-10A[20]. Also a ferrocenecarboxylate modified with a pyrrole group, 4-(1H-pyrrol-1-yl)phenyl ferrocenecarboxylate, (Fc-CO_2-Ph-4-Py), has been reported showing good anti-proliferative activity on MCF-7[20].

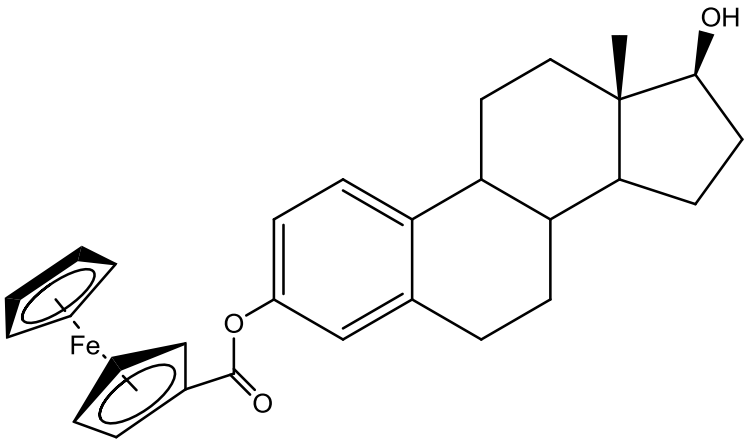

Figure 2. 1. Chemical structure of ferrocenoyl 17β-hydroxy-estra-1,3,5(10)-trien-3-olate complex ("Fc-CO_2-estradiol").

The mechanism of action of those ferrocene or ferrocenium complexes has been investigated on MCF-7 and MCF-10A[29] The ferrocenium based complexes can generate

H_2O_2 by autooxidation, forming Fc^+ which induce DNA oxidative damage and 8-oxoguanine as an initial product of guanine oxidation[30–32]. The DNA oxidative damage can be expressed as DNA fragmentation. The DNA fragmentation can be measured using a well established procedure by Fenech and coworkers[33–36]. The cytokinesis-block micronucleus assay (CBMN) measure the micronuclei (MNi) formation, represented in **Figure 2.2,** that originates from chromosome fragments or whole chromosomes that lag behind at anaphase during nuclear division[34-39]. In addition, a reactive oxygen induction assay (ROS) was performed to corroborate the genotoxic effects. ROS induction assay consists in measurements of a fluorescent product 2′,7′-dichlorofluorescein (DCF) that result from the oxidation in the cell[29].

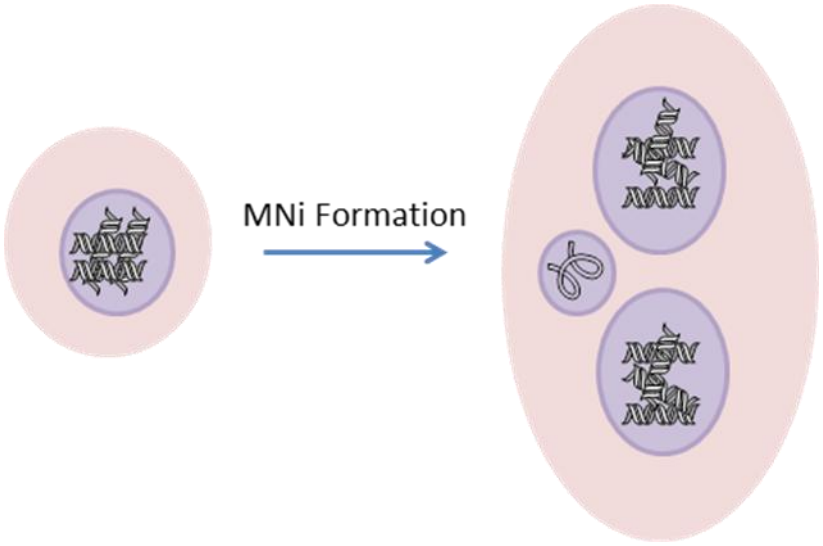

Figure 2. 2 Micronuclei formation during cell division in the cytokinesis-block micronucleus assay.

2.2 Experimental Section

2.2.1 General Procedure

All reactions were performed under an atmosphere of dry nitrogen using Schlenk glassware or a glovebox, unless otherwise stated. Reaction vessels were flame dried under a stream of nitrogen, and anhydrous solvents were transferred by oven-dried syringes or cannula. CH_2Cl_2 was dried and deoxygenated by distillation over CaH_2 under nitrogen. Infrared spectra were recorded on a Perkin Elmer Spectrum ATR spectrometer in solid. The NMR spectra were obtained on a 500MHz Bruker spectrometer. Electrochemical characterizations were carried out on a BAS CV-50W voltammetric analyzer. Elemental analyses were obtained from Atlantic Microlab Inc. Silica gel was heated at about 200°C while a slow stream of dry nitrogen was passed through it prior to use. 4-(1*H*-Pyrrol-1-yl)phenol, ferroceneacetic acid and ferrocenedicarboxylic acid were purchased from Aldrich and used as received.

Hydrolytic stability studies of Fc-(CO_2-Ph-4-Py)CO_2H, and Fc-CH_2CO_2-Ph-4-Py were performed by ^{1}H NMR using a solvent mixture of 5% DMSOd_6–95% D2O (v/v). The complex solutions were prepared first by dissolving the corresponding ferrocene in DMSO-d_6 and then D_2O was added to a final composition of 5% DMSOd_6–95% D_2O. The ^{1}H NMR spectrum of the complex solution was then recorded at 0 h, 24 h and 72 h. Attempts to study the hydrolytic stability of Fc-(CO_2-Ph-4-Py)$_2$ was hampered by the limited solubility of this compound on aqueous solution.

2.2.2 Synthesis and characterization

2.2.2.1 Synthesis of 1,1'-4-(1H-pyrrol-1-yl)phenyl ferrocenedicarboxylate ("Fc-(CO_2-Ph-4-Py)$_2$")

In a 50 mL three neck round bottom flask, 1,1'-ferrocenedicarboxylic acid (0.2741g, 0.001 mol), oxalyl chloride (174.5 µL, 0.002 mol) and pyridine (161 µL, 0.002 mol) were reacted in 20 mL of dichloromethane (DCM) under nitrogen atmosphere at room temperature. The reaction was carried out for 12 h to obtain 1,1'-ferrocenoyl dichloride. For esterification, 1,1'-ferrocenyl chloride was reacted with 4-(1H-pyrrol-1-yl)phenol (0.1592g, 0.001 mol) and pyridine (161 µL, 0.002 mol) for 12 h. After that period, three consecutive washing with 0.01 M HCl were carried out. The organic phase was then dried over sodium sulfate. From the reaction a mixture of three components were obtained; 4-(1H-pyrrol-1-yl)phenyl ferrocenecarboxylate, *("Fc-CO_2-Ph-4-Py")*[14], 1,1'-4-(1H-pyrrol-1-yl)phenyl ferrocenedicarboxylate, *("Fc-(CO_2-Ph-4-Py)$_2$"),* and 1-4-(1H-pyrrol-1-yl)phenyl, 1'-carboxyl ferrocenecarboxylate *("Fc-(CO_2-Ph-4-Py)CO_2H").* The products were separated by column chromatography using silica gel and DCM as mobile phase. The three products, Fc-CO_2-Ph-4-Py, Fc-(CO_2-Ph-4-Py)$_2$, and Fc-(CO_2-Ph-4-Py)CO_2H were isolated in 3 – 9% yield, 12 – 15 % yield, and 45 – 47% yield respectively. The characterization of 4-(1H-pyrrol-1-yl)phenyl ferrocenecarboxylate, *("Fc-CO_2-Ph-4-Py")* was previously reported[20].

Crystallization of 1,1'-4-(1H-pyrrol-1-yl)phenyl ferrocenedicarboxylate was performed inside an NMR tube containing CD_2Cl_2 for a period of two weeks, obtaining block-type orange crystals suitable for X-ray diffraction. Crystal data, data collection and structure refinement details are summarized in **Table 2.1.** The crystallographic data was collected on

a Bruker APEX_II Instrument. The structure solution and refinement was performed using SHELXT 2014/4 (Sheldrick, 2014). H atoms were positioned in idealized locations.

1,1'-4-(1H-pyrrol-1-yl)phenyl ferrocenedicarboxylate ("Fc-(CO_2-Ph-4-Py)$_2$"):

^{1}HNMR (500 MHz, $CDCl_3$) (δppm): 7.37 (2H, d, ph; ^{3}J = 8.8 Hz), 7.25 (2H, d, py; ^{3}J = 2.8 Hz), 7.03 (2H, dd, ph; ^{3}J = 1.3 Hz), 6.34 (2H, dd, py; ^{3}J = 1.6 Hz), 5.08 (2H, overlapping doublets, AA', Cp), 4.64(2H, overlapping doublets, BB', Cp).

^{13}CNMR (125 MHz, $CDCl_3$) (δppm): 169.0 (C=O), 148.3, 138.6, 122.9, 121.5, 119.5, 110.5, 73.4, 72.4, 72.0.

ATR-IR(cm^{-1}): 3145, 3092, 2925, 2841, 1727 (C=O), 1523, 1265, 1205, 1106, 848, 796, 727.

Anal. Calc. for $C_{32}H_{24}O_4FeN_2$: C, 69.05; H, 4.40 Found: C, 68.62; H, 4.46.

1-4-(1H-pyrrol-1-yl)phenyl, 1'-carboxyl ferrocenecarboxylate ("Fc-(CO_2-Ph-4-Py)CO_2H"): ^{1}HNMR (500 MHz, $CDCl_3$): 7.45 (2H, d, ph; ^{3}J = 8.5 Hz), 7.31 (2H, d, py; ^{3}J = 8.5 Hz), 7.08 (2H, dd, ph; ^{3}J = 1.6 Hz), 6.37 (2H, dd, py; ^{3}J = 1.6 Hz), 5.01 (2H, overlapping doublets, AA', Cp), 4.95 (2H, overlapping doublets, BB', Cp), 4.57 (2H, overlapping doublets, AA', Cp'), 4.56 (2H, overlapping doublets, BB' Cp')

^{13}CNMR (125 MHz, $CDCl_3$) (δppm): 168.9 (C=O)', 166.4 (C=O), 148.3, 138.5, 122.9, 121.5, 119.5, 110.5, 74.3, 73.8, 73.4, 72.5, 72.1, 71.0.

ATR-IR (cm^{-1}): 3410(COOH), 3137, 3032, 2963, 1772(C=O), 1697 (C=O)', 1515, 1250, 1068, 1015, 825, 712.

ESI-MS (positive mode), m/z (relative intensity, P4): [Fc-(CO_2-Ph-4-Py)CO_2H-H]+ 413(5), 415(100), 416(23), 417(4). Anal. Calc. for $C_{22}H_{17}O_4NFe(CH_2Cl_2)_{0.125}$: C, 62.40; H, 4.08 Found: C, 62.59; H, 4.28.

2.2.2.2. Synthesis of 4-(1H-pyrrol-1-yl)phenyl ferroceneacetylate ("Fc-CH_2CO_2-Ph-4-Py")

In a 50 mL three neck round bottom flask, ferroceneacetic acid (0.0600g, 0.25 mmol), oxalyl chloride (21.8 µL, 0.25 mmol), pyridine (20.1 µL, 0.25 mmol) and 4-(1H-pyrrol-1yl)phenol (0.0398g, 0.25 mmol) were reacted in 10 mL of dichloromethane (DCM) under nitrogen atmosphere at room temperature. The reaction was carried out for 12 h to get 4(1H-pyrrol-1-yl)phenyl ferroceneacetylate. After that period three consecutive washing with 0.01 M HCl were carried out. The organic phase was then dried over sodium sulfate. The product was separated by column chromatography using silica gel and DCM as mobile phase. Fc-CH_2CO_2-Ph-4-Py was isolated in 62% yield.

4-(1H-pyrrol-1-yl)phenyl ferroceneacetylate ("Fc-CH_2CO_2-Ph-4-Py"):

^{1}HNMR (500 MHz, $CDCl_3$): 7.44 (2H, d, ph; ^3J = 8.8 Hz), 7.18 (2H, d, py; ^3J = 8.8 Hz), 7.01(2H, dd, ph; ^3J = 1.9 Hz), 6.36 (2H, dd, py; ^3J = 1.9 Hz), 4.32 (2H, bs, Cp), 4.19 (2H, bs, Cp', 5H), 3.62 (2H, s, CH_2, 2H).

^{13}CNMR (125 MHz, $CDCl_3$) (δppm): 169.5 (C=O), 148.32, 138.6, 122.6, 121.6, 119.54, 110.5, 79.7, 68.8, 68.1, 35.6.

ATR-IR (cm^{-1}): 3092, 2963, 2917, 1750(C=O), 1508, 1334, 1143, 1098, 810, 727.

ESI-MS (positive mode), m/z (relative intensity, P4): [Fc-CH_2CO_2-Ph-4-Py]+ 384(5), 386(100), 387(22). Anal. Calc. for $C_{22}H_{19}O_2NFe(CH_2Cl_2)_{0.06}$: C, 67.88; H, 4.94 Found: C, 67.99; H, 5.04.

2.2.3 Anti-proliferative studies

Biological activity was determined using the colorimetric MTT assay originally described by Mossman [40,41] but using 10% Triton in isopropanol as a solvent for the MTT formazan crystals[40,41]. The breast adenocarcinoma cell line MCF-7 and MCF-10A were purchased from American Type Culture Collection (ATCC HTB22 and CRL-10317) and were grown under sterile conditions in a culture chamber at 37°C and 95%Air/5%CO_2. Breast adenocarcinoma cell line MCF-7 was grown in Eagles's Minimum Essential medium supplemented with 10% (v/v) fetal bovine serum, 1% (v/v) penicillin/streptomycin, and 0.01 mg/mL bovine insulin. Non-tumorigenic human breast epithelial cell line MCF-10A, was grown in Dulbecco's modified Eagle's medium (DMEM), 5% horse serum, 0.5 µg/mL hydrocortisone (Sigma Cat. no. H-0888), 10 µg/mL insulin (Sigma-ca. no. I1882), 20 ng/mL epidermal growth factor (Sigma Cat. no. E-9644). HT-29 cells were maintained at 37°C and 95% Air–5% CO_2 in McCoy's 5A (ATCC) complete medium, which had been supplemented with 10% (v/v) fetal bovine serum (ATCC) and 1% (v/v) penicillin/streptomycin (Sigma). Asynchronously growing cells were seeded at 1.0 x 10^5 cells per well in 96-well plates containing 100 µL of complete growth medium, and allowed to recover overnight. Various concentrations of the complexes (10–1300 mM) dissolved in 5% DMSO–95% medium were added to the wells (eight wells per concentration; experiments performed in quadruplicate plates). The complex solutions were prepared first by dissolving the corresponding ferrocene in DMSO and then medium was added to a final composition of 5% DMSO–95% medium. In addition to the cells treated with the ferrocenes, two controls experiments were run: one without any addition of solvent mixture (5% DMSO–95% medium) and one adding 5% DMSO–95% medium to the cells. Both control experiments behaved identically, showing that 5% of DMSO in the medium

did not render toxic to these types of cells. The cells were incubated for an additional 70 h. After this time, MTT dissolved in complete growth medium was added to each well to a final concentration of 1.0 mg mL^{-1} and incubated for two additional hours. After this period of time, all MTT containing medium was removed, cells were washed with cold PBS and dissolved with 200 mL of a 10% (v/v) Triton X-100 solution in isopropanol. After complete dissolution of the formazan crystals, absorbances were recorded in triplicate on a 340ATTC microplate reader (SLTLab Instruments) at 570 nm with background subtraction at 630 nm. Concentrations of compounds required to inhibit cell proliferation by 50% (IC_{50}) were calculated by fitting data to a four-parameter logistic plot by means of Sigma Plot software from SPSS (SPSS; Chicago, IL).

2.2.4 Electrochemistry

Cyclic voltammetric experiments were performed in deoxygenated CH_3CN solutions of ferrocene complexes with 0.1 M $[NBu^n_4]PF_6$ as supporting electrolyte and ferrocene complex concentration of 2 x 10^{-3} M. The three electrodes used were platinum disk as the working electrode, Ag/AgCl as a reference electrode, and Pt wire as an auxiliary electrode. The working electrode was polished with 0.05 µm alumina slurry for 1-2 minutes, and then rinsed with double-distilled and deionized water. This cleaning process is done before each CV experiment and a sweep between 0 and 2000 mV is performed on the electrolyte solution to detect any possible deposition of ferrocene on the electrode surface.

2.2.5 Cytokinesis-block micronucleus assay (CBMN)

Cytokinesis-block micronucleus assay (CBMN) was performed as a modified procedure from Fenech M.[33]. Breast adenocarcinoma cells (MCF-7) were seeded in a 75 cm^2 flask with 20 mL of growth media and incubated for about 72 h. Following disaggregation with trypsin/EDTA and re-suspension in complete medium, with concentration of 1 x 10^6 cells/mL, the cells were seed on a six well plate. After 24 h the medium was replaced with a solution at different concentrations of ferrocene complexes. Various concentrations (10 to 0.01 µM) of the corresponding ferrocene were set below IC_{50}. Ferrocene solutions were prepared first by dissolving the corresponding ferrocene in DMSO and then medium was added to a final composition of 5% DMSO–95% medium. The different solutions of the desired ferrocene were added to individual wells, in addition to solutions of a negative control (cells without treatment) and a positive control (cell with methyl methane sulphonate, MMS). Methyl methane sulphonate concentration was selected according to Decordier *et al.*[42]. After 72 h of drug exposure, the solution of ferrocene complex was then replaced with fresh media containing only 6µg/mL of cytochalasin-β and incubated for another 24 h. The cells were washed with phosphate-buffer saline (PBS) and disaggregated with trypsin/EDTA. Following by centrifugation, the cells were re-suspended in 50µL of medium and then fixed with methanol and stained with hemacolor stain set (Harleco, cat# 65044-93). For each treatment condition, micronuclei in 500 binucleated MCF-7 cells for three experiments were scored (mean ± SD). Mitotic rate was assessed as per cent of binucleated cells (mean ± SD). Probability values (P) were estimated by Student's t-test comparing treated cells versus control.

2.2.6 Measurements of reactive oxygen species (ROS)

The ROS production was determined on MCF-7 treated with the oxidation-sensitive dye, 2′,7′-dichlorodihydrofluoresceindiacetate (H_2DCF-DA, Sigma-Aldrich). The exposure of cells to H_2DCF-DA generates a fluorescent product 2′,7′-dichlorofluorescein (DCF) which has an excitation/emission maxima of ~495/529 nm. The breast cancer cells (MCF-7) were seeded in 96-well plates at a concentration of 5 x 10^4 cells/mL containing 100 μL of complete growth medium, and allowed to recover overnight. Various concentrations of the complexes (10–1300 mM) dissolved in 5% DMSO–95% medium were added to the wells (eight wells per concentration; experiments performed in quadruplicate plates). The complex solutions were prepared first by dissolving the corresponding ferrocene in DMSO and then medium was added to a final composition of 5% DMSO–95% medium. In addition to the cells treated with the ferrocenes, two controls experiments were run: one without any addition of solvent mixture (5% DMSO–95% medium) and one adding 5% DMSO–95% medium to the cells. Both control experiments behaved identically, showing that 5% of DMSO in the medium did not render toxic to these types of cells. The cells were incubated for an additional 70 h. After this time, the cells were treated with 10 μM of H_2DCF-DA and incubated for 40 minutes at 37^{o}C after which time ROS production was evaluated at 605 nm.

2.3. Results and discussion

2.3.1 Synthesis and characterization

The subject ferrocenoyl esters were synthesized by an established procedure treating the 1,1´-ferrocenoyl dicarboxilic acid (**Figure 2.3**) with oxalyl chloride to produce 1,1´-ferrocenoyl dichloride. Then 1,1´-ferrocenoyl dichloride was treated with 4-(1H-pyrrol-1-yl)phenol until reaction is completed. However, the reaction (**Figure 2.3**) rendered not very efficient since in the synthesis of Fc-(CO_2-Ph-4-Py)$_2$, the desired complex was isolated in low yield (12-15%) and it yielded two by-products: Fc-CO_2-Ph-4-Py and Fc-(CO_2-Ph-4-Py)CO_2H. The second by-product undergoes a decarboxylation process into the Cp' ring when extractions with HCl were performed. The mechanism of decarboxylation for Fc-(CO_2-Ph-4-Py)CO_2H is shown of **Figure 2.4.** The first step on decarboxylation is the proton removal of the carboxylic proton by the pyridine in the reaction to form the carboxyl anion. Then on an acid media the carboxyl anion undergoes a decarboxylation. The resulting product was previously reported[20]. The third ferrocene derivative was synthesized from a modified procedure reacting ferrocene acetyl chloride (**Figure 2.5)** with 4-(1H-pyrrol-1-yl)phenol for about 12 h. This reaction was simply performed without important by-products. The desired product was isolated in 62% yield.

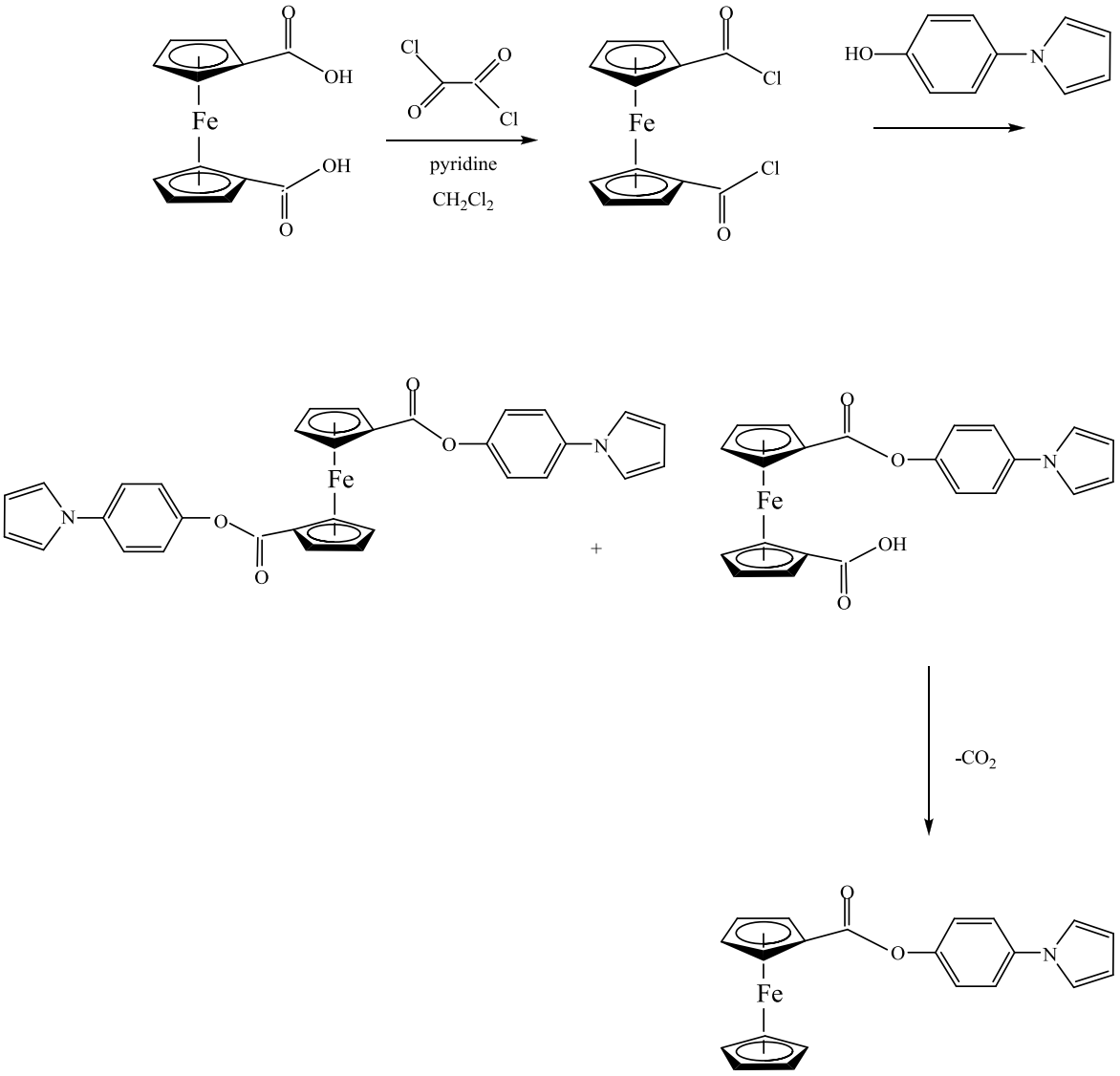

Figure 2. 3. Synthesis of ferrocenoyl esters containing 4-(1H-pyrrol-1-yl)phenolate as pendant group. First and second complexes are the principal products of the reaction. The last product results from decarboxylation of the cyclopentadiene.

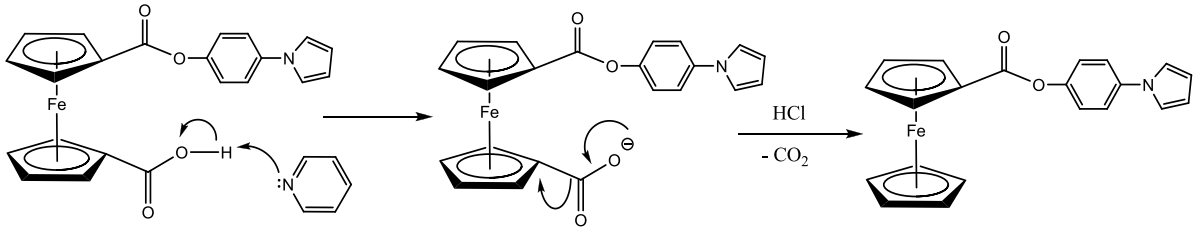

Figure 2. 4 Decarboxylation mechanism of 1-4-(1H-pyrrol-1-yl)phenyl, 1'-carboxyl ferrocenecarboxylate.

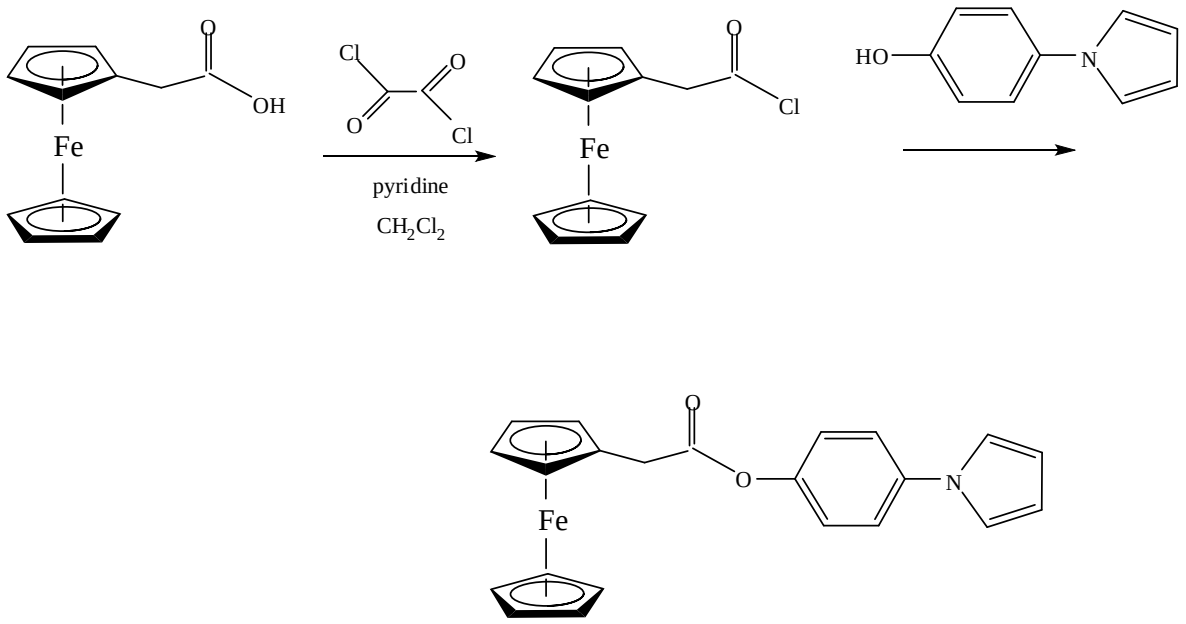

Figure 2. 5. Synthesis of 4(1H-pyrrol-1-yl)phenyl ferroceneacetylate.

The three new synthesized ferrocene were characterized by IR and NMR. The IR spectra (**Figure 2.6**) showed bands in the 1727 - 1772 cm^{-1} region indicating the presence of the carbonyl stretching of the ester groups on the ferrocene. Fc-$(CO_2$-Ph-4-Py$)_2$, shows a carbonyl stretching at 1727 cm^{-1} meanwhile Fc-$(CO_2$-Ph-4-Py$)CO_2H$ showed two carbonyl

stretching bands, one at 1772 cm^{-1}, corresponding to the functionalized Cp ring and a second carbonyl stretching at 1697 cm^{-1} of the carbonyl attached to the unsubstituted Cp ring. The Fc-(CO_2-Ph-4-Py)CO_2H also showed a broad band at 3410 cm^{-1} indicating the presence of the carboxyl OH group attached on the other Cp ring. The difference in the carbonyl stretching wavenumber of the different complexes shows the effect of the pendant group.

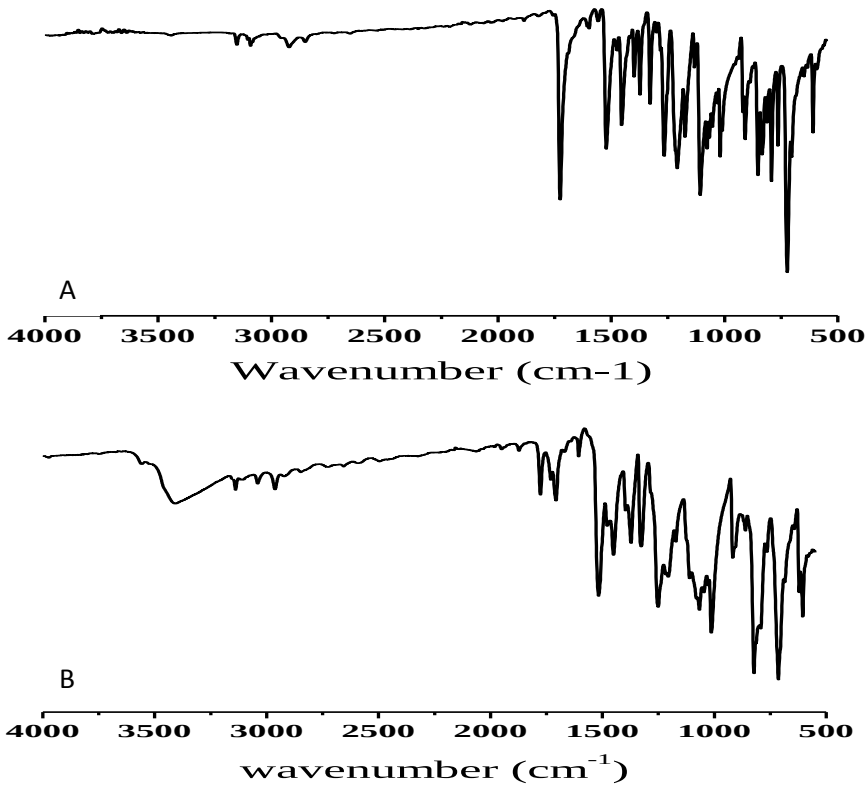

Figure 2. 6. Infrared Spectra of ferrocene derivatives using an ATR-Infrared Spectrometer. A) Fc-(CO_2-Ph-4-Py)$_2$, B) Fc-(CO_2-Ph-4-Py)CO_2H.

The ^{13}C NMR spectra of the three ferrocenes exhibit signals about 169 ppm corresponding to the carbonyl groups. The Fc-(CO_2-Ph-4-Py)CO_2H showed a second

carbonyl signal as expected at 166 ppm attributed to the carboxyl group. The ^{1}H NMR spectral data (**Figure 2.7**) for Fc-(CO_2-Ph-4-Py)CO_2H showed a singlet near 12.33 ppm corresponding of the carboxyl proton. Fc-CH_2CO_2-Ph-4-Py showed a singlet corresponding to the unsubstituted Cp ring and two overlapping signals with AA'BB" pattern corresponding to the monosubstituted Cp ring. Likewise, for Fc-(CO_2-Ph-4-Py)$_2$ and Fc-(CO_2-Ph-4-Py)CO_2H, the Cp signals appear as overlapping doublets in a AA'BB' pattern. The phenyl and pyrrole groups appear in the aromatic and conjugated vinylic regions respectively as doublets or doublet of doublet splitting pattern.

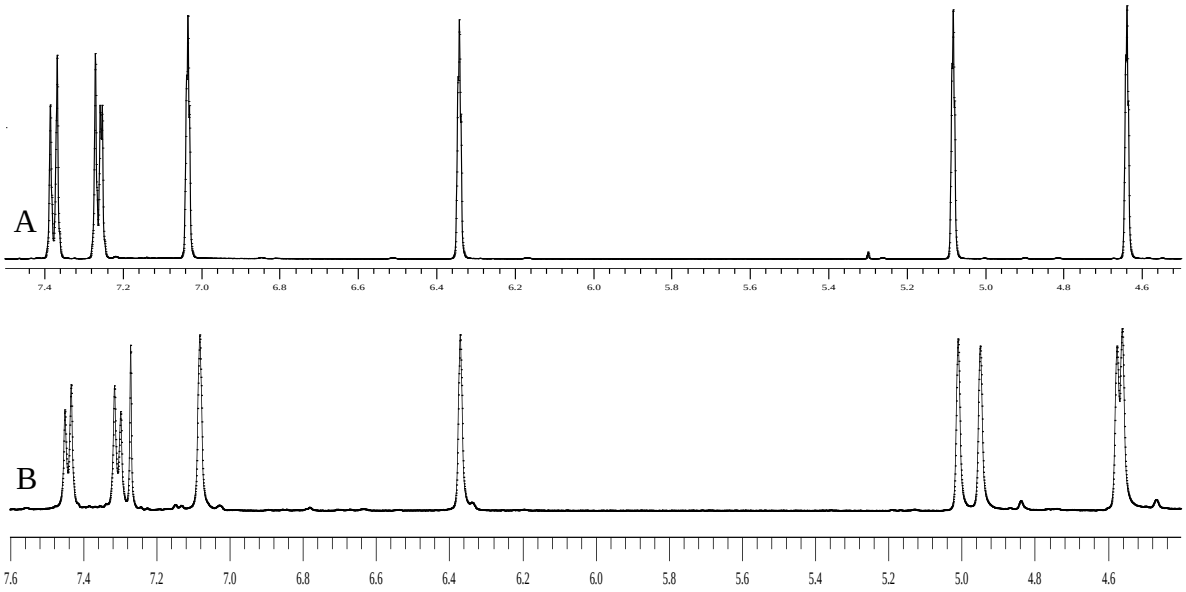

Figure 2. 7. ^{1}HNMR spectra of: A) Fc-(CO_2-Ph-4-Py)$_2$ and B) Fc-(CO_2-Ph-4-Py)CO_2H.

2.3.2 Crystal structure of 1,1'-4-(1H-pyrrol-1-yl)phenyl ferrocenedicarboxylate

The 1,1'-4-(1H-Pyrrol-1-yl)phenyl ferrocenedicarboxylate (Fc-(CO_2-Ph-4-Py)$_2$) was crystallized into a NMR tube by evaporation of deuterated dichloromethane for two weeks. After this time, crystals with plates shape were obtained, and the crystal structure of Fc-(CO_2-Ph-4-Py)$_2$ was elucidated by X-ray diffraction. Attempts to crystallize the Fc-(CO_2-

Ph-4-Py)CO_2H and Fc-CH_2CO_2-Ph-4-Py were unsuccessful due to decomposition of the complexes.

The Fc-(CO_2-Ph-4-Py)$_2$ complex crystallizes in the orthorombic space group *Pbca* (**Figure 2.8**), Table 2.1 with the Fe^{2+} positioned on an inversion center. The symmetry of the Fc-(CO_2-Ph-4-Py)$_2$ complex is implied by the NMR data where only one set of signals were found for the H(2)/H(5) and H(3)/H(4) of Cp rings as well as the H(2)/H(6) and H(3)/H(5) of the phenyl and H(2)/H(5) and H(3)/H(4) of the pyrrole groups. Figure 2.9 presents the solid state structure of Fc-(CO_2-Ph-4-Py)$_2$ complex. The average bond distance for the Fe-C(Cp) is 2.044 Å, which is very similar to that reported for ferrocene[48] and other previously reported structures in our lab[49]. The Fe-C(1) bond distance (2.032 Å) is shorter than the Fe-C bond distances of the unsubstituted carbon atoms due to the inductive effect of the carboxylate functional group attached to the Cp ring. The Figure 2.10 shows the twist angles of the carboxylate group and the phenyl group of the ligand with respect of the Cp ring plane. The carboxylate group is oriented backward with a twist angle of 14.38^o with respect to the Cp ring plane. The twist angle between the Cp ring and the aromatic ring is 70.20^0 above the Cp ring plane.

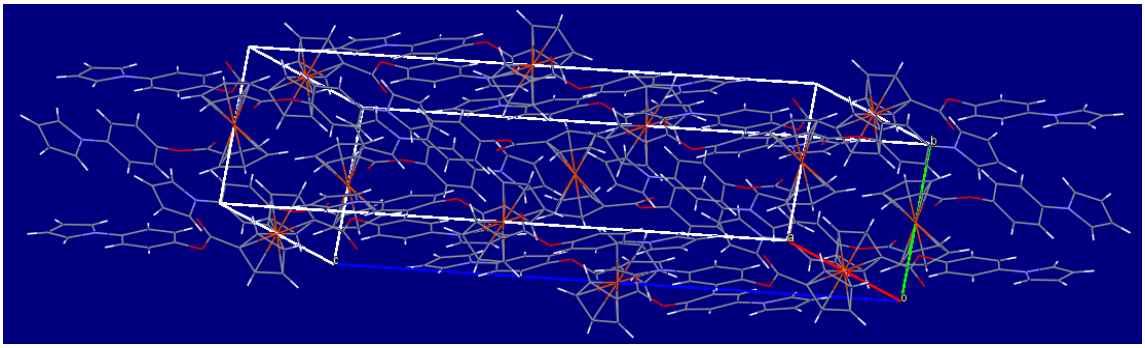

Figure 2. 8. Representation of the orthorombic space group *Pbca* crystallization of 1,1'-4-(1H-pyrrol-1-yl)phenyl ferrocenedicarboxylate.

Table 2. 1. Crystal data and structure refinement for 1,1'-4-(1H-pyrrol-1-yl)phenyl ferrocenedicarboxylate.

Empirical formula	$C_{32}H_{24}FeN_2O_4$
Formula weight	556.38
Temperature	100(2) K
Wavelength	0.71073 Å
Crystal system	Orthorhombic
Space group	*P b c a*
Unit cell dimensions	a = 10.6386(15) Å α = 90°. b = 7.3948(10) Å β = 90°. c = 30.554(4) Å γ = 90°.
Volume	2403.7(6) $Å^3$
Z	4
Density (calculated)	1.537 Mg/m^3
Absorption coefficient	0.673 mm^{-1}
F(000)	1152
Crystal size	0.280 x 0.260 x 0.230 mm^3
Theta range for data collection	2.666 to 28.395°.
Index ranges	-13<=h<=14, -9<=k<=9, -37<=l<=40
Reflections collected	12444
Independent reflections	2999 [R(int) = 0.0769]
Completeness to theta = 25.000°	99.80%
Absorption correction	Multi-scan
Refinement method	Full-matrix least-squares on F^2
Data / restraints / parameters	2999 / 0 / 178
Goodness-of-fit on F^2	1.015
Final R indices [I>2sigma(I)]	$R1$ = 0.0441, $wR2$ = 0.1049
R indices (all data)	$R1$ = 0.0651, $wR2$ = 0.1166
Largest diff. peak and hole	0.339 and -0.622 e.$Å^{-3}$

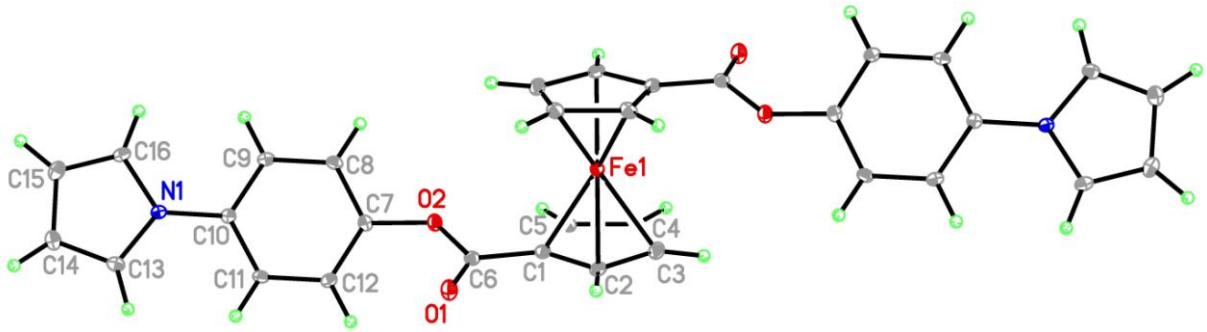

Figure 2. 9. Solid state structure of 1,1´-4-(1H-pyrrol-1-yl)phenyl ferrocenedicarboxylate (Fc-(CO_2-Ph-4-Py)$_2$).

The crystal structure of the new ferrocene derivative Fc-(CO_2-Ph-4-Py)$_2$ is comparable with the previously reported 4-bromophenyl and 4-chlorophenyl ferrocenecarboxylates (Fc-CO_2-Ph-4-Br and Fc-CO_2-Ph-4-Cl)[20]. The Fc-CO_2-Ph-4-Br and Fc-CO_2-Ph-4-Cl contains only one Cp functionalized and a phenyl group attached to the carboxylate, but with Br and Cl instead of pyrrole in the 4-position. Structural data of Fc-CO_2-Ph-4-Br and Fc-CO_2-Ph-4-Cl is presented on **Figures 2.11 and 2.12 and Table 2.3[20]**. The first structural difference between the Fc-CO_2-Ph-4-Br,Fc-CO_2-Ph-4-Cl and Fc-(CO_2-Ph-4-Py)$_2$ is observed on the position of the Cp rings. In the Fc-CO_2-Ph-4-Br and Fc-CO_2-Ph-4-Cl derivatives, the Cp rings are positioned in a nearly eclipsed conformation and parallel with stagger angles < 3^0 and Cp tilt angles of 0.48-1.25^0. Whilst in Fc-(CO_2-Ph-4-Py)$_2$ the Cp rings are positioned in a perfect anti-conformation. The second structural difference is observed on the twist angle between the Cp ring and the carboxylate group. This twist angle for Fc-(CO_2-Ph-4-Py)$_2$ (14.38^o) is larger than the same twist angle on Fc-CO_2-Ph-4-Br and Fc-CO_2-Ph-4-Cl (6.75^o-10.15^o). The third difference was found on the carbonyl oxygen of Fc-(CO_2-Ph-4-Py)$_2$ which lies above the Cp plane whereas for the Fc-

CO_2-Ph-4-Br and Fc-CO_2-Ph-4-Cl complexes, the carbonyl oxygen lies below the Cp plane. Finally, the twist angle between the Cp and the aromatic ring on Fc-(CO_2-Ph-4-Py)$_2$ is 70.20^0 while Fc-CO_2-Ph-4-Br and Fc-CO_2-Ph-4-Cl the two rings are placed at higher angles approaching a perpendicular position.

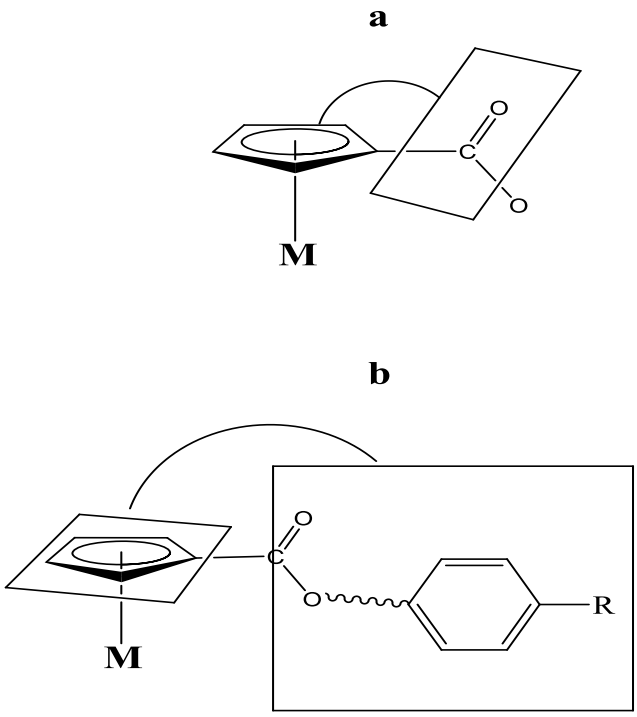

Figure 2. 10. Twist angle between the Cp ring and the carboxylate group (a) and the twist angles between the Cp plane and the aromatic ring (b).

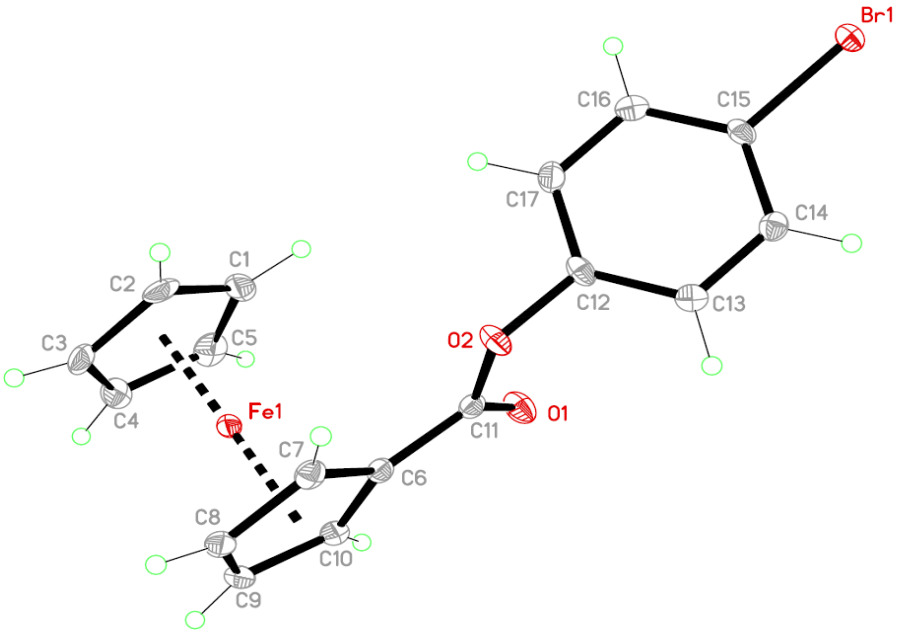

Figure 2. 11 Solid-state structure of 4-bromophenyl ferrocenecarboxylate. Only one of two chemically equivalent molecules is presented. Reproduced with permission of the J. Organometallic Chemistry.

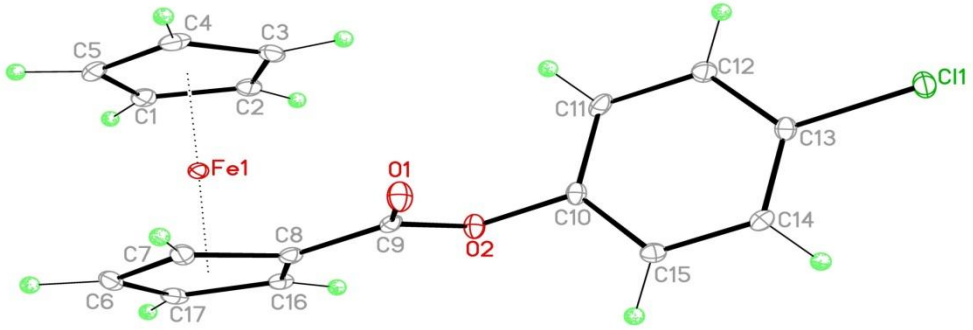

Figure 2. 12 Solid-state structure of 4-chlorophenyl ferrocenecarboxylate. Only one of two chemically equivalent molecules is presented. Reproduced with permission of the J. Organometallic Chemistry.

The crystal structures of Fc-(CO_2-Ph-4-Py)$_2$, Fc-CO_2-Ph-4-Br, and Fc-CO_2-Ph-4-Cl also have some structural similarities. The geometry of the carbonyl carbon in the three ferrocene complexes is similar presenting a distorted trigonal planar. The Fe-C(Cp*) average bond distances of the substituted Cp rings is 2.044 Å which is identical, within the experimental error, in the Fc-(CO_2-Ph-4-Py)$_2$,.Fc-CO_2-Ph-4-Br, and Fc-CO_2-Ph-4-Cl derivatives. Another similarity of the Fc-(CO_2-Ph-4-Py)$_2$ with the Fc-CO_2-Ph-4-Br, and Fc-CO_2-Ph-4-Cl derivatives is found on the Fe-C bond distance of the substituted carbon atom. The pattern of Fe-C bond distance where the pendant group is attached, is substantially shorter than the remaining distances of the Fe-C(Cp) on the three structures. The C(Cp)-C(CO) bond distance in Fc-(CO_2-Ph-4-Py)$_2$ C(1)-C(6), is shorter than a typical C-C single bond, (1.473(3) versus 1.54 Å (single bond))[50]. This bond distance suggests a partial double bond character and delocalization with the Cp π system in analogous manner as for Fc-CO_2-Ph-4-Br, and Fc-CO_2-Ph-4-Cl derivatives.

In comparison with the structure of a disubstituted ferrocene, 1,1'-methyl ferrocenedicarboxylate, Fe($C_5H_4CO_2CH_3$)$_2$, **Figure 2.13**[49], the average Fe-C(Cp) bonds are 2.048/2.049 Å, similar to the subject complex. The Cp rings on Fe($C_5H_4CO_2CH_3$)$_2$, adopt an eclipsed conformation with a stagger angle of 2.37 Å in contrast with the anti-conformation of the Cp rings in Fc-(CO_2-Ph-4-Py)$_2$. Also the functional groups are not positioned perfectly anti to each other. The Fe-C(Cp)-C(CO) bond of Fe($C_5H_4CO_2CH_3$)$_2$, 1.477(4) is notably shorter than the distance for a typical C-C single bond (1.54 Å), in a similar manner to our subject complex, suggesting delocalization with the Cp π system. Finally, Fc-(CO_2-Ph-4-Py)$_2$ contain two π ring system, 4-(1H-pyrrol-1-yl)phenyl, which in principle could do intramolecular π-π or C-H--π stacking as do other 1,1'-disubstituted

ferrocenes with extended π ring system[51-53]. However, such π-π or C-H--π stacking is not observed in Fc-$(CO_2$-Ph-4-Py$)_2$ since the Cp rings adopt an anti-conformation.

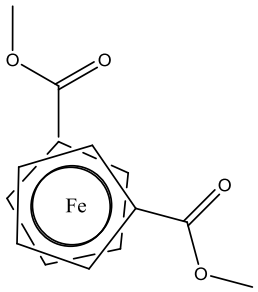

Figure 2. 13. Structure of $Fe(C_5H_4CO_2CH_3)_2$.

Table 2. 2 Selected bond distances [Å] and angles [°] of 1,1´-4-(1H-pyrrol-1-yl)phenyl ferrocenedicarboxylate.

Bond distances [Å]		Bond angles [°]	
Fe-Cp(av)	2.044(10)	C(1)-Fe(1)-C(1)#1	180
Fe(1)-C(5)	2.035(2)	C(1)-Fe(1)-C(5)#1	138.91(8)
Fe(1)-C(3)	2.050(2)	C(2)#1-Fe(1)-C(2)	180.00(12)
Fe(1)-C(2)	2.051(2)	C(3)#1-Fe(1)-C(3)	180
N(1)-C(13)	1.382(3)	C(4)#1-Fe(1)-C(4)	180
N(1)-C(10)	1.422(3)	C(5)#1-Fe(1)-C(5)	180.00(11)
Fe-C(1) (subst)	2.032(2)	O(1)-C(6)-C(1)	126.17(19)
Fe(1)-C(4)	2.055(2)	O(2)-C(6)-C(1)	109.97(18)
O(1)-C(6)	1.201(3)	C(6)-O(2)-C(7)	119.52(16)
O(2)-C(6)	1.366(2)	O(1)-C(6)-O(2)	123.84(18)
O(2)-C(7)	1.407(2)	C(8)-C(7)-O(2)	116.66(18)
N(1)-C(16)		C(12)-C(7)-O(2)	122.16(18)
		C(13)-N(1)-C(16)	107.58(17)
		C(13)-N(1)-C(10)	126.34(17)
		C(16)-N(1)-C(10)	126.08(18)
		C(14)-C(13)-N(1)	108.78(19)
		C(15)-C(16)-N(1)	108.9(2)
Tilt angle between Cps [°]	0		
Twist angle between Cp and carboxylate [°] 14.38			
Twist angle between Cp and aromatic ring [°] 70.20			

Table 2. 3 Selected bonding parameters for 4-chlorophenyl ferrocenecarboxylate and 4-bromophenyl ferrocenecarboxylate.

4-chlorophenyl ferrocenecarboxylate			
Bond lengths [Å]		Molecule 1	Molecule 2
Fe-C_{av}(Cp subt.)		2.044	2.043
Fe-C(8)	2.0259(18)		
Tilt angle between Cp rings [°]		0.54	1.25
Twist angle between Cp and carboxylate [°]		6.75	10.15
Twist angle between Cp plane and the aromatic ring [°]		87.58	78.06
Cp stagger angle [°]		2.95	1.19

4-bromophenyl ferrocenecarboxylate			
Bond lengths [Å]		Molecule 1	Molecule 2
Fe-C_{av} (Cp subst.)		2.044	2.040
Fe-C(6)	2.026(2)		
Tilt angle between Cp rings [°]		0.48	1.11
Twist angle between Cp and carboxylate [°]		7.97	9.03
Twist angle between Cp plane and the aromatic ring [°]		84.11	81.26
Cp stagger angle [°]		1.74	1.24

2.3.3 Electrochemical characterization

The ferrocenium ion (Fc^+) production is involved in the formation of reactive oxygen species (ROS) which induce the oxidation of the guanine to oxo-guanine resulting in DNA damage[20,29]. The electrochemical characterizations of the three new species were pursued by CV to determine the redox properties of the new complexes to assess the DNA damage (**Figure 2.14**). **Table 2.4** presents the redox properties of the subject complexes. The CV of the three new ferrocene complexes were performed on 0.1 M $[NBu^n_4]PF_6$ as supporting electrolyte due to the low solubility of these complexes under pseudo physiological conditions. All three complexes showed reversible redox processes with i_{pa}/i_{pc} ratios close to one.

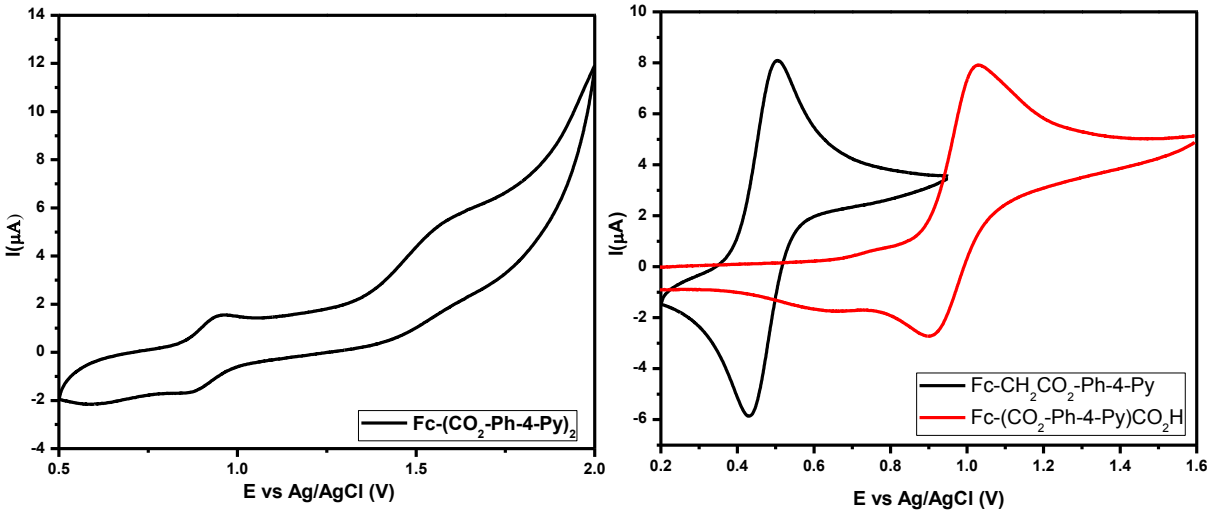

Figure 2. 14. Cyclic Voltamograms of 1,1´-ferrocendicarboxylic acid, 1-4-(1H-pyrrol-1yl)phenyl, 1-carboxyl ferrocenecarboxylate and 4(1H-pyrrol-1yl)phenyl Ferroceneacetylate in CH_3CN with 0.1M $[NBu_4^n]PF_6$ as supporting electrolyte and complex concentrations of 1mM at room temperature. The working electrode was a platinum disk, reference electrode was Ag/AgCl and scan rate was 100 mVs^{-1}.

Fc-$(CO_2$-Ph-4-Py$)_2$ (E_{pa} = 958 mV) and Fc-$(CO_2$-Ph-4-Py$)CO_2H$ (E_{pa} = 1027 mV) showed oxidation potentials higher than Fc (494 mV), while Fc-CH_2CO_2-Ph-4-Py showed similar oxidation potential (E_{pa} = 503 mV) to ferrocene. The phenyl group attached to the Cp ring through an ester linkage can delocalize the electrons away from the metal center due to its conjugated system. This electron delocalization makes the ferrocene robust for oxidation, increasing its E_{pa}. For Fc-CH_2CO_2-Ph-4-Py, the CH_2 group between the ferrocene and the functional group isolates the metal center from the conjugated system avoiding electron delocalization between the ferrocene unit and the 4(1H-pyrrol-1-yl)phenylcarboxylate. In order to get more insight in the mechanism of action and the possible correlation with the oxidation potentials, a comparison with previously reported potentials of biologically active ferrocene, Fc-CO_2-estradiol and 4-bromophenyl ferrocenecarboxylate (Fc-CO_2-Ph-4-Br), in MCF-7 and HT-29 cancer cell lines is needed.

From the electrochemical point of view, Fc-CO_2-Ph-4-Br does not have a pyrrole group available and as a consequence, electron delocalization is reduced as well as the oxidation potential. Meanwhile, Fc-CO_2-estradiol has a steroid group, a conjugated system, which is able to delocalize electrons resulting in higher E_{pa}. In spite of these differences, Fc-CO_2-estradiol and Fc-CO_2-Ph-4-Br have identical anti-proliferative activities in MCF-7 and HT-29 cancer cell lines thereby the correlation between oxidation potential and cytotoxicity cannot be made.

Table 2. 4. Redox potentials of functionalized ferrocenes in CH_3CN with 0.1 M $[NBu_4^n]PF_6$ at a scan rate of 100 mVs^{-1}, using Ag/AgCl saturated as reference electrode.

Complexes	**E_{pa}(mV)**	**E_{pc} (mV)**	**ΔE (mV)**	**$E_{1/2}$ (mV)**
Fc-(CO_2-Ph-4-Py)$_2$	958	862	96	910
Fc-(CO_2-Ph-4-Py)CO_2H	1027	901	126	964
Fc-CH_2CO_2-Ph-4-Py	503	431	73	467
Fc-CO_2-estradiol[19]	801	711	90	756
Fc-CO_2-Ph-4-Br[20]	580	484	96	532
Fc/Fc^+	494	414	80	454

2.3.4 Anti-proliferative activity studies

Cytotoxic activity of the three new ferrocenes complexes and their starting materials were determined by MTT-colorimetric assays. The MTT measurements were performed

after 72 h of drug exposure in two malignant human cell lines, MCF-7 breast cancer and HT-29 colon cancer, and a non-tumorigenic breast cell line, MCF-10A[40,41]. Their IC_{50} values listed on **Table 2.5** are compared with our two most active compounds at the present time in MCF-7 cell line, Fc-CO_2-estradiol and Fc-CO_2-Ph-4-Br[19,20]. All three starting materials 1-1'ferrocenedicarboxilic acid, ferroceneacetic acid and 4-(1H-pyrrol-1-yl)phenol showed low cytotoxic effects except 1-1'ferrocenedicarboxilic acid which is none-active in MCF-7 and MCF-10A. In MCF-7 cell line, all ferrocene derivatives showed dose dependent relationship. Two of the three ferrocene complexes, Fc-(CO_2-Ph-4-Py)$_2$ (45.5(6) μM) and Fc-(CO_2-Ph-4-Py)CO_2H (57(7) μM) showed moderate anti-proliferative activity on MCF-7 and low anti-proliferative activity non-tumorigenic human breast epithelial cell line MCF-10A. Nonetheless, their anti-proliferative activities on MCF-7 do not exceed those of Fc-CO_2-estradiol and Fc-CO_2-Ph-4-Br[19,20]. Fc-CH_2CO_2-Ph-4-Py has low activity on all cell lines, MCF-7, MCF-10A and HT-29. We should point out that none of the complexes have higher anti-proliferative activity on MCF-7 and HT-29 than Fc-CO_2-estradiol, and Fc-CO_2-Ph-4-Br.

Table 2. 5. Anti-proliferative activities of ferrocene derivatives studied on MCF-7 breast cancer, MCF-10A normal breast, and HT-29 colon cancer cell lines, as determined using MTT assay after 72 h of drug exposure.

Complex	**IC_{50} (μM), MCF-7**	**IC_{50}(μM), MCF-10A**	**IC_{50} (μM), HT-29**
Fc-(CO_2-Ph-4-Py)$_2$	45.5(6)	298(5)	189(16)
Fc-(CO_2-Ph-4-Py)CO_2H	57(7)	219(21)	121(8)
Fc-CH_2CO_2-Ph-4-Py	103(6)	288(57)	283(11)
Fc-CO_2-estradiol	9(2)[19]	119(8)	24.4(6)[19]
Fc-CO_2-Ph-4-Br[20]	9.2(8)	353(8)	24(6)
1,1´-ferrocenedicarboxilic acid	N/A	N/A	410(21)
Ferroceneacetic acid	590(25)	86(7)	253(10)
4-(1H-pyrrol-1yl)phenol	249(5)	553(76)	211(44)
Ferricenium tetrafluoroborate[19]	150		180

IC_{50} values based on quadruplicate experiments and standard deviation in parenthesis. N/A is non-active.

2.3.5 Cytokinesis-block micronucleus assay

The cytokinesis block micronucleus assay (CBMN) is a well-established technique used to measure the DNA damage on human or mammalian cells, measuring the quantity of binucleated cells with micronuclei (MNi)[33,33,36]. A micronuclei (MNi) is formed by whole chromosomes or chromosome fragments that result from DNA breakage during anaphase

nuclear division and expressed just before cytokinesis[34–39]. The cytokinesis is the final step in the mitosis represented on **Figure 2.14.** In the CBMN assay, divided cells are the one that can express MNi and are recognized by their binucleated appearance[34,36,38]. Different mechanism of DNA damage may induce micronuclei-forming activity. For example, the estrogens produces metabolites which may involve DNA adduct formation and free radical by redox cycling of estrogens through microsomal, mitochondrial or nuclear processes[43–46]. For ferrocene derivatives, DNA damage may be caused by oxygen free radical species, inducing oxidative damage to the DNA. Those radical species oxidize the guanine to oxo-guanine resulting in DNA fragmentation[18–20,30,31,34]. The DNA fragments results in micronucleated cells during anaphase cell stage.

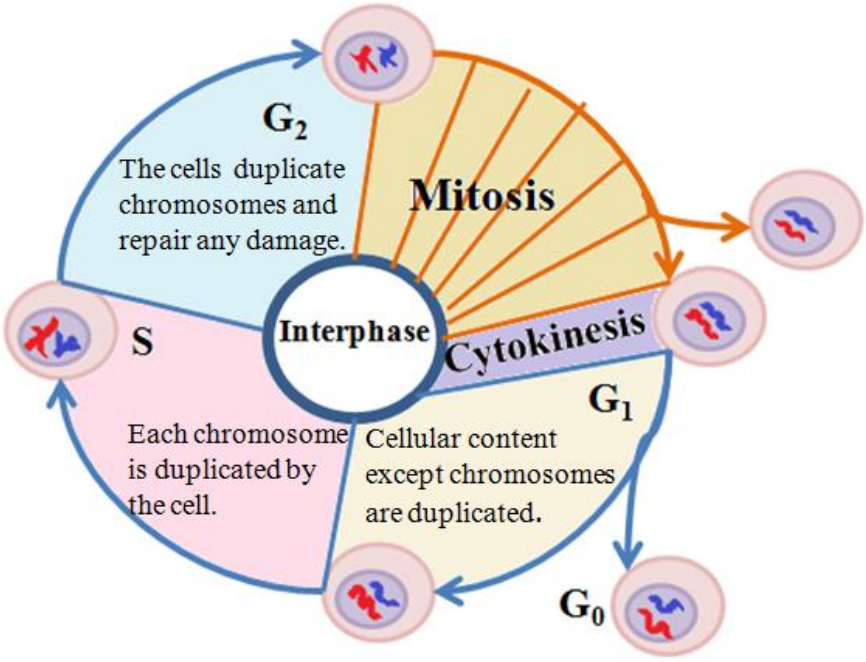

Figure 2. 15.Schematic representation of the cell cycle. Cytokinesis is the final step of the mitosis.

The level of DNA damage caused by the three new ferrocenes and Fc-CO_2-estradiol was studied on MCF-7 cells using cytokinesis-block micronucleus (CBMN) assay. The genotoxic effects of, Fc-(CO_2-Ph-4-Py)CO_2H, Fc-CH_2CO_2-Ph-4-Py, and Fc-(CO_2-Ph-4-Py)$_2$ were studied after 72 h of treatment with these compounds. Micronuclei were scored in 500 binucleated MCF-7 cells as micronucleated binucleated cells. **Figure 2.15** presents the photomicrographs of the MCF-7 cells in the CBMN assay without the presence of the drugs to demonstrate the appearance of mononucleated cell, binucleated cell and binucleated cell containing one micronucleus.

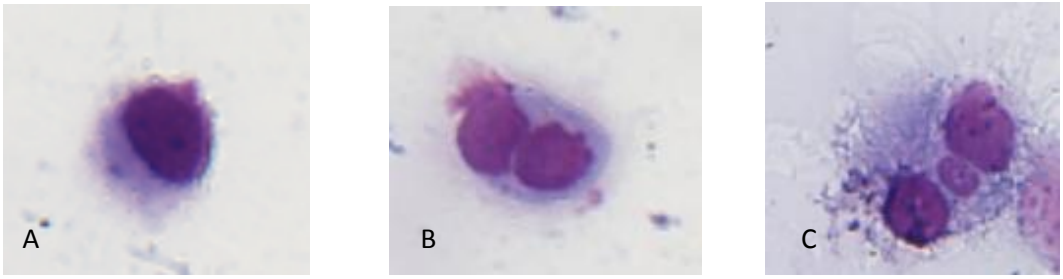

Figure 2. 16. Photomicrographs of the MCF 7 cells scored in the CBMN assay taken with an electronic microscope Olympus BX60. A) Mononucleated cell; B) binucleated cell; C) binucleated cell containing one micronucleus. All cells were treated with 6 µg/mL Cytochalasin-ß for 24 hours.

The concentrations of each ferrocene complex were selected below IC_{50} values of the corresponding ferrocene. For Fc-CO_2-estradiol with an IC_{50} of 9(2) µM the concentrations selected were 1µM, 0.1µM, and 0.01µM. For Fc-(CO_2-Ph-4-Py)$_2$, Fc-(CO_2-Ph-4-Py)CO_2H, and Fc-CH_2CO_2-Ph-4-Py with IC_{50} values between 45 to 103 µM, the concentrations were 10 µM, 1µM, and 0.1µM. The induction of micronucleus forming activity was characterized by an increase in the number of binucleated cells containing one micronucleus relative to untreated cells. A positive control was selected to verify the effectiveness of the method. Methyl methane sulphonate (MMS) was selected as positive control due to its well-known genotoxic activity[30]. After drug exposure time, the cells were

treated with cytochalasin-β, an inhibitor of the cytokinetic stage during the cell mitosis. The micronucleus formation can only be expressed in divided cells during the anaphase. Mononucleated, binucleated and micronucleated binucleated scored cells after 24 h of cytochalasin-β addition are represented in **Figure 2.15**. Micronucleus formation in binucleated cells is associated to the genotoxic effect of the complex under study.

Figure 2.16 shows the micronuclei-forming activity of the ferrocene complexes as total micronucleated binucleated MCF-7 cells in 500 scored cells. The micronucleus-forming activity of each complex was evaluated as the fold increases in the number of micronucleated binucleated cells of each concentration over the number of micronucleated binucleated cells of the untreated cells. A statistical student's t-test was used to evaluate the significance of the results compared with the control.

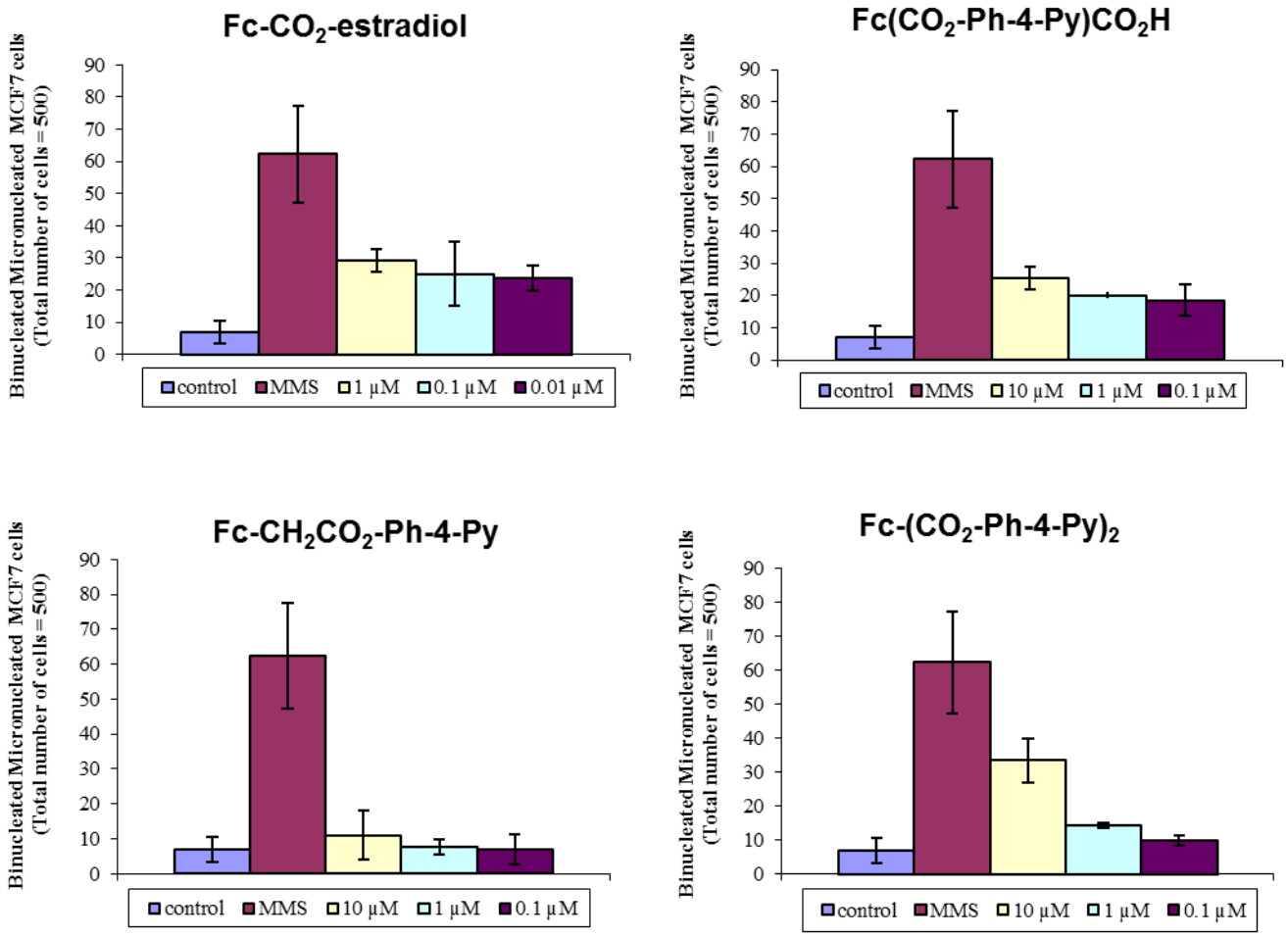

Figure 2. 17 Micronucleus forming activity of Fc-CO_2-estradiol, Fc-(CO_2-Ph-4-Py)CO_2H, Fc-CH_2CO_2-Ph-4-Py and Fc-(CO_2-Ph-4-Py)$_2$ on MCF-7 cells (mean ± SD).

Induction of single micronucleus formation in binucleated cells was found for Fc-CO_2-estradiol, Fc-(CO_2-Ph-4-Py)CO_2H, and Fc-(CO_2-Ph-4-Py)$_2$. Binucleated cells with more than one micronucleus were not significantly formed. Fc-CO_2-estradiol at concentrations of 1μM (mean 29, $P < 0.0001$) and 0.1μM (mean 25, $P < 0.01$) and Fc-(CO_2-Ph-4-Py)CO_2H at a concentration of 10 μM (mean 25.5, $P < 0.01$) showed a 4-fold increase in micronucleus forming activity compared to the control experiment (untreated cells). At a concentration of 0.01μM (mean 24, $P < 0.0004$) Fc-CO_2-estradiol has a 3-fold increase in micronucleus forming activity while Fc-(CO_2-Ph-4-Py)CO_2H shows similar micronuclei-forming activity for the two lower concentrations (1μM (mean 20, $P < 0.01$), and 0.1μM (mean 18.5, $P < 0.03$)). Fc-(CO_2-Ph-4-Py)$_2$ exhibits higher micronucleus forming activity than Fc-CO_2-estradiol and Fc-(CO_2-Ph-4-Py)CO_2H at a concentration of 10 μM (up to 5-fold, mean 33.5, $P < 0.05$) meanwhile, at 0.1μM Fc-(CO_2-Ph-4-Py)$_2$ has no significant (mean 10, $P < 0.1$) increase in micronucleus forming activity compared to our control experiment. Fc-CH_2CO_2-Ph-4-Py has no significant ($P < 1$) micronucleus forming activity at any concentration.

The increase in micronucleus-forming activity with concentration suggests a direct relation of genotoxic effect with concentration. Important differences in micronucleus forming activity depending on concentrations for Fc-CO_2-estradiol, Fc-(CO_2-Ph-4-Py)CO_2H, and Fc-(CO_2-Ph-4-Py)$_2$ can be observed. For instance, a considerable increase in the number of total micronucleated binucleated cells at a concentration close to IC_{50} was observed for Fc-(CO_2-Ph-4-Py)$_2$. Likewise, Fc-CO_2-estradiol and Fc-(CO_2-Ph-4-Py)CO_2H showed similar genotoxic effect on MCF-7 cells at concentrations close to their IC_{50}. Fc-CH_2CO_2-Ph-4-Py with the lowest cytotoxicity appears to have no significant genotoxic

effect on MCF-7 cells. For Fc-CO_2-estradiol, Fc-(CO_2-Ph-4-Py)CO_2H, and Fc-(CO_2-Ph-4-Py)$_2$, the micronucleus forming activity decrease as concentration decreases suggesting a dose dependent relation. The micronucleus forming activities in Fc-CO_2-estradiol, Fc-(CO_2-Ph-4-Py)CO_2H, Fc-CH_2CO_2-Ph-4-Py, and Fc-(CO_2-Ph-4-Py)$_2$ are lower than activity for positive control (MMS) at all concentrations.

The mitotic rate effects on MCF-7 cells after 72 h treatment was also assessed with CBMN. The mitotic rate effect is presented on **Table 2.6** as percent of binucleated cells following cytokinesis block. Statistical correlation of the percent of binucleated cells and untreated cells was estimated by Student's t-test. A decrease in the mitotic rate is observed upon a treatment of MCF-7 cells with all four ferrocene complexes and the positive control (MMS), in comparison with untreated cells. However, those results reflect no significant differences ($P < 1$).

Table 2. 6. Micronucleus forming activity values of control (untreated cells), MMS, Fc-CO_2-estradiol, Fc-(CO_2-Ph-4-Py)CO_2H, Fc-CH_2CO_2-Ph-4-Py, and Fc-(CO_2-Ph-4-Py)$_2$ on MCF-7 cells (mean ± SD) after 72 h of treatment.

Ferrocene Complex	Concentrations (μM)	Micronucleus (MNi) (mean ± SD)	%Binucleated cells (Mitotic rate)
Control (untreated cells)		7 (4)	40 (15)
(MMS)	94.4	62 (6)***	28 (3)*
Fc-CO_2-estradiol	1.0	29 (4)****	34 (9)*
	0.1	25 (10)***	39 (9)*
	0.01	23 (4)****	33 (2)*
Fc-(CO_2-Ph-4-Py)$_2$	10.0	34 (6)***	25 (6)*
	1.0	15 (1)**	33 (13)*
	0.1	10 (1)**	18 (7)*
Fc-(CO_2-Ph-4-Py)CO_2H	10.0	26 (4)***	12 (2)*
	1.0	20 (1)***	16 (6)*
	0.1	19 (5)***	13 (3)*
Fc-CH_2CO_2-Ph-4-Py	10.0	11 (7)*	38 (12)*
	1.0	8 (2)*	41 (15)*
	0.1	7 (4)*	33 (21)*

Mitotic rate values represented as per cent binucleated MCF-7 cells (mean ± SD). * P < 1, ** P < 0.1, *** P < 0.05, **** P < 0.0005 (treatment versus control) as determined by Student's t-test.

The mechanistic route for Fc-CO_2-estradiol was recently elucidated. Fc-CO_2-estradiol binds to the alpha estrogen receptor, ERα, causing a conformational change acting as an antagonist.[19]. Additionally, studies with confocal microscopy revealed that Fc-CO_2-estradiol migrate through the cell and reach the nucleus after 2 h of drug exposure[18]. Once Fc-CO_2-estradiol reaches the nucleus it generates oxygen free radical species resulting in DNA fragmentation. The results for the micronucleus assay shows an increase in micronucleus-forming activity up to 4-fold at a concentration near IC_{50}. These results can be considered a moderate genotoxic effect of the Fc-CO_2-estradiol on MCF-7 cells. Meanwhile, studies reported by Yared *et al*.[43] using β-estradiol on MCF-7 cells show a 3-fold increase in the micronucleus-forming activity. The differences in activity of Fc-CO_2-estradiol and β-estradiol can be attributed to the redox activity ferrocenoyl group.

Fc-(CO_2-Ph-4-Py)CO_2H, Fc-(CO_2-Ph-4-Py)$_2$, and Fc-CH_2CO_2-Ph-4-Py showed important differences in the anti-proliferative activity and genotoxicity. Fc-(CO_2-Ph-4-Py)CO_2H with a pyrrole group and a carboxylic group is less cytotoxic than Fc-(CO_2-Ph-4-Py)$_2$. Both Fc-(CO_2-Ph-4-Py)CO_2H and Fc-(CO_2-Ph-4-Py)$_2$ are the one with higher oxidation potentials than ferrocene. Fc-(CO_2-Ph-4-Py)CO_2H present up to 4-fold increase in micronucleus-forming activity close to IC_{50} while Fc-(CO_2-Ph-4-Py)$_2$ shows up to 5-fold increase. The difference in micronucleus activity of these two ferrocene complexes may be attributed to the number of pyrrole groups attached to the Cp rings. This pendant group, 4-(1H-pyrrol-1-yl)phenol, exhibit a oxidation potential close to 1.6 V providing an additional redox center which could induce redox processes (oxidative stress) in the cell and enhancing the cytotoxic activity. In addition, 4-(1H-pyrrol-1-yl)phenol, could enhance the permeability of the ferrocene complex through the cell[23]. In contrast, Fc-CH_2CO_2-Ph-4-Py

which possess a CH_2 between the Cp ring and the pendant group, and unsubstituted Cp ring exhibit the lower cytotoxicity, and lower genotoxic effect. This ferrocene derivative has an oxidation potential similar to ferrocene and shows slightly damage to DNA. As a result, it exhibits a mild reduction on mitotic rate compared to the untreated cells due to its low cytotoxicity.

Recently our laboratory reports a series of ferrocene derivatives using phenol pendant groups with various substituents on the 4-position (Fc-CO_2-Ph-4-X, X = F, Cl, Br, I, pyrrole)[20]. *In vitro* studies on MCF-7 combined with docking studies on the ERα revealed that their anti-proliferative activities are not associated to the anti-estrogenic properties of the ferrocene but rather to the cytotoxic activity of the metallocene unit[20]. Noteworthy, the binding affinity of Fc-CO_2-Ph-4-Py in the ERα is lower than for the Fc-CO_2-Ph-4-X (X = F, Cl, Br, I) complexes[20]. Additionally, Fc-CO_2-Ph-4-Py has high anti-proliferative activity on hormone-dependent breast cancer cell line MCF-7, but it also has high anti-proliferative activity on non-tumorigenic human breast epithelial cell line MCF-10A. Thus, ERα is not responsible for the anti-proliferative activity of Fc-CO_2-Ph-4-Py.

2.3.6. Measurements of reactive oxygenated species (ROS)

Measurements of reactive oxygen species (ROS) induction assay were performed on MCF-7 to prove the relation of the cytotoxic and genotoxic effect of the ferrocenoyl derivatives: Fc-CO_2-estradiol, Fc-(CO_2-Ph-4-Py)CO_2H, Fc-(CO_2-Ph-4-Py)$_2$, and Fc-CH_2CO_2-Ph-4-Py (**Figure 2.17**). Fc-CO_2-estradiol and Fc-(CO_2-Ph-4-Py)$_2$ the ones with the higher genotoxic activity shows significant increase in ROS production with concentration. Those results suggest a direct correlation between concentration and ROS production and a

significant increase around 1000 µM. The amount of ROS formation by Fc-CO_2-estradiol and Fc-(CO_2-Ph-4-Py)$_2$ are similar to ferrocene ($FeCp_2$) but lower than ferrocenium ($[FeCp_2]BF_4$) as reported by Acevedo et al[29]. Although these results suggest that the genotoxic activities of Fc-CO_2-estradiol and Fc-(CO_2-Ph-4-Py)$_2$ are likely correlated to the ROS formation, other possible mechanisms cannot be ruled out. Along this line, the ROS formation of Fc-(CO_2-Ph-4-Py)CO_2H is the lowest, but the IC_{50} is comparable to Fc-(CO_2-Ph-4-Py)$_2$. Meanwhile, the ROS production for Fc-CH_2CO_2-Ph-4-Py, is low in comparison with $FcCp_2$[29] and it has no relationship to concentrations. However, this last result was expected considering the low cytotoxic effect and micronucleus forming activity of Fc-CH_2CO_2-Ph-4-Py. The results of ROS induction assay agree with the genotoxic and cytotoxic findings.

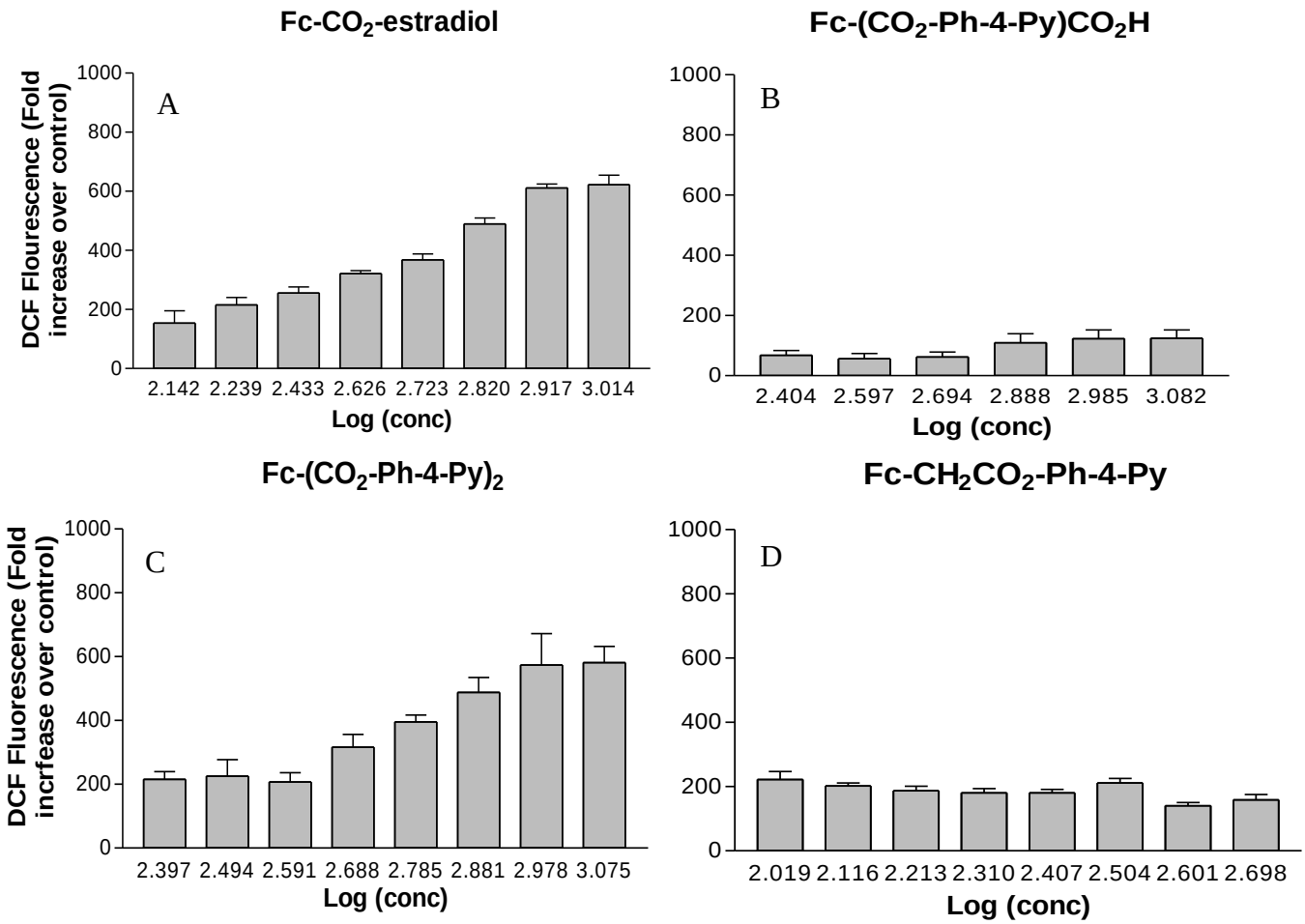

Figure 2. 18. ROS production induced by (A)Fc-CO_2-estradiol, (B) Fc-(CO_2-Ph-4-Py)CO_2H, (C) Fc-(CO_2-Ph-4-Py)$_2$, and (D) Fc-CH_2CO_2-Ph-4-Py generated on MCF-7 at 72 h.

2.4 Concluding Remarks

The antiproliferative and genotoxic activity of three new functionalized ferrocenes with 4-(1H-pyrrol-1-yl)phenol as pendant group and Fc-CO_2-estradiol was assessed in order to determine the influence of the redox active pendant groups on ferrocene on breast cancer cell line. The cytotoxic activity was evaluated on MCF-7, MCF-10A and HT-29 cells using a colorimetric MTT assay. The new ferrocene synthesized Fc-(CO_2-Ph-4-Py)$_2$ displayed moderate cytotoxic activity on MCF-7 nonetheless its activity does not exceed the previously reported Fc-CO_2-estradiol and Fc-CO_2-Ph-4-Br which both have IC_{50} values of 9.2 μM.

The genotoxic activity on MCF-7 of Fc-(CO_2-Ph-4-Py)$_2$, Fc-(CO_2-Ph-4-Py)CO_2H, Fc-CH_2CO_2-Ph-4-Py, and Fc-CO_2-estradiol was evaluated using the cytokinesis-block micronucleus assay and ROS induction assay to measure the amount of DNA damage (genotoxic effects). These results were compared with the electrochemical data to establish a correlation between the redox potential with the ROS induction and the micronucleus forming activity. **Table 2.7** summarizes the results obtained from electrochemical data, cytotoxic and genotoxic experiments for the three new ferrocenes and Fc-CO_2-estradiol. First, in comparison to Fc-CO_2-estradiol and Fc-CO_2-Ph-4-Br which both have IC_{50} values of 9.2 μM but different redox potentials (756 and 532 mV respectively), we observe similar trends among the three new ferrocene-pyrrole complexes. That is, there is no correlation between the anti-proliferative activity of the new ferrocenes and their redox potentials. Second, Fc-CO_2-estradiol has the higher micronucleus-forming activity on MCF-7 cell line followed by Fc-(CO_2-Ph-4-Py)$_2$ > Fc-(CO_2-Ph-4-Py)CO_2H > Fc-CH_2CO_2-Ph-4-Py. This trend is correlated to their IC_{50} values. The ROS production assay confirmed the genotoxic

activity of Fc-CO_2-estradiol and Fc-(CO_2-Ph-4-Py)$_2$ due to reactive oxygen species formation.

Table 2. 7 Summary of the oxidation potentials, IC50 values, micronucleus forming activity and reactive oxygen species induction results of MCF-7 cells.

Ferrocene Complexes	**E_{pa}, (mV)**	**IC_{50} (µM) MCF-7**	**MNi**	**ROS**
Fc-(CO_2-Ph-4-Py)$_2$	958	45.5(6)	34(6)	High
Fc-(CO_2-Ph-4-Py)CO_2H	1027	57(7)	26(4)	Low
Fc-CH_2CO_2-Ph-4-Py	503	103(6)	11(7)	Low
Fc-CO_2-estradiol	801	9(2)*	29(4)	High

Thus, this study provides evidence that the pendant groups have influence in the anti-proliferative activity and in less degree to the DNA damage on MCF-7 breast cancer cell line. However, the anti-estrogenic effects of Fc-CO_2-estradiol and analogous ferrocenes functionalized with phenols in the alpha estrogen receptor (ERα) revealed that Fc-CO_2-estradiol acts as an antagonist whereas the analogous ferrocenes not[19,20]. Comparing these results with our complexes we can suggest that the genotoxic effects of these new functionalized ferrocene complexes come mainly from the ferrocene moiety and not from the anti-estrogenic effects.

2.5 References

(1) Miller, S. A.; Tebboth, J. A.; Tremaine, J. F. 114. Dicyclopentadienyliron. *J. Chem. Soc. Resumed* **1952**, 632.

(2) Atkinson, R. C. J.; Gibson, V. C.; Long, N. J. The Syntheses and Catalytic Applications of Unsymmetrical Ferrocene Ligands. *Chem. Soc. Rev.* **2004**, *33*, 313.

(3) Kealy, T. J.; Pauson, P. L. A New Type of Organo-Iron Compound. *Nature* **1951**, *168*, 1039–1040.

(4) Köpf-Maier, P.; Köpf, H.; Neuse, E. W. Ferricenium Complexes: A New Type of Water-Soluble Antitumor Agent. *J. Cancer Res. Clin. Oncol.* **1984**, *108*, 336–340.

(5) Togni, A. *Ferrocenes: Homogeneous Catalysis, Organic Synthesis, Materials Science*; John Wiley & Sons, 2008.

(6) Gómez Arrayás, R.; Adrio, J.; Carretero, J. C. Recent Applications of Chiral Ferrocene Ligands in Asymmetric Catalysis. *Angew. Chem. Int. Ed.* **2006**, *45*, 7674–7715.

(7) Togni, A.; Hayashi, T. *Ferrocenes: Homogeneous Catalysis, Organic Synthesis, Materials Science*; VCH Publishers: Weinheim; New York, 1995.

(8) Braga, S. S.; Silva, A. M. S. A New Age for Iron: Antitumoral Ferrocenes. *Organometallics* **2013**, *32*, 5626–5639.

(9) Gasser, G.; Ott, I.; Metzler-Nolte, N. Organometallic Anticancer Compounds. *J. Med. Chem.* **2011**, *54*, 3–25.

(10) *Medicinal Organometallic Chemistry*; Jaouen, G.; Metzler-Nolte, N.; Alberto, R., Eds.; Topics in organometallic chemistry; Springer-Verlag: Heidelberg ; New York, 2010.

(11) Fouda, M. F. R.; Abd-Elzaher, M. M.; Abdelsamaia, R. A.; Labib, A. A. On the Medicinal Chemistry of Ferrocene. *Appl. Organomet. Chem.* **2007**, *21*, 613–625.

(12) Jaouen, G. *Bioorganometallics: Biomolecules, Labeling, Medicine*; John Wiley & Sons, 2006.

(13) Van Staveren, D. R.; Metzler-Nolte, N. Bioorganometallic Chemistry of Ferrocene. *Chem. Rev.* **2004**, *104*, 5931–5986.

(14) Nguyen, A.; Top, S.; Pigeon, P.; Vessières, A.; Hillard, E. A.; Plamont, M.-A.; Huché, M.; Rigamonti, C.; Jaouen, G. Synthesis and Structure-Activity Relationships of Ferrocenyl Tamoxifen Derivatives with Modified Side Chains. *Chem. - Eur. J.* **2009**, *15*, 684–696.

(15) Top, S.; Vessières, A.; Leclercq, G.; Quivy, J.; Tang, J.; Vaissermann, J.; Huché, M.; Jaouen, G. Synthesis, Biochemical Properties and Molecular Modelling Studies of Organometallic Specific Estrogen Receptor Modulators (SERMs), the Ferrocifens and Hydroxyferrocifens: Evidence for an Antiproliferative Effect of Hydroxyferrocifens on Both Hormone-Dependent and Hormone-Independent Breast Cancer Cell Lines. *Chem. - Eur. J.* **2003**, *9*, 5223–5236.

(16) Vessières, A.; Top, S.; Beck, W.; Hillard, E.; Jaouen, G. Metal Complex SERMs (selective Oestrogen Receptor Modulators). The Influence of Different Metal Units on Breast Cancer Cell Antiproliferative Effects. *Dalton Trans.* **2006**, 529.

(17) Vessières, A.; Top, S.; Pigeon, P.; Hillard, E.; Boubeker, L.; Spera, D.; Jaouen, G. Modification of the Estrogenic Properties of Diphenols by the Incorporation of Ferrocene. Generation of Antiproliferative Effects in Vitro. *J. Med. Chem.* **2005**, *48*, 3937–3940.

(18) Meléndez, E. Metallocenes as Target Specific Drugs for Cancer Treatment. *Inorganica Chim. Acta* **2012**, *393*, 36–52.

(19) Vera, J.; Gao, L. M.; Santana, A.; Matta, J.; Meléndez, E. Vectorized Ferrocenes with Estrogens and Vitamin D2: Synthesis, Cytotoxic Activity and Docking Studies. *Dalton Trans.* **2011**, *40*, 9557.

(20) Vera, J. L.; Rullán, J.; Santos, N.; Jiménez, J.; Rivera, J.; Santana, A.; Briggs, J.; Rheingold, A. L.; Matta, J.; Meléndez, E. Functionalized Ferrocenes: The Role of the Para Substituent on the Phenoxy Pendant Group. *J. Organomet. Chem.* **2014**, *749*, 204–214.

(21) Ghorab, M. M.; Alsaid, M. S.; Ceruso, M.; Nissan, Y. M.; Supuran, C. T. Carbonic Anhydrase Inhibitors: Synthesis, Molecular Docking, Cytotoxic and Inhibition of the Human Carbonic Anhydrase Isoforms I, II, IX, XII with Novel Benzenesulfonamides Incorporating Pyrrole, Pyrrolopyrimidine and Fused Pyrrolopyrimidine Moieties. *Bioorg. Med. Chem.* **2014**, *22*, 3684–3695.

(22) Abou El Ella, D. A.; Ghorab, M. M.; Noaman, E.; Heiba, H. I.; Khalil, A. I. Molecular Modeling Study and Synthesis of Novel pyrrolo[2,3-D]pyrimidines and Pyrrolotriazolopyrimidines of Expected Antitumor and Radioprotective Activities. *Bioorg. Med. Chem.* **2008**, *16*, 2391–2402.

(23) Chatzopoulou, M.; Patsilinakos, A.; Vallianatou, T.; Prnova, M. S.; Žakelj, S.; Ragno, R.; Stefek, M.; Kristl, A.; Tsantili-Kakoulidou, A.; Demopoulos, V. J. Decreasing

Acidity in a Series of Aldose Reductase Inhibitors: 2-Fluoro-4-(1H-Pyrrol-1-Yl)phenol as a Scaffold for Improved Membrane Permeation. *Bioorg. Med. Chem.* **2014**, *22*, 2194–2207.

(24) Mohamed, M. S.; Kamel, R.; Abd El-hameed, R. H. Evaluation of the Anti-Inflammatory Activity of Some pyrrolo[2,3-D]pyrimidine Derivatives. *Med. Chem. Res.* **2013**, *22*, 2244–2252.

(25) Hassan, S. M.; El-Maghraby, A. A.; Abdel Aal, M. M.; Bashandy, M. S. Heteroaromatization with Sulfonamido Phenyl Ethanone, Part I: Synthesis of Novel Pyrrolo[2,3-D]Pyrimidine and Pyrrolo[3,2-E][1,2,4]Triazolo[1,5-C]Pyrimidine Derivatives Containing Dimethylsulfonamide Moiety. *Phosphorus Sulfur Silicon Relat. Elem.* **2009**, *184*, 291–308.

(26) Esteves, M. A.; Ortet, O.; Capelo, A.; Supuran, C. T.; Marques, S. M.; Santos, M. A. New Hydroxypyrimidinone-Containing Sulfonamides as Carbonic Anhydrase Inhibitors Also Acting as MMP Inhibitors. *Bioorg. Med. Chem. Lett.* **2010**, *20*, 3623–3627.

(27) Clark, M. P.; George, K. M.; Bookland, R. G.; Chen, J.; Laughlin, S. K.; Thakur, K. D.; Lee, W.; Davis, J. R.; Cabrera, E. J.; Brugel, T. A.; et al. Development of New Pyrrolopyrimidine-Based Inhibitors of Janus Kinase 3 (JAK3). *Bioorg. Med. Chem. Lett.* **2007**, *17*, 1250–1253.

(28) Merighi, S.; Mirandola, P.; Varani, K.; Gessi, S.; Leung, E.; Baraldi, P. G.; Tabrizi, M. A.; Borea, P. A. A Glance at Adenosine Receptors: Novel Target for Antitumor Therapy. *Pharmacol. Ther.* **2003**, *100*, 31–48.

(29) Morantes, C. Y. A.-. Cytotoxicity and Reactive Oxygen Species Generated by Ferrocenium and Ferrocene on MCF7 and MCF10A Cell Lines. *J. Cancer Sci. Ther.* **2012**, *04*.

(30) Tabbì, G.; Cassino, C.; Cavigiolio, G.; Colangelo, D.; Ghiglia, A.; Viano, I.; Osella, D. Water Stability and Cytotoxic Activity Relationship of a Series of Ferrocenium Derivatives. ESR Insights on the Radical Production during the Degradation Process. *J. Med. Chem.* **2002**, *45*, 5786–5796.

(31) Osella, D.; Mahboobi, H.; Colangelo, D.; Cavigiolio, G.; Vessières, A.; Jaouen, G. FACS Analysis of Oxidative Stress Induced on Tumour Cells by SERMs. *Inorganica Chim. Acta* **2005**, *358*, 1993–1998.

(32) Kovjazin, R.; Eldar, T.; Patya, M.; Vanichkin, A.; Lander, H. M.; Novogrodsky, A. Ferrocene-Induced Lymphocyte Activation and Anti-Tumor Activity Is Mediated by Redox-Sensitive SiNGaling. *FASEB J.* **2003**, *17*, 467–469.

(33) Fenech, M. Cytokinesis-Block Micronucleus Cytome Assay. *Nat. Protoc.* **2007**, *2*, 1084–1104.

(34) Fenech, M. The in Vitro Micronucleus Technique. *Mutat. Res.* **2000**, *455*, 81–95.

(35) Fenech, M.; Morley, A. A. Measurement of Micronuclei in Lymphocytes. *Mutat. Res.* **1985**, *147*, 29–36.

(36) Fenech, M.; Morley, A. A. Cytokinesis-Block Micronucleus Method in Human Lymphocytes: Effect of in Vivo Ageing and Low Dose X-Irradiation. *Mutat. Res.* **1986**, *161*, 193–198.

(37) Heddle, J. A Rapid in Vivo Test for Chromosomal Damage☆. *Mutat. Res. Mol. Mech. Mutagen.* **1973**, *18*, 187–190.

(38) Schmid, W. The Micronucleus Test. *Mutat. Res.* **1975**, *31*, 9–15.

(39) Fenech, M.; Morley, A. Solutions to the Kinetic Problem in the Micronucleus Assay. *Cytobios* **1985**, *43*, 233–246.

(40) Denizot, F.; Lang, R. Rapid Colorimetric Assay for Cell Growth and Survival. *J. Immunol. Methods* **1986**, *89*, 271–277.

(41) Mosmann, T. Rapid Colorimetric Assay for Cellular Growth and Survival: Application to Proliferation and Cytotoxicity Assays. *J. Immunol. Methods* **1983**, *65*, 55–63.

(42) Decordier, I. Influence of Caspase Activity on Micronuclei Detection: A Possible Role for Caspase-3 in Micronucleation. *Mutagenesis* **2005**, *20*, 173–179.

(43) Yared, E.; McMillan, T. J.; Martin, F. L. Genotoxic Effects of Oestrogens in Breast Cells Detected by the Micronucleus Assay and the Comet Assay. *Mutagenesis* **2002**, *17*, 345–352.

(44) Fischer, W. H.; Keiwan, A.; Schmitt, E.; Stopper, H. Increased Formation of Micronuclei after Hormonal Stimulation of Cell Proliferation in Human Breast Cancer Cells. *Mutagenesis* **2001**, *16*, 209–212.

(45) Stopper, H.; Schmitt, E.; Gregor, C.; Mueller, S. O.; Fischer, W. H. Increased Cell Proliferation Is Associated with Genomic Instability: Elevated Micronuclei Frequencies in Estradiol-Treated Human Ovarian Cancer Cells. *Mutagenesis* **2003**, *18*, 243–247.

(46) Fleck, S. C.; Hildebrand, A. A.; Pfeiffer, E.; Metzler, M. Catechol Metabolites of Zeranol and 17β-Estradiol: A Comparative in Vitro Study on the Induction of Oxidative

DNA Damage and Methylation by Catechol-O-Methyltransferase. *Toxicol. Lett.* **2012**, *210*, 9–14.

(47) Drummond, T. G.; Hill, M. G.; Barton, J. K. Electrochemical DNA Sensors. *Nat. Biotechnol.* **2003**, *21*, 1192–1199.

(48) J.D.Dunitz, L. E. Orgel, andA. Rich, "The crystal structure of ferrocene," *Acta Cryst.* 1956, *9(4)*, 373–375.

(49) Gao, L.M.; Hernández, R.; Matta, J.; Meléndez, E. Synthesis, Structure, Electrochemistry, and Cytotoxic Properties of Ferrocenyl Ester Derivatives. Metal Based Drugs **2009**, Article ID 420784, doi:10.1155/2009/420784.

(50) L. Pauling, The Nature of the Chemical Bond, third ed. Cornell University Press, Ithaca, NewYork, 1960.

(51) Takashi Okabe, Keisuke Nakazaki, Tsuyoshi Igaue, Naotake Nakamura, Bertrand Donnio, Daniel Guillon and Jean-Louis Gallani. Synthesis and physical properties of ferrocene derivatives. XXI. Crystal structure of a liquid crystalline ferrocene derivative,1,1'-bis[3-[4-(4-methoxyphenoxycarbonyl)phenoxy]propyloxycarbonyl] ferrocene. *J. Appl. Cryst*. **2009**. *42*, 63–68.

(52)Antonio Togni, Markus Hobi, Grety Rihs, Gunther Rist, Albert Albinati, Piero Zanello, Damian Zech, and Hugo Keller. 1,l'-Disubstituted Ferrocenes as Donors for Charge-Transfer Complexes. Synthesis, Structure, Conductivity, and Magnetic Properties. *Organometallics* **1994**,*13*, 1224-1234

(53) Francois Gelin and Randolph P. Thummel. Structural Features of 1,l'-Bis(azaary1)-Substituted Ferrocenes. *J. Org. Chem.* **1992,**57*(14).*

Chapter III

Nanostructured gold dsDNA sensor for early detection of breast cancer by beta protein 1 (BP_1)

3.1 Introduction

Breast cancer is the second leading cause of death in women after lung cancer. According to the American Cancer Society over 232,670 new cases of invasive breast cancer will be diagnosed in the United States in 2014. Meanwhile 2,360 new cases of invasive breast cancer will be diagnosed in men during 2014. The principal incidence of breast cancer is related to estrogen receptor-positive (ER+) breast cancer while estrogen receptor-negative (ER-) breast cancer is less diagnosed[1]. According to a statistical study, about 90% of the breast cancer patients diagnosed with carcinoma in stage 0 will survive[2]. During the past decade researchers focus their attention to find different biomarkers for early detection of breast cancer. In 2002, Sidney et al. reports the correlation of the expression of beta protein 1 (BP_1, a homeobox gene), and estrogen receptor in breast cancer cells[3]. BP_1 was first expressed in leukemia and found to play an important role in oncogenic pathway[4]. However, BP_1 has a remarkably expression of 100% in estrogen receptor negative tumors and 73% expression in estrogen receptor positive tumors[3,5,6]. Estrogen receptor negative breast tumors are more invasive and typically have poor diagnosis in comparison to the ER+ tumors. Meanwhile, lack of BP_1 expression was found in ER- normal breast cells and low-level expression in ER+ normal breast cells. In addition, frequent expression of BP_1 was also found in all tumor grades. Therefore this protein is a perfect biomarker for early detection of breast cancer[3,5,6].

Nanostructured gold (NG) sensors are commonly used to develop sensitive electrochemical detection of different analytes due to its conductivity, large surface area, and high stability[7-10]. Most NG sensors are modified with DNA to characterize the binding event of the analyte through DNA electrochemical charge transport[11-16]. DNA, a biorecognition element, is anchored in the surface functioning as a transducer[11,12]. A series of conjugated charge donors or acceptors are employed as redox active probes interacting by π-stacked base pairs in DNA to monitor the electrochemical binding event[14,17-24].

In this research, an electrochemical NG sensor was modified with the BP_1 genomic sequence DNA[3,5,6] containing a thiol C_6 linker. Methylene blue (MB) was used as redox-active probe intercalated to DNA by non-covalent interactions with the π-stacked base pairs. BP_1 binging event was characterized by monitoring the redox cycle of MB with different concentrations of BP_1. This NG biosensor provides a new sensitive tool for early detection of breast cancer. Thus, this work proposes for the first time (1) the detection of a clinically-relevant transcription factor biomarker, (2) the electrochemical detection of a transcription factor using a double-stranded DNA probe on a nanostructured gold electrode, and (3) a detection limit of 1.2 nM.

3.2 Experimental Section

3.2.1 Materials

SRS Quartz crystal microbalance (QCM) Ti/Au, 5MHz electrode used were purchased from Stanford Research Systems. Methylene blue 82%, 6-mercapto-1-hexanol (MCH) 97%, and tris(hydroxymethyl)-aminomethane 99.9% were obtained from Sigma-Aldrich. The DNA sequences containing the BP_1 binding motif ATATATATG were the

following: Forward 5'-TTAAAAAGATATATATATATGTTTTTCTAATGT-3', (modified with 5'end thiol C_6 linker) and reverse 5'-ACATTAGAAAAACATATATAT-ATATCTTTT-TAA-3'[5,6]. The following sequences without the BP_1 binding sequence where used as the dsDNA negative control (Forward: 5'-TCTTAGAGGGAGGGCTGAGGGTTTGAAGTCCAACTCCTAAGCC-3'; Reverse: 5'-AGAATCTCCCTCCCGACTCCCAAACTTCAGGTTGAGGATTCGG-3')[5]. All DNA probes were obtained from Eurofins Genomics and the BP_1 protein was obtained from Gen Way and used as received. Deionized water (18.2 MΩ) was used for all experiments.

3.2.2 Equipment

CP-II VEECO atomic force microscope (AFM) with scanning probe microscopy and lateral force microscopy and nanomanipulation capabilities with 100 _ 100 lm scanning area capacity is used to characterize the surface morphology. Scanning electron microscopy (SEM) is used to characterize the surface morphology of the nanostructured electrode using a Field Emission Scanning Electron Microscope Supra 35 (Zeiss). The equipment allows analysis of features in the nanometer range using low accelerating voltage (3kV). Electrochemical experiments were carried on an Epsilon Potentiostat/Galvanostat (Bioanalytical Systems, Inc.) using a specially designed three-electrode electrochemical cell having gold as working electrode, a platinum wire as counter (auxiliary) and Ag/AgCl paste covered wire as reference electrode.

3.2.3 Synthesis and characterization of gold nanoparticles

The gold electrode surface was polished prior to use with 0.5 µm alumina for 3 minutes and then cleaned in an ultrasonic bath with ethanol and deionized water for 5 minutes. The gold electrode is then electrochemically cleaned by cyclic voltammetry (CV) in 0.5 M sulfuric acid at 100 mVs^{-1} scan rate, between -0.35 to 1.5 V until no changes in voltamograms. After electrochemical cleaning of the gold electrode, the thick hydrous gold oxide layer accumulated on the gold electrode was removed in 0.5 M sulfuric acid by using repetitive square-wave voltammetry (SWV), with a potential range between −0.8 V and 2.5 V (versus silver/silver chloride electrode) at 2,000 Hz for 5 minutes. In the following step, the potential is held at -0.8 V until complete electro-reduction of the hydrous gold oxide layer is accomplished. The NG surface was characterized by cyclic voltametry in 0.5 H_2SO_4 between -0.35 to 1.5 V (versus silver/silver chloride electrode) at 100 mVs^{-1}. After synthesis of gold nanoparticles, the gold reduction peak current at 0.942 V increases considerably. SEM was used to characterize the surface morphology of the nanostructured electrode. In addition, atomic force microscopy (AFM) was used to measure the surface topography.

3.2.4 Immobilization of dsDNA onto Nanostructured gold sensor.

The BP_1 binding sequence oligonucleotides were resuspended in an annealing buffer consisting of 10 mM Tris, pH 7.5, 50 mM NaCl, 1 mM EDTA. Equimolar concentrations of the forward and reversed oligonucleotides were annealed at 94^{o}C for 4 minutes and then cooled at room temperature for 40 minutes. The resulting dsDNA was self-assembled into the NG surface for 18-24 h. After dsDNA addition to the NG surface, it

was exposed to a solution of 1.0 mM mercaptohexanol (MCH) for 1 h (**Figure 3.1**) to allow for surface passivation[37]. The co-adsorption of MCH onto DNA-modified gold surface removes the weakly, unspecifically adsorbed nucleic acids by forming a dense MCH sublayer. DNA sensor was then immersed in a solution on 20 µM MB for 20 minutes to intercalate it as redox-active probe[25,26]. Characterization of dsDNA and its binding to the NG surface were performed using CV to monitor changes in MB redox cycle. The CV experiments were performed between -0.450 to 0 V at 100 mVs^{-1} in 20 mM Tris, 100 mM NaCl, pH 7.5, at room temperature under an inert atmosphere. A three-compartment electrochemical cell is used with a Pt wire auxiliary electrode, silver/silver chloride electrode as reference, and a 0.02 cm^2 NG working electrode.

3.2.5 Electrochemical characterization of DNA-binding event of BP_1

The BP_1 binding event was characterized by CV between -0.450 to 0 V (vs. Ag/AgCl) in 20 mM Tris, 100 mM NaCl, 20 µM MB, pH 7.5 at 100 mVs^{-1}, using silver/silver chloride as reference, Pt wire as supporting electrode and NG/dsDNA/MCH as the working electrode. A stock solution of BP_1 was prepared dissolving 0.01 mg of the protein in buffer. For the binding event characterization, the redox cycle current of MB was monitored with different dilutions of the BP_1 stock solution (5.30 to 33.78 nM). Regeneration of the NG/dsDNA/MCH sensor was performed by a simple rinse in deionized water. Square wave voltametry (SWV) was also performed after regeneration to confirm the BP_1 binding event. This was carried out in 20 mM Tris, 100 mM NaCl, 20 µM MB, pH 7.5 from -0.6 to 0 V (vs. Ag/AgCl) at 600 Hz with an amplitude of 25 mV and a step size of 1 mV. It should be mentioned that both, CV and SWV can be used to monitor and quantify the BP_1 binding.

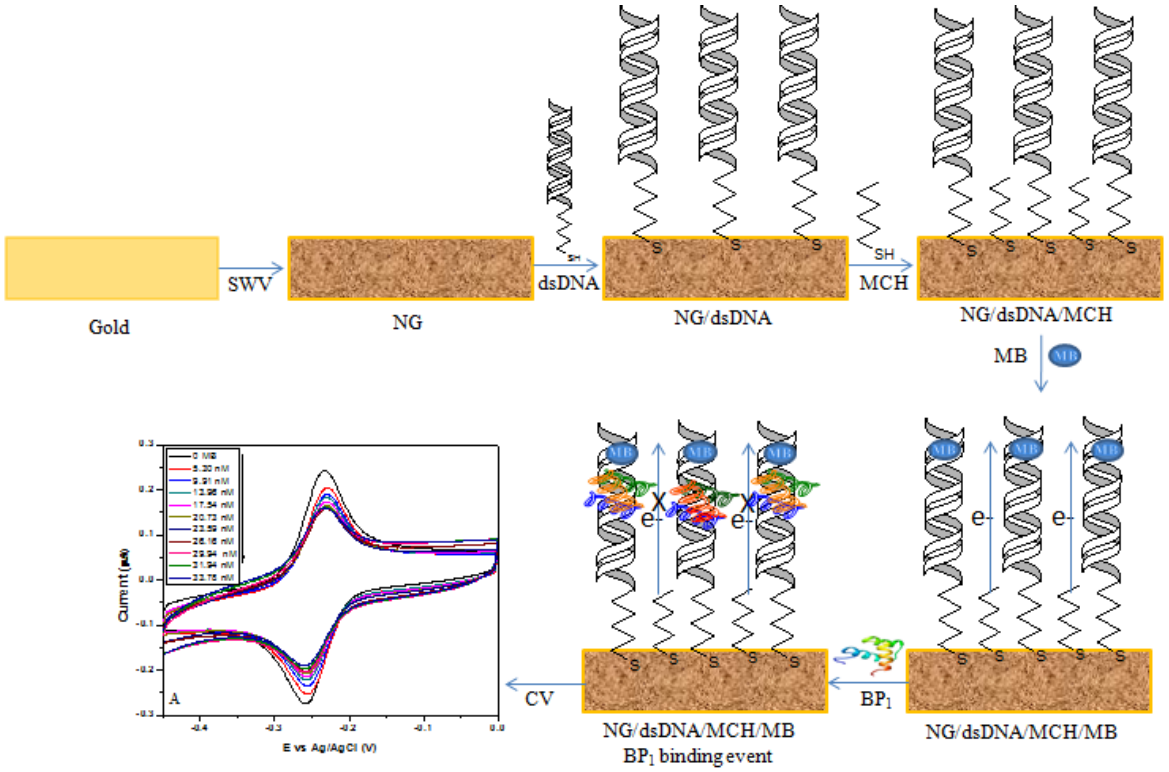

Figure 3. 1. Schematic representation of NG/dsDNA/MB sensor construction.

3.3. Results and discussion

3.3.1 Synthesis and Characterization of gold nanostructures

The gold sensor was nanostructured by a modified procedure[7] using square wave voltametry in 0.5 M H_2SO_4 at 2,000 Hz for five minutes followed by electro-reduction at a fixed potential of -800 V. **Figure 3.2** shows the cyclic voltammograms (CV) in 0.5 M H_2SO_4 at 100 mVs^{-1} of the gold electrode before electroreduction (black) and after electroreduction (red). The CV of the clean gold electrode display two oxidation peaks for the formation of gold oxides at 1.09 and 1.27 V and a reduction peak at 0.95 V[19]. When the process of electroreduction is finished, the current of gold reduction peak at 0.95 V increase

about 18 µA compared to the non-nanostructured gold electrode. The increase in reduction current of the gold reduction peak indicates the formation of gold nanostructures. Those results are related to the formation of the NG which has large surface area and greater conductivity[19].

The NG surface topography was measured by AFM, represented in **Figure 3.3**. The gold surface topography before electro-reduction (**Figure 3.3 A**) shows a smooth surface topography with an average roughness of 2.089 nm while the NG electrode surface (**Figure 3.3 B**) has a rough appearance with an average roughness of 7.202 nm. The increase in average roughness is consistent with the changes in surface area due to gold nanostructures formation. SEM images of clean gold electrode (**Figure 3.3 C**) shows gold particles with a uniform size while the SEM images of NG (**Figure 3.3 D**) shows small grains and a brain like particles as reported in literature[19].

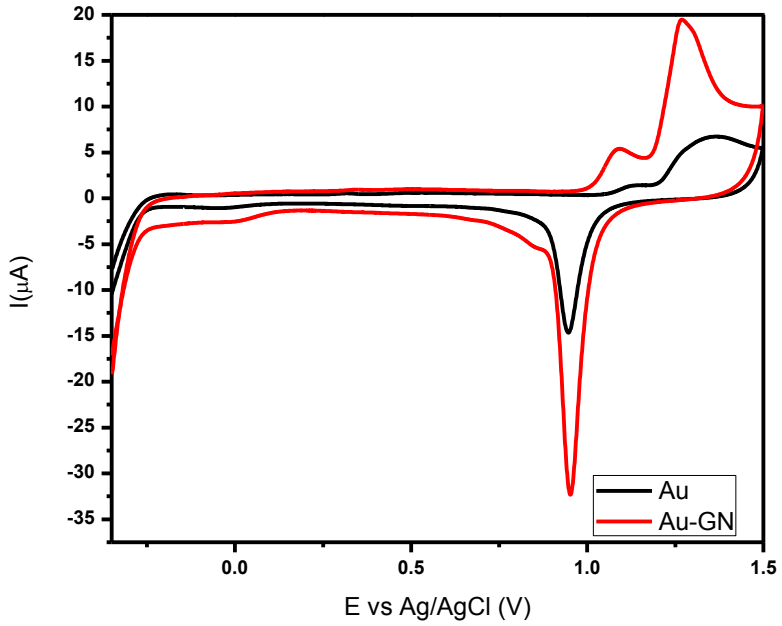

Figure 3. 2. Cyclic voltamograms of clean gold electrode (black) and nanostructured gold electrode (red) performed in 0.5 M H_2SO_4 at a scan rate of 100 mVs^{-1}.

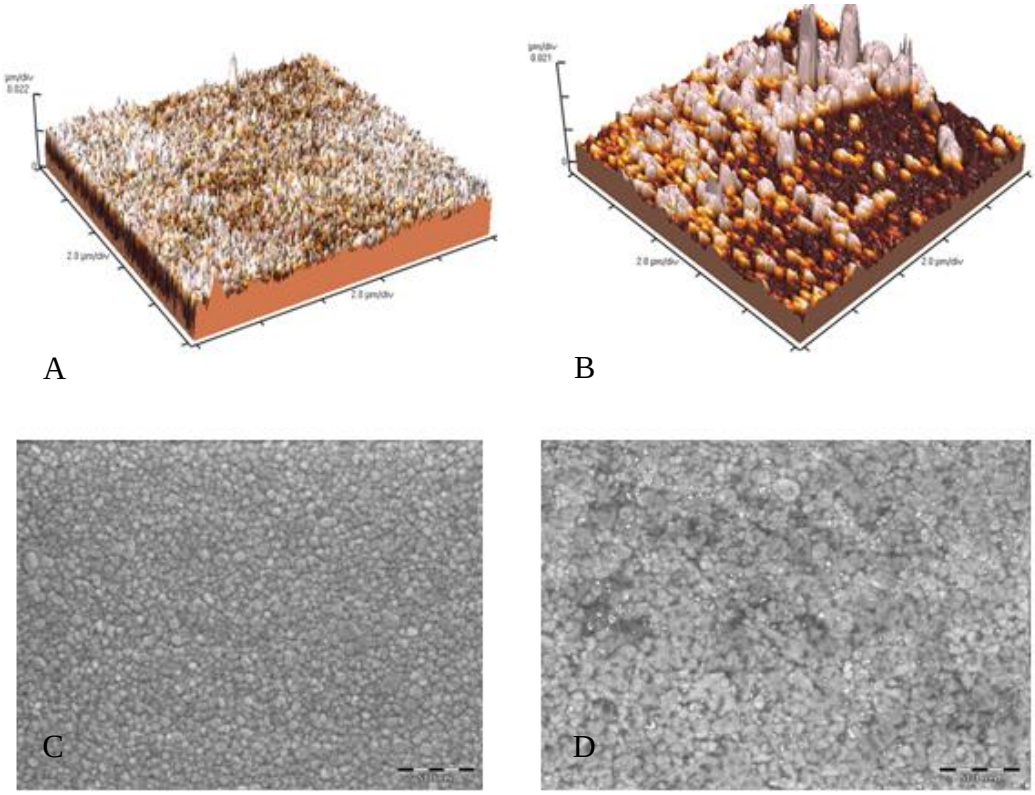

Figure 3. 3. A) AFM image of clean gold electrode, B) AFM image of gold nanostructed electrode, C) SEM image of clean gold electrode, and D) SEM image of NG electrode.

3.3.2 Immobilization of dsDNA onto Nanostructured gold sensor

DNA oligonucleotide with the BP_1 binding sequence were first annealed by mixing them in equimolar concentrations on a thermostatic bath at 95 ^{o}C for 4 min, and cooled to room temperature for 40 min. Subsequently, the annealed oligo duplex was exposed in contact with NG electrode[14,17]. The forward strand of the BP_1 DNA is modified with a thiol terminal which has strong affinity for gold. The annealed oligo duplex is adsorbed on the nanostructured gold surface due to its thiol C_6 linker. The dsDNA nanostructured gold surface is then exposed to MCH to passivate the surface. The MCH is introduced into the uncovered gold surface to avoid interactions of the analyte with the sensor surface. Hereby, the protein only can interact with the dsDNA attached to the gold surface and not directly with the gold surface. After this process, the redox-active probe (MB) is incorporated on the system through intercalation into the dsDNA.

The presence of the dsDNA self assembled into the gold electrode was confirmed by cyclic voltammetry of the redox-active probe intercalated into the dsDNA (**Figure 3.4**). **Figure 3.4 A** shows the CV of MB using the NG electrode (blue). The MB has an anodic peak in -0.188 V, when it is intercalated onto the dsDNA attached to the NG electrode, the anodic peak potential was shifted to -0.253 V (**Figure 3.4 A**, pink). The anodic peak potential shift of the MB is due to the intercalation into dsDNA. An increase in anodic peak current was also observed due to the DNA electron charge transport.

Hybridization of the oligos was verified to detect any mismatch in the double strand formation (**Figure 3.5**). The mismatch was detected through reduction of MB in presence of potassium ferricyanide. The current flows through the well-stacked DNA transferring one electron to the MB intercalated to it. The MB is then reduced to produce

leucomethylene blue (LB) who reduces ferricyanide to reoxidize MB[26,27]. The electro-reduction cycle results in amplification of the MB signal. Meanwhile, if the dsDNA have any mismatch, the MB reduction to LB does not occur resulting in a decrease in the oxidation current of MB[11,13].

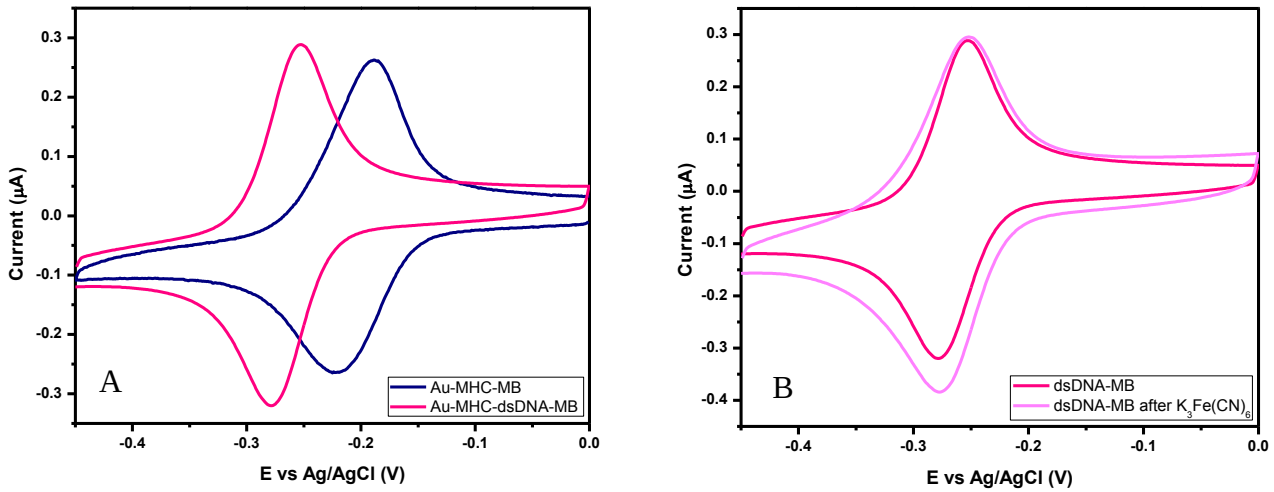

Figure 3. 4. Cyclic voltammograms of; A) NG/MCH sensor in 20 mM Tris, 100 mM NaCl, 20 µM MB (blue) and NG-MCH-dsDNA with MB intercalated into dsDNA (pink). B) CV of NG/MCH/dsDNA in 20 mM Tris, 100 mM NaCl, 20 µM MB (pink) and with 0.1M $K_2Fe(CN)_6$. MCH = 6-mercapto-1-hexanol.

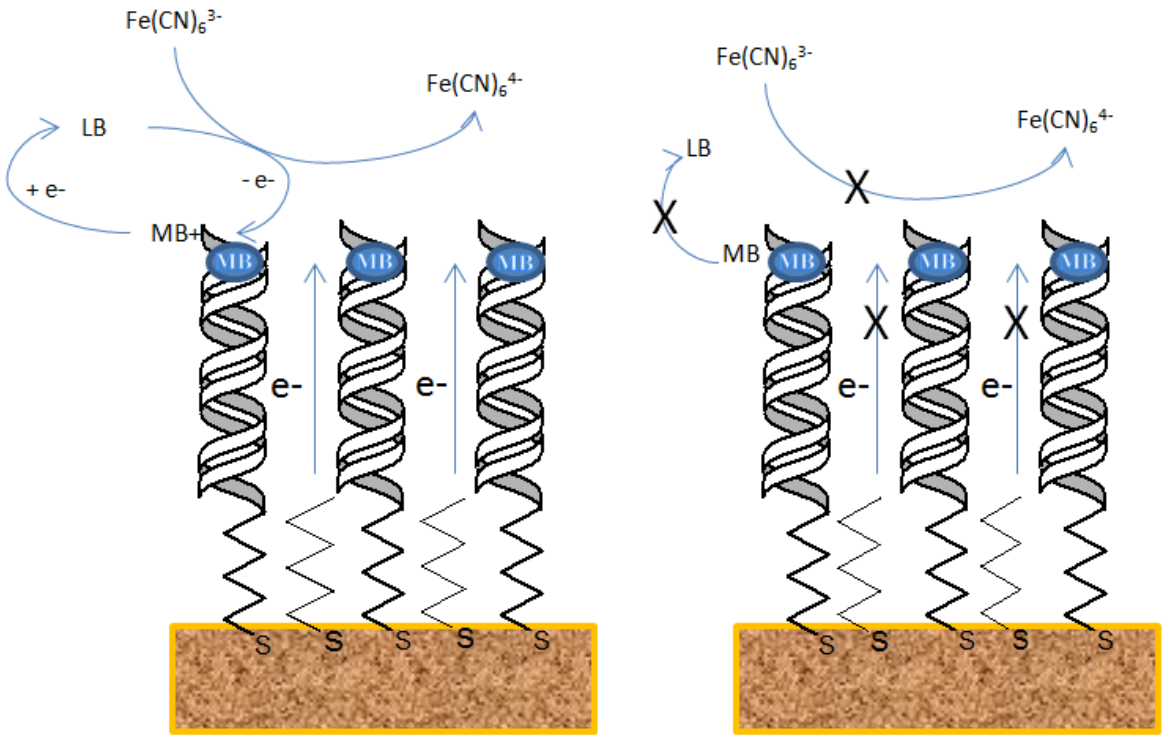

Figure 3. 5 Mismatch identification on the dsDNA hybridization by monitoring the redox of MB intercalated onto the DNA. On the left: the current flows to the well-stacked dsDNA to reduce MB intercalated onto the DNA to leucomethylene blue (LB) which reduce ferricyanide in solution. Ferricyanide regenerates MB to complete the electron cycle. On the right: if the dsDNA have some mismatch the MB reduction to LB does not occur.

3.3.3 Characterization of the binding event of beta protein 1 (BP_1) to dsDNA

Characterization of the binding event of BP_1 was performed by cyclic voltammetry and square wave voltammetry (SWV) monitoring the redox-active probe, methylene blue (MB). Methylene blue is a well-known organic molecule that binds to DNA by intercalation[18,20,28-30]. The MB was intercalated into a dsDNA containing the binding site (ATATATATG) for BP_1 transcription factor reported in literature[5]. The electron charge transport reaction in taken between the NG surfaces through the dsDNA to the MB. The electrochemical signal of the MB is then monitored by CV or SWV to determine the possible changes in current when the protein BP_1 binds to the dsDNA. A schematic

illustration of the binding event of the BP_1 to the genomic sequence dsDNA is shown in **Figure 3.1**.

The MB intercalation is positioned on the top of the dsDNA allowing the binding site interactions with the protein. The NG/dsDNA/MB sensor is then exposed to different concentrations of BP_1 and monitored by CV or SWV. When BP_1 binds to the genomic sequence in the dsDNA, the charge transport through the dsDNA to the MB is interrupted. The interruption in the charge transport system results in attenuation of the current generated by the redox-active probe[14]. **Figure 3.6** shows the cyclic voltammograms of MB intercalated on the dsDNA linked to the NG surface (NG/dsDNA/MB) at different concentrations of transcription factor BP_1. The anodic peak current of MB decreases significantly after first addition of BP_1. The anodic peak current of MB continues to a gradual decrease while concentration of BP_1 increases. The percent of response after first addition of BP_1 is 16% compared to the anodic current of MB in absence of BP_1. The significant decrease in current at the lowest concentration reflects the effects of the binging event of BP_1 onto the dsDNA. Whenever BP_1 interacts with the binding site on the dsDNA genomic sequence it perturbs the charge transport resulting in attenuation of the oxidation or reduction signal of the MB.

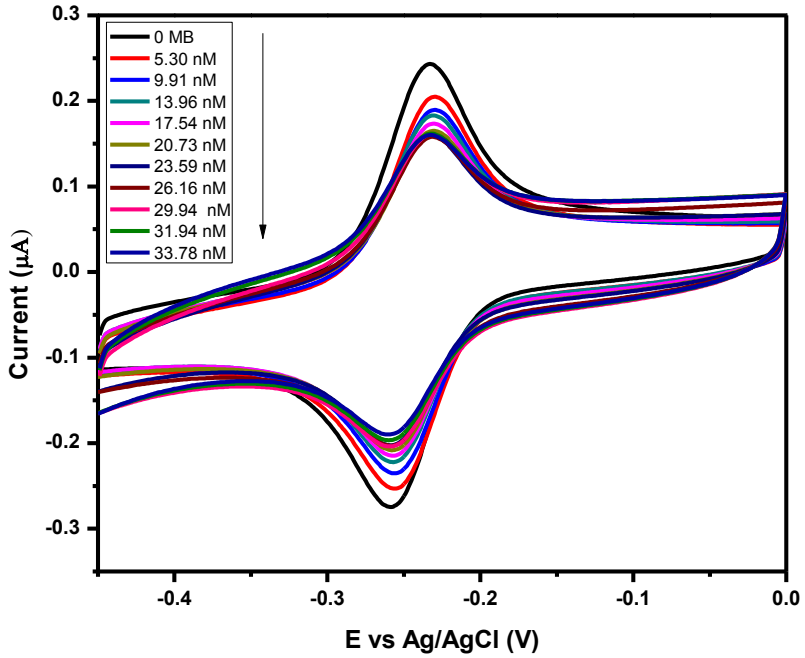

Figure 3. 6. Cyclic voltamograms of NG/dsDNA/MB containing 20 µM MB, in 20 mM tris, 100 mM NaCl at 100 mVs^{-1} in presence of different concentrations of BP_1.

3.3.4 Analytical performance of the biosensor

The analytical performance of the NG/dsDNA/MB sensor was evaluated using three independent measures using the same electrode. A significant attenuation of the MB current response was observed while the BP_1 concentration increases. The percent of current attenuation follows a good linear relation with BP_1 concentrations (**Figure 3.7**), with a linear range from 5.3 to 23.6 nM and a correlation coefficient of 0.998 ± 0.39. The linear regression equation is $\%\Delta I = 8.551 + 1.152\ C$ (C units of nM), and a limit of detection of 1.2 nM. The SD obtained from the data was of 0.39 indicating a good reproducibility of the biosensor. The NG/dsDNA/MB sensor also demonstrates to be stable and reusable with reproducible results. Comparing the NG/dsDNA/MB with other

biosensors (summarized in **Table 3.1**), our biosensor based on protein interaction is specific for breast cancer cells, take instant measurements and is reusable.

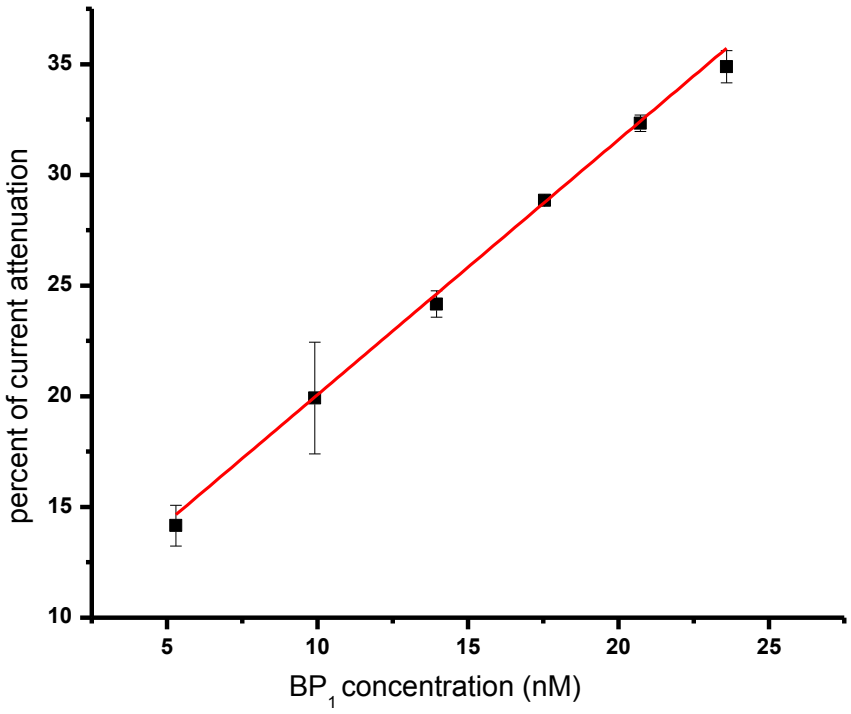

Figure 3. 7. Calibration curve of NG/dsDNA/MB illustrating the percent of current change vs BP_1 concentration (nM).

Table 3. 1. Comparison of detection agent, linear range, advantages anddisadvantages of electrochemical biosensor for breast cancer detection.

Modified electrodes	Detection Agent	Linear range	Advantages/disadvantages	References
anti-HER-3	HER-3	0.2 to 1.4 pg/mL	HER-3 is present in a wide range to tumors cell lines Incubation of 1 h with HER-3 sample Single use electrode	[31]
SAM-assisted SiNW	Erα	1 pM to 1 fM	Erα is present in breast cancer cell lines and non-tumorigenic breast cells Incubation of 1 h with cells sample Single use electrode	[32]
Avastin-MGO-Au	VEGF	31.25 - 2000 pg/mL	VEGF is present in many human cancers Incubation of 30 min with sample Reusable	[33]
VEGF-R1		10 - 70 pg/mL	VEGF is secreted by tumor cells Incubation of 1 h with VEGF sample Single use electrode	[34]
NG/dsDNA/MB	BP_1	5.3 - 23.6 nM	BP_1 is expressed in $Er\alpha^+$ and $Er\alpha^-$ breast cancer cells Instant sample measurements Reusable	This work

HEGF-3 = human epidermal growth factor-3, SAM = self-assembled monolayer, SiNW = silicon nanowire, ERE = estrogen receptor element, Erα = Estrogen receptor alpha MGO = magnetic graphene oxide, VEGF-R1 = vascular endothelial growth factor receptor 1

3.3.5 Regeneration of the fabricated DNA sensor

The NG/dsDNA/MB is a simple and easy to use sensor for early detection of breast cancer by recognition of BP_1 transcription factor. This DNA sensor is not only simple to use but it can be regenerated and reused. For regeneration of NG/dsDNA/MB sensor, a simple wash with deionized water for 30 seconds remove all the protein bound to the dsDNA resulting in a re-appearance of the MB original signal[14,23]. After wash with deionized water, the MB signal is completely restored and new measurements of BP_1 can be performed. New measurements of BP_1 were realized by square wave voltammetry (SWV) to prove the stability of the DNA sensor. Selection of the square wave frequency was performed to determine MB redox signal at different frequencies after regeneration. The frequency with better signal of MB was reached at 600 Hz (**Figure 3.8**). Different SWV experiments were made with additions of BP_1 transcription factor. A rapid response (less than 30 s) for the lowest concentration of BP_1 was observed with a signal of about 14% less than MB initial signal. Subsequent attenuation response while the concentration of BP_1 increased was obtained (**Figure 3.9**).

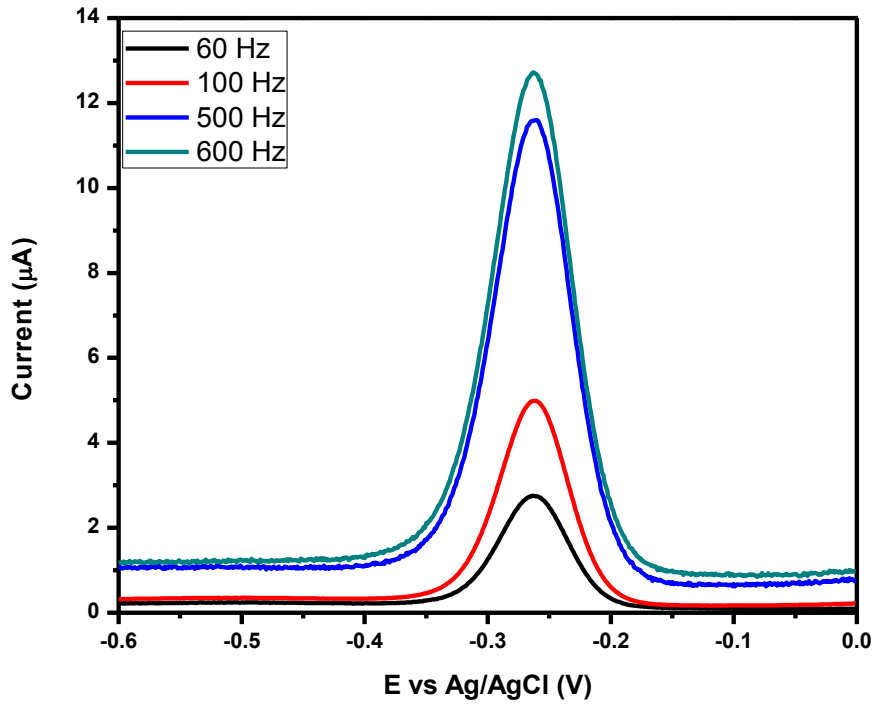

Figure 3. 8 Square wave voltammetry of MB in NG/dsDNA/MB sensor after regeneration at different frequencies. SWV was carried out in 20 mM Tris, 100 mM NaCl from 60 Hz to 600 Hz with amplitude of 25 mV and a step size of 1 mV.

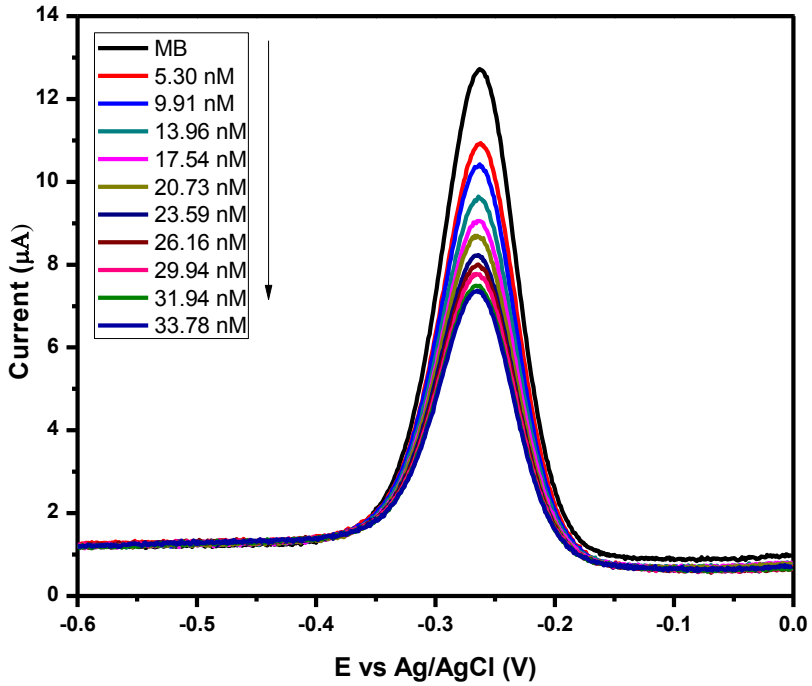

Figure 3. 9. Square wave voltammetry of MB in NG/dsDNA/MB sensor after regeneration at different concentrations of BP_1. SWV was carried out in 20 mM Tris, 100 mM NaCl at 600 Hz with amplitude of 25 mV and a step size of 1 mV.

3.3.6 Selectivity of NG/dsDNA/MB biosensor

A negative control sequence, a dsDNA sequence with no binding site to PB_1, was used to verify the selectivity of the biosensor. The sequence of dsDNA without the binding site of BP_1 was previously reported in the literature by Togni, A^5. **Figure 3.10** shows the SWV of MB in NG sensor modified with the negative control sequence. The MB intercalated onto the negative control sequence (black) shows a higher reduction current than MB intercalated onto the DNA genomic sequence (blue). However, only a 3% of signal attenuation was observed with the negative control sequence (red) compared to a 16% of attenuation signal with the genomic sequence at the same concentration of BP_1 (cyan). No significant changes in attenuation response were observed with higher concentrations of BP_1. Those results suggest that NG/dsDNA/MB sensor has a good selectivity due to the specific sequence for the BP_1 binding site. In addition, NG/dsDNA/MB sensor was stable after two weeks of its preparation.

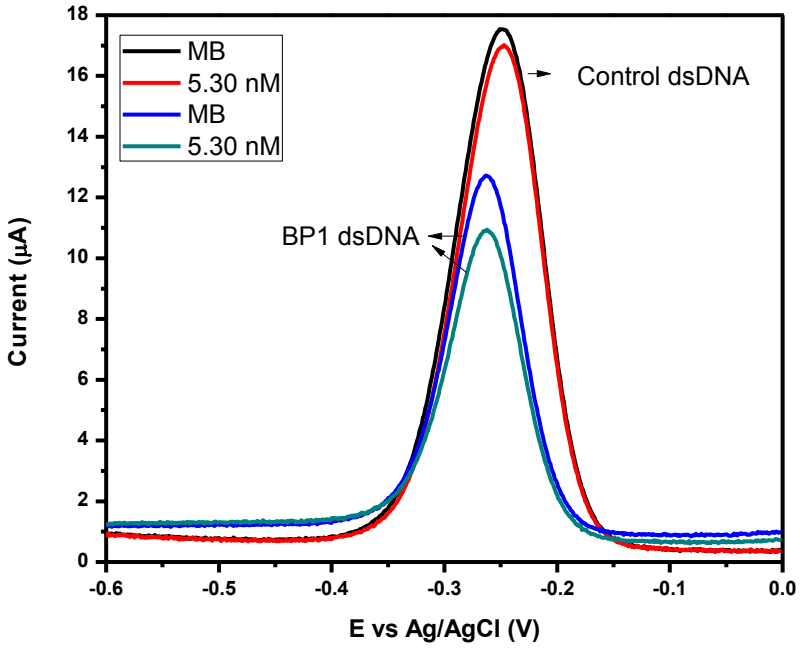

Figure 3. 10. Square wave voltammetry of MB in NG/dsDNA/MB sensor modified with the negative control DNA (black and red) and NG/dsDNA/MB with the genomic sequence (blue and cyan). SWV was carried out in 20 mM tTis, 100 mM NaCl at 600 Hz with amplitude of 25 mV and a step size of 1 mV.

3.4. Concluding remarks

A nanostructured gold biosensor based on dsDNA genomic sequence for the detection of the binding event of BP_1 was fabricated in a simple manner. First, the gold nanoparticles were synthesized and characterized by cyclic voltammetry (CV), atomic force microscopy (AFM), and scanning electron microscopy (SEM). The increase in reduction current of the gold electrode demonstrated the formation of the gold nanoparticles. The presence of characteristic morphology and topography of the gold nanoparticles was confirmed by the surface analysis with AFM and SEM. Second, the dsDNA was annealed and then immobilized onto the gold surface through the thiol end incorporated to one of the DNA stand. The intercalation of the organic compound methylene blue as redox-active probe allows the simple monitoring of the electrochemical response without causing damage to the dsDNA. The NG/dsDNA/MB electrochemical response to the binding event of BP_1 results in attenuation of the current generated by the charge transport through the dsDNA to the MB. The resulting signal response to different concentrations of BP_1 has linear range from 5.3 to 23.6 nM and a correlation coefficient of 0.998 ± 0.39. Also, it has been demonstrated that NG/dsDNA/MB sensor is stable and can be regenerated. Regeneration of the sensor provides the advantage of a reusable sensor. Through the selective detection of BP_1 at low concentrations, NG/dsDNA/MB sensor is suitable for early detection of breast cancer. Nanostructured gold dsDNA sensor is demonstrated to be sensitive, selective, stable, and reusable allowing it to be potentially used at clinical level.

3.5 References

[1] DeSantis, C.; Ma, J.; Bryan, L.; Jemal, A. Breast Cancer Statistics, 2013: Breast Cancer Statistics, 2013. *CA. Cancer J. Clin.* **2014**, *64*, 52–62.

[2] McDaniel, R. E.; Maximov, P. Y.; Jordan, V. C. Estrogen-Mediated Mechanisms to Control the Growth and Apoptosis of Breast Cancer Cells. In *Vitamins & Hormones*; Elsevier, 2013; Vol. 93, pp. 1–49.

[3] Fu, S. W.; Schwartz, A.; Stevenson, H.; Pinzone, J. J.; Davenport, G. J.; Orenstein, J. M.; Gutierrez, P.; Simmens, S. J.; Abraham, J.; Poola, I.; et al. Correlation of Expression of BP1, a Homeobox Gene, with Estrogen Receptor Status in Breast Cancer. *Breast Cancer Res. BCR* **2003**, *5*, R82–87.

[4] Haga, S. B.; Fu, S.; Karp, J. E.; Ross, D. D.; Williams, D. M.; Hankins, W. D.; Behm, F.; Ruscetti, F. W.; Chang, M.; Smith, B. D.; et al. BP1, a New Homeobox Gene, Is Frequently Expressed in Acute Leukemias. *Leukemia* **2000**, *14*, 1867–1875.

[5] Kluk, B. J.; Fu, Y.; Formolo, T. A.; Zhang, L.; Hindle, A. K.; Man, Y.; Siegel, R. S.; Berg, P. E.; Deng, C.; McCaffrey, T. A.; et al. BP1, an Isoform of DLX4 Homeoprotein, Negatively Regulates BRCA1 in Sporadic Breast Cancer. *Int. J. Biol. Sci.* **2010**, *6*, 513–524.

[6] Chase, M. B.; Fu, S.; Haga, S. B.; Davenport, G.; Stevenson, H.; Do, K.; Morgan, D.; Mah, A. L.; Berg, P. E. BP1, a Homeodomain-Containing Isoform of DLX4, Represses the Beta-Globin Gene. *Mol. Cell. Biol.* **2002**, *22*, 2505–2514.

[7] Zhong, G. Detection of Femtomolar Level Osteosarcoma-Related Gene via a Chronocoulometric DNA Biosensor Based on Nanostructure Gold Electrode. *Int. J. Nanomedicine* **2012**, 527.

[8] Thaxton, C. S.; Georganopoulou, D. G.; Mirkin, C. A. Gold Nanoparticle Probes for the Detection of Nucleic Acid Targets. *Clin. Chim. Acta Int. J. Clin. Chem.* **2006**, *363*, 120–126.

[9] Wang, W.; Chen, C.; Qian, M.; Zhao, X. S. Aptamer Biosensor for Protein Detection Using Gold Nanoparticles. *Anal. Biochem.* **2008**, *373*, 213–219.

[10] Tansil, N. C.; Gao, Z. Nanoparticles in Biomolecular Detection. *Nano Today* **2006**, *1*, 28–37.

[11] Gorodetsky, A. A.; Buzzeo, M. C.; Barton, J. K. DNA-Mediated Electrochemistry. *Bioconjug. Chem.* **2008**, *19*, 2285–2296.

[12] Genereux, J. C.; Barton, J. K. Mechanisms for DNA Charge Transport. *Chem. Rev.* **2010**, *110*, 1642–1662.

[13] Drummond, T. G.; Hill, M. G.; Barton, J. K. Electrochemical DNA Sensors. *Nat. Biotechnol.* **2003**, *21*, 1192–1199.

[14] Gorodetsky, A. A.; Ebrahim, A.; Barton, J. K. Electrical Detection of TATA Binding Protein at DNA-Modified Microelectrodes. *J. Am. Chem. Soc.* **2008**, *130*, 2924–2925.

[15] Bonham, A. J.; Hsieh, K.; Ferguson, B. S.; Vallée-Bélisle, A.; Ricci, F.; Soh, H. T.; Plaxco, K. W. Quantification of Transcription Factor Binding in Cell Extracts Using an Electrochemical, Structure-Switching Biosensor. *J. Am. Chem. Soc.* **2012**, *134*, 3346–3348.

[16] Kelley, S. O.; Jackson, N. M.; Hill, M. G.; Barton, J. K. Long-Range Electron Transfer through DNA Films. *Angew. Chem. Int. Ed.* **1999**, *38*, 941–945.

[17] Pheeney, C. G.; Barton, J. K. DNA Electrochemistry with Tethered Methylene Blue. *Langmuir* **2012**, *28*, 7063–7070.

[18] Pan, D.; Zuo, X.; Wan, Y.; Wang, L.; Zhang, J.; Song, S.; Fan, C. Electrochemical Interrogation of Interactions between Surface-Confined DNA and Methylene Blue. *Sensors* **2007**, *7*, 2671–2680.

[19] Zhong, G.; Liu, A.; Chen, X.; Wang, K.; Lian, Z.; Liu, Q.; Chen, Y.; Du, M.; Lin, X. Electrochemical Biosensor Based on Nanoporous Gold Electrode for Detection of PML/RARα Fusion Gene. *Biosens. Bioelectron.* **2011**, *26*, 3812–3817.

[20] Tuite, E.; Kelly, J. M. The Interaction of Methylene Blue, Azure B, and Thionine with DNA: Formation of Complexes with Polynucleotides and Mononucleotides as Model Systems. *Biopolymers* **1995**, *35*, 419–433.

[21] Zhao, G.-C.; Zhu, J.-J.; Zhang, J.-J.; Chen, H.-Y. Voltammetric Studies of the Interaction of Methylene Blue with DNA by Means of B-Cyclodextrin. *Anal. Chim. Acta* **1999**, *394*, 337–344.

[22] Cañete, S. J. P.; Yang, W.; Lai, R. Y. Folding-Based Electrochemical DNA Sensor Fabricated by "click" Chemistry. *Chem. Commun.* **2009**, 4835–4837.

[23] Rowe, A. A.; White, R. J.; Bonham, A. J.; Plaxco, K. W. Fabrication of Electrochemical-DNA Biosensors for the Reagentless Detection of Nucleic Acids, Proteins and Small Molecules. *J. Vis. Exp.* **2011**.

[24] Rohs, R.; Sklenar, H. Methylene Blue Binding to DNA with Alternating AT Base Sequence: Minor Groove Binding Is Favored over Intercalation. *J. Biomol. Struct. Dyn.* **2004**, *21*, 699–711.

[25] Arinaga, K.; Rant, U.; Tornow, M.; Fujita, S.; Abstreiter, G.; Yokoyama, N. The Role of Surface Charging during the Coadsorption of Mercaptohexanol to DNA Layers on Gold: Direct Observation of Desorption and Layer Reorientation. *Langmuir* **2006**, *22*, 5560–5562.

[26] Kelley, S. Single-Base Mismatch Detection Based on Charge Transduction through DNA. *Nucleic Acids Res.* **1999**, *27*, 4830–4837.

[27] Boon, E. M.; Ceres, D. M.; Drummond, T. G.; Hill, M. G.; Barton, J. K. Mutation Detection by Electrocatalysis at DNA-Modified Electrodes. *Nat. Biotechnol.* **2000**, *18*, 1096–1100.

[28] Bradley, D. F.; Stellwagen, N. C.; O'konski, C. T.; Paulson, C. M. Electric Birefringence and Dichroism of Acridine Orange and Methylene Blue Complexes with Polynucleotides. *Biopolymers* **1972**, *11*, 645–652.

[29] Nordén, B.; Tjerneld, F. Structure of Methylene blue–DNA Complexes Studied by Linear and Circular Dichroism Spectroscopy. *Biopolymers* **1982**, *21*, 1713–1734.

[30] Tuite, E.; Norden, B. Sequence-Specific Interactions of Methylene Blue with Polynucleotides and DNA: A Spectroscopic Study. *J. Am. Chem. Soc.* **1994**, *116*, 7548–7556.

[31] Canbaz, M. Ç.; Şimşek, Ç. S.; Sezgintürk, M. K. Electrochemical Biosensor Based on Self-Assembled Monolayers Modified with Gold Nanoparticles for Detection of HER-3. *Anal. Chim. Acta* **2014**, *814*, 31–38.

[32] Zhang, G.-J.; Huang, M. J.; Ang, J. J.; Liu, E. T.; Desai, K. V. Self-Assembled Monolayer-Assisted Silicon Nanowire Biosensor for Detection of protein–DNA Interactions in Nuclear Extracts from Breast Cancer Cell. *Biosens. Bioelectron.* **2011**, *26*, 3233–3239.

[33] Lin, C.-W.; Wei, K.-C.; Liao, S.; Huang, C.-Y.; Sun, C.-L.; Wu, P.-J.; Lu, Y.-J.; Yang, H.-W.; Ma, C.-C. M. A Reusable Magnetic Graphene Oxide-Modified Biosensor for Vascular Endothelial Growth Factor Detection in Cancer Diagnosis. *Biosens. Bioelectron.* **2015**, *67*, 431–437.

[34] Sezgintürk, M. K. A New Impedimetric Biosensor Utilizing VEGF Receptor-1 (Flt-1): Early Diagnosis of Vascular Endothelial Growth Factor in Breast Cancer. *Biosens. Bioelectron.* **2011**, *26*, 4032–4039.

Appendixes

Appendix A: NMR Data

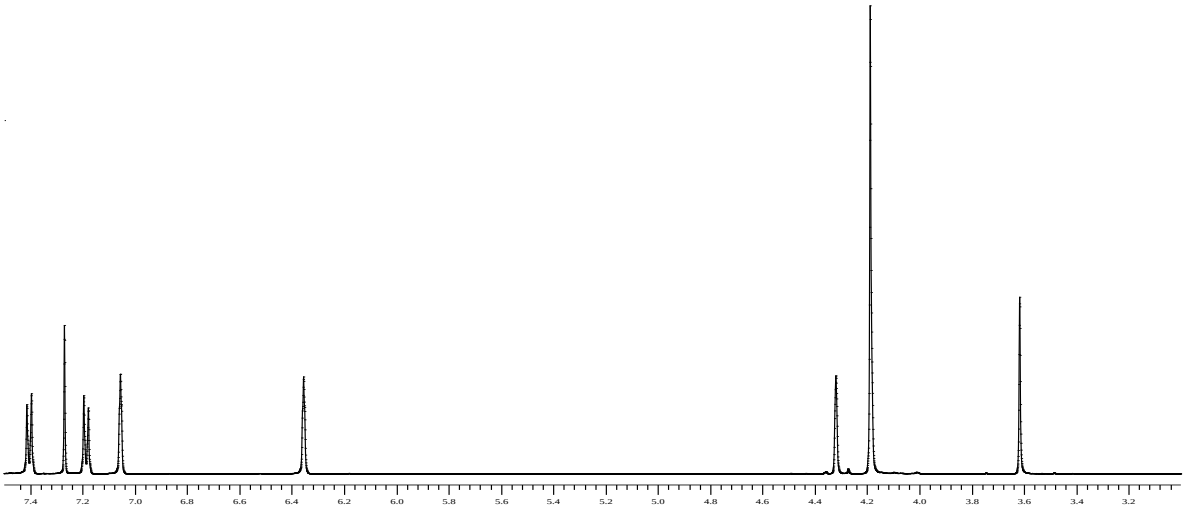

Figure A1: 4-(1H-pyrrol-1-yl)phenyl ferroceneacetylate ("Fc-CH_2CO_2-Ph-4-Py"): ^{1}HNMR (500 MHz, $CDCl_3$): 7.44 (2H, d, ph; ^{3}J = 8.8 Hz), 7.18 (2H, d, py; ^{3}J = 8.8 Hz), 7.01(2H, dd, ph; ^{3}J = 1.9 Hz), 6.36 (2H, dd, py; ^{3}J = 1.9 Hz), 4.32 (2H, bs, Cp), 4.19 (2H, bs, Cp', 5H), 3.62 (2H, s, CH_2, 2H).

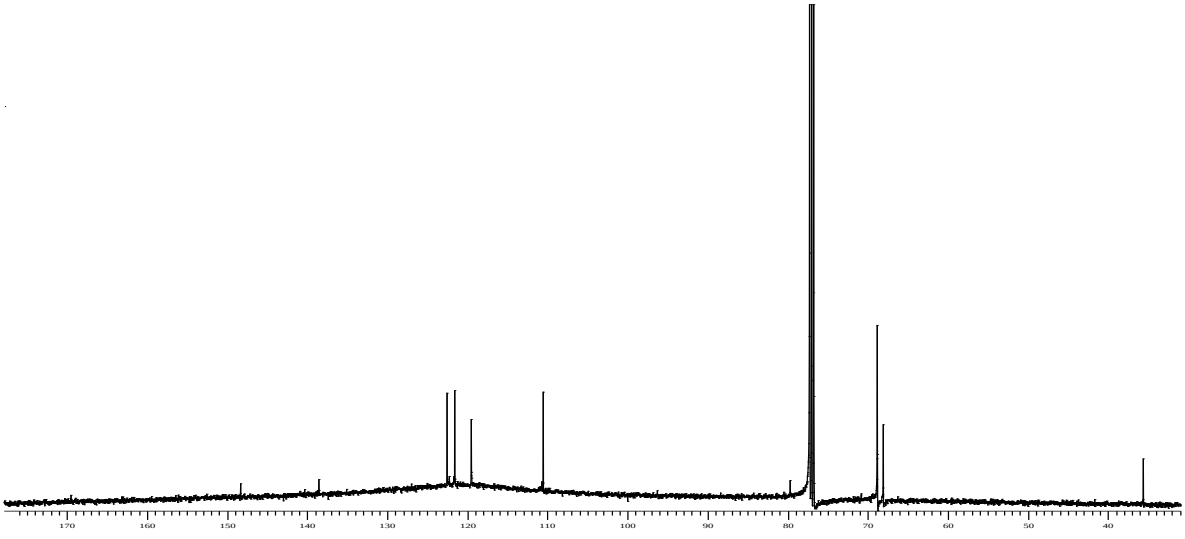

Figure A2: 4-(1H-pyrrol-1-yl)phenyl ferroceneacetylate ("Fc-CH_2CO_2-Ph-4-Py"): ^{13}CNMR (125 MHz, $CDCl_3$) (δppm): 169.5 (C=O), 148.32, 138.6, 122.6, 121.6, 119.54, 110.5, 79.7, 68.8, 68.1, 35.6.

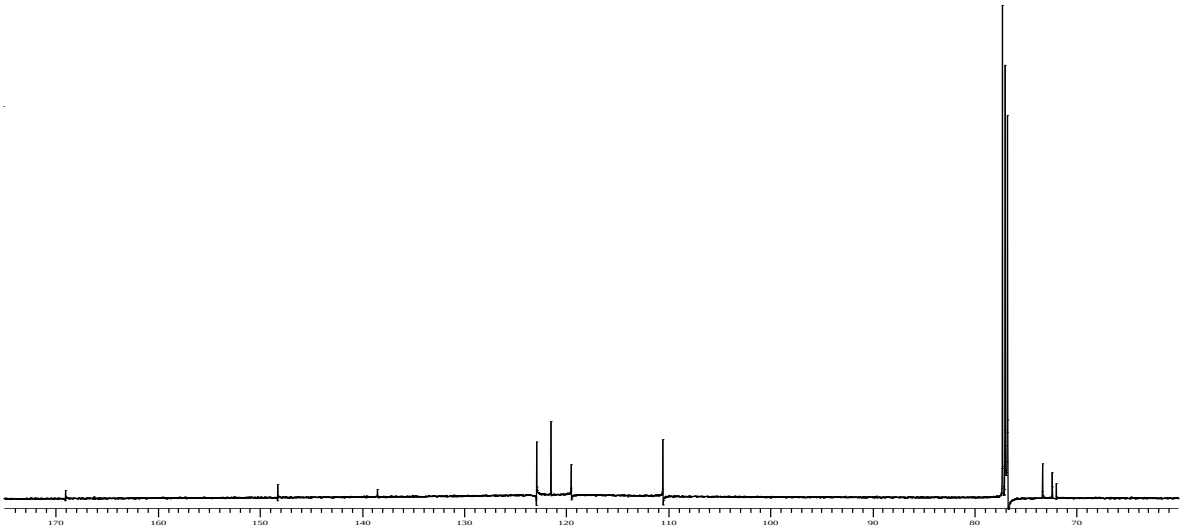

Figure A3: 1,1'-4-(1H-pyrrol-1-yl)phenyl ferrocenedicarboxylate ("Fc-(CO_2-Ph-4-Py)$_2$"): ^{13}CNMR (125 MHz, $CDCl_3$) (δppm): 169.0 (C=O), 148.3, 138.6, 122.9, 121.5, 119.5, 110.5, 73.4, 72.4, 72.0.

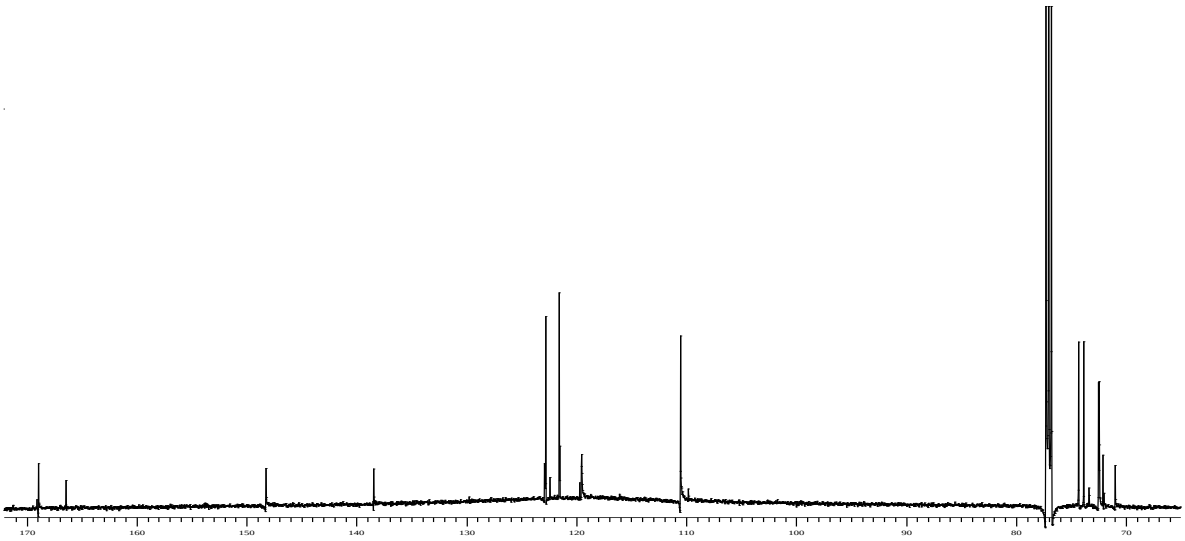

Figure A4: 1-4-(1H-pyrrol-1-yl)phenyl, 1'-carboxyl ferrocenecarboxylate ("Fc-(CO_2-Ph-4-Py)CO_2H"): ^{13}CNMR (125 MHz, $CDCl_3$) (δppm): 168.9 (C=O)', 166.4 (C=O), 148.3, 138.5, 122.9, 121.5, 119.5, 110.5, 74.3, 73.8, 73.4, 72.5, 72.1, 71.0.

Appendix B: Infrared Data

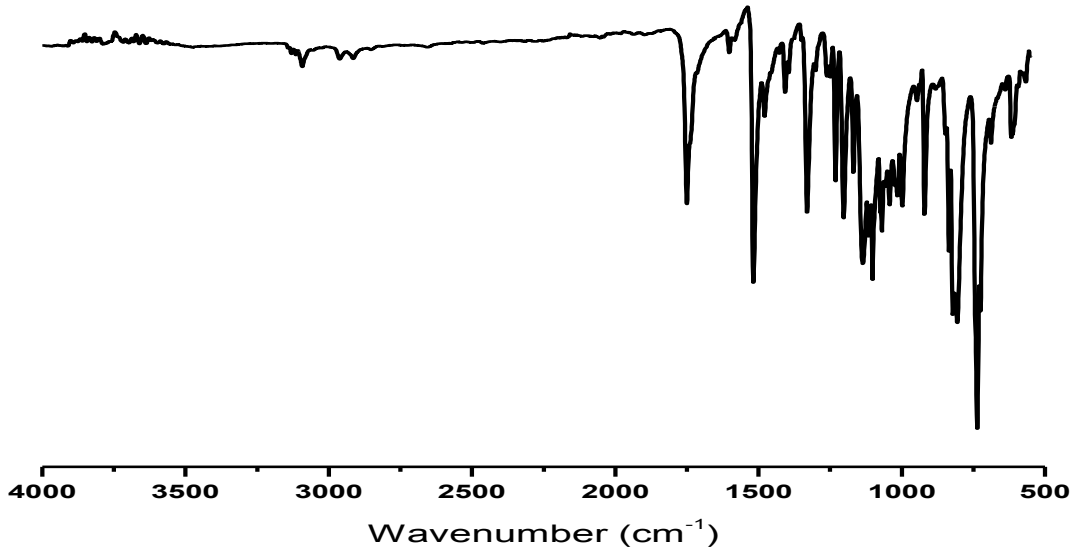

Figure B1: Infrarred spectra of 4-(1H-pyrrol-1-yl)phenyl ferroceneacetylate ("Fc-CH_2CO_2-Ph-4-Py"): ATR-IR (cm^{-1}): 3092, 2963, 2917, 1750(C=O), 1508, 1334, 1143, 1098, 810, 727.

Appendix C: IC_{50} Data of MCF-7

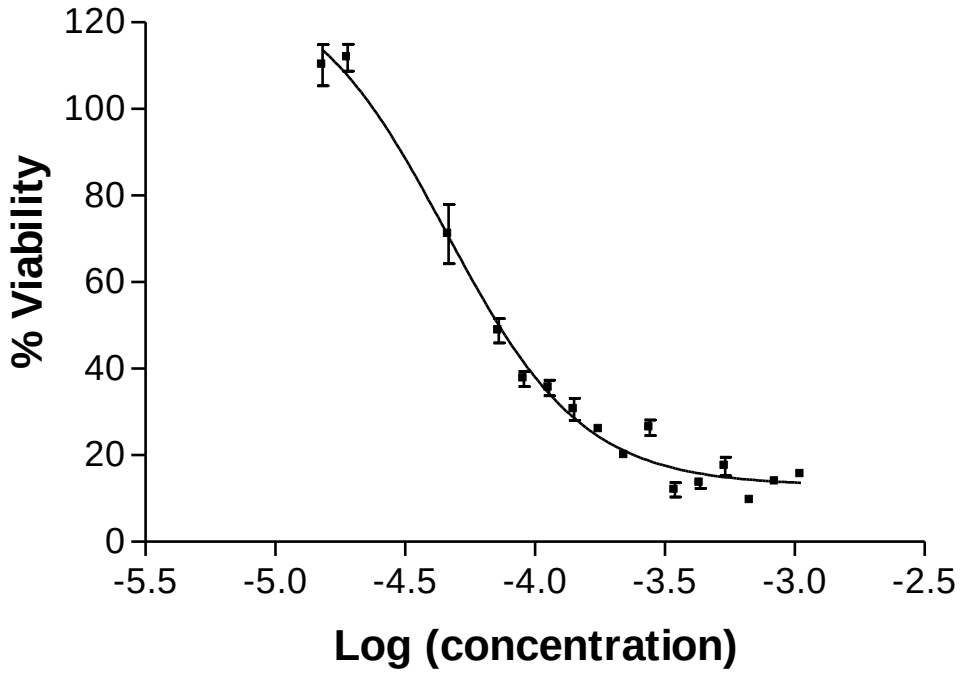

Figure C1: IC_{50} values for 1,1'-4-(1H-pyrrol-1-yl)phenyl ferrocenedicarboxylate ("Fc-(CO_2-Ph-4-Py)$_2$").

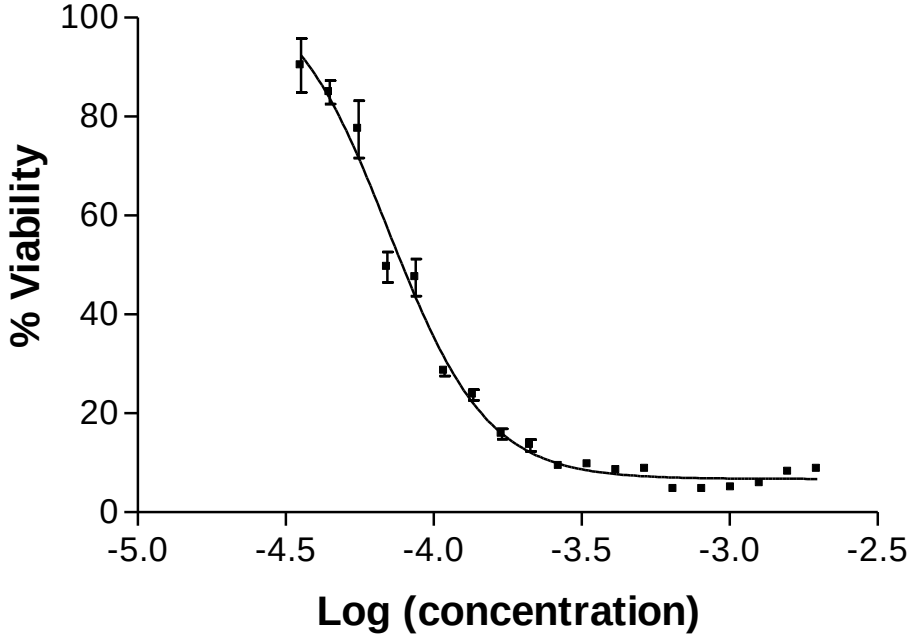

Figure C2: IC_{50} values for 1-4-(1H-pyrrol-1-yl)phenyl, 1'-carboxyl ferrocenecarboxylate ("Fc-(CO_2-Ph-4-Py)CO_2H").

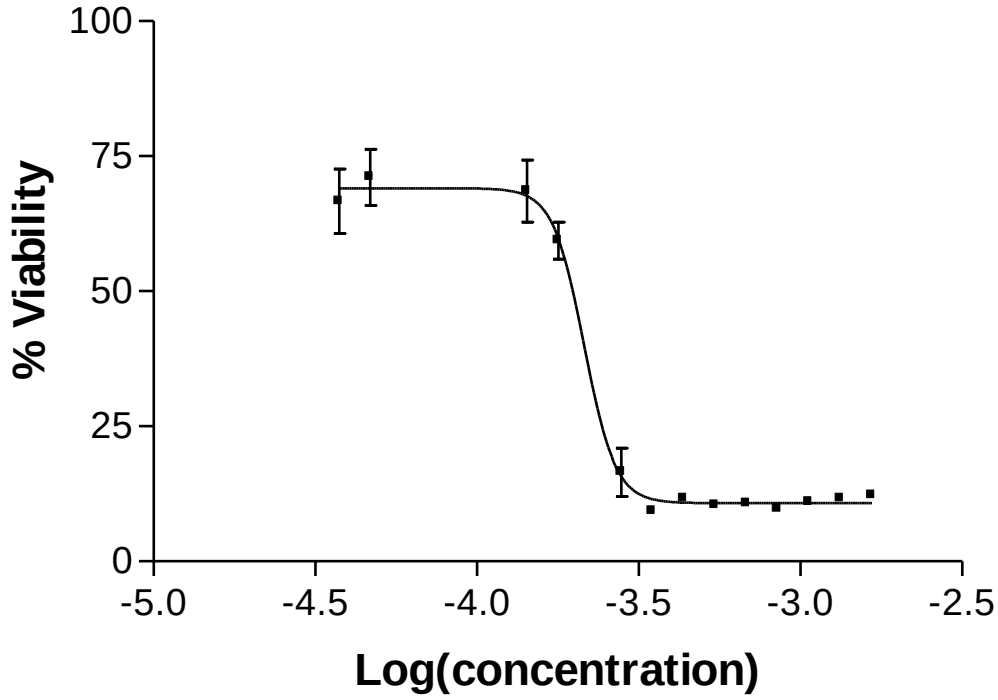

Figure C3: IC_{50} values for 4-(1H-pyrrol-1-yl)phenyl ferroceneacetylate ("Fc-CH_2CO_2-Ph-4-Py").

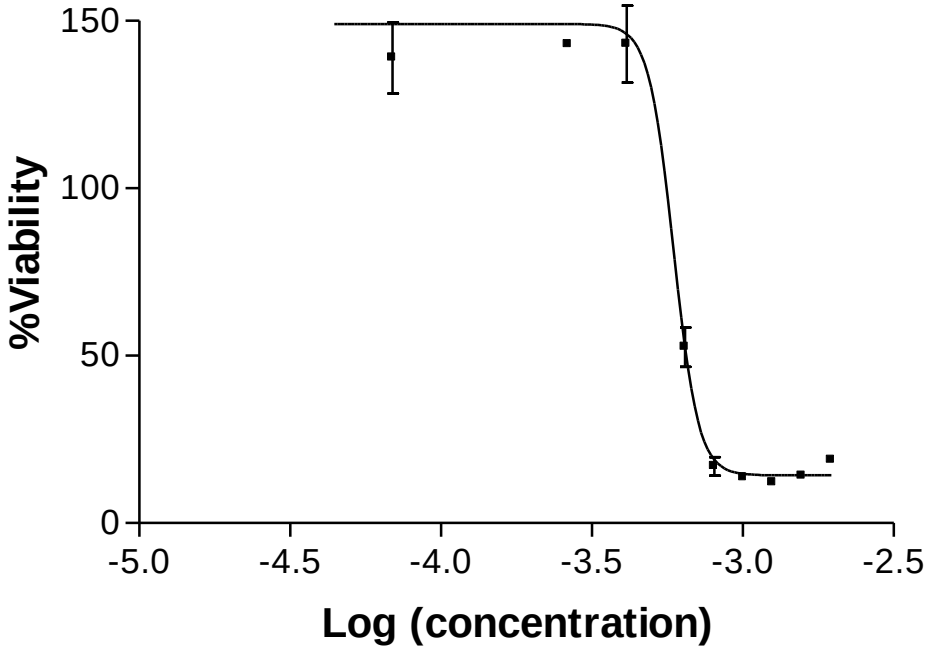

Figure C4: IC_{50} values for ferroceneacetic acid.

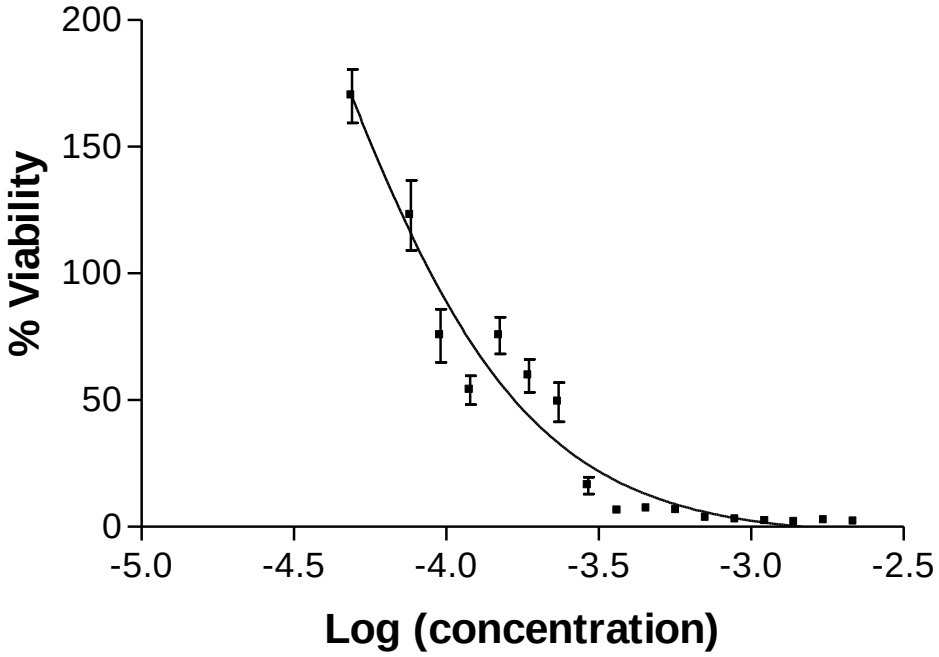

Figure C5: IC_{50} values for 4-(1H-pyrrol-1yl)phenol.

Appendix D: IC_{50} Data of MCF-10A

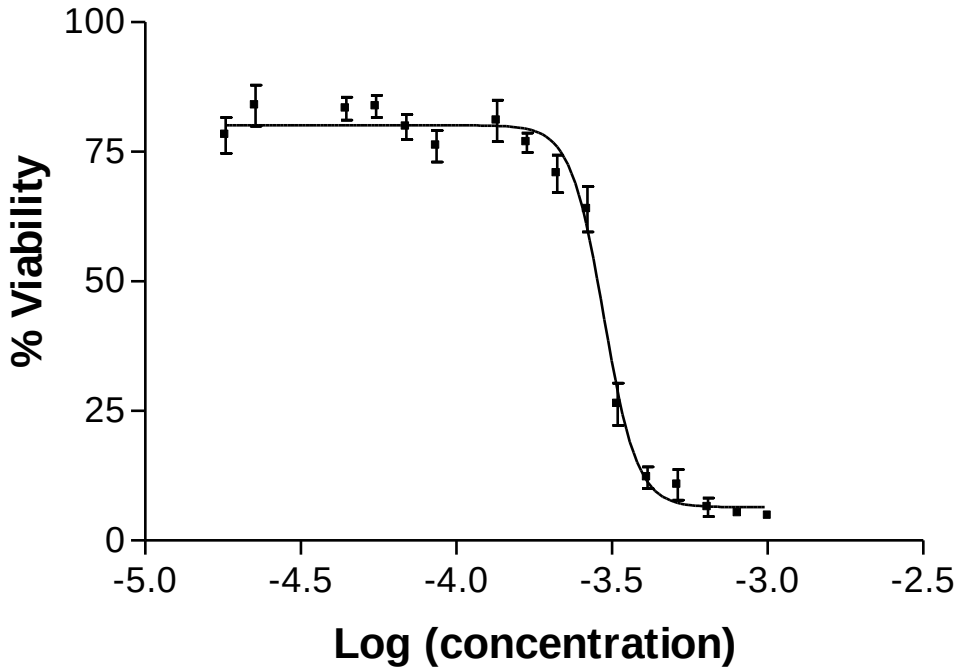

Figure D1: IC_{50} values for 1,1'-4-(1H-pyrrol-1-yl)phenyl ferrocenedicarboxylate ("Fc-$(CO_2$-Ph-4-Py$)_2$").

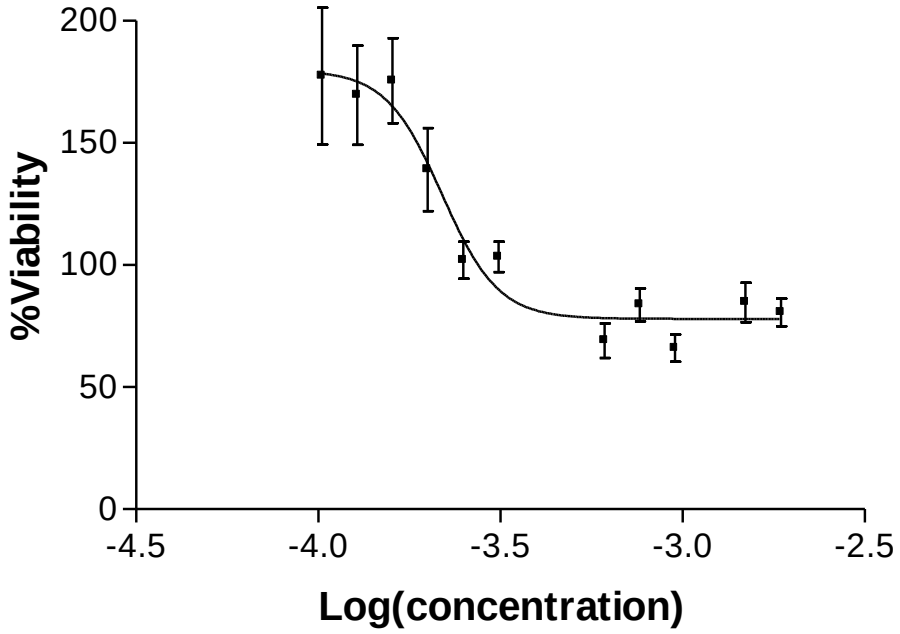

Figure D2: IC_{50} values for 1-4-(1H-pyrrol-1-yl)phenyl, 1'-carboxyl ferrocenecarboxylate ("Fc-$(CO_2$-Ph-4-Py$)CO_2$H").

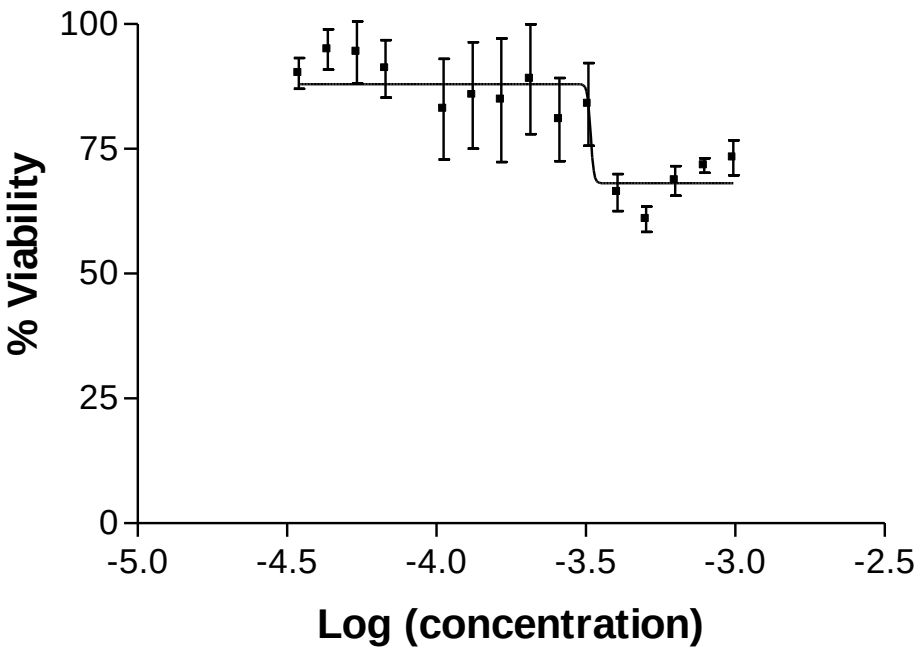

Figure D3: IC_{50} values for 4-(1H-pyrrol-1-yl)phenyl ferroceneacetylate ("Fc-CH_2CO_2-Ph-4-Py").

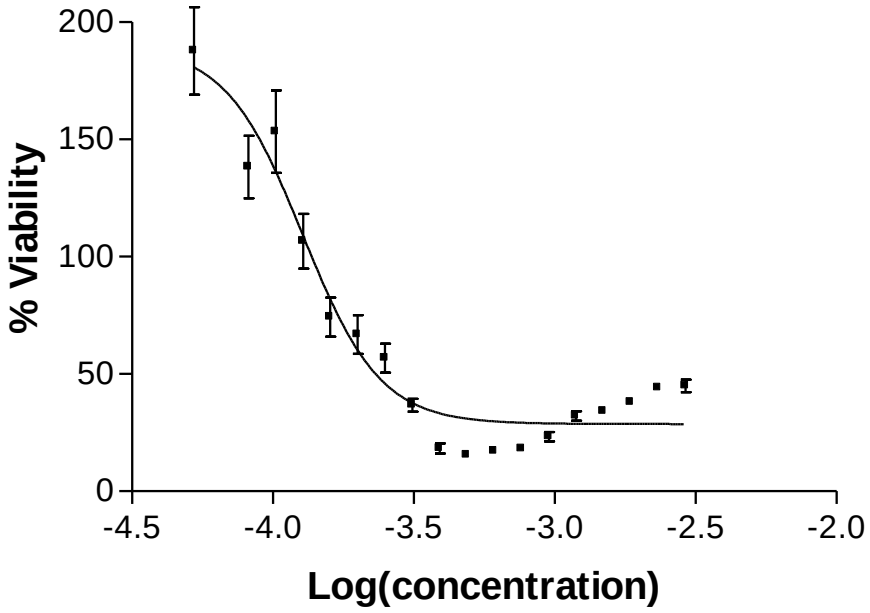

Figure D4: IC_{50} values for ferrocenoyl 3b-estra1,3,5(10)-trien-17-one-3-olate (Fc-CO_2-estradiol).

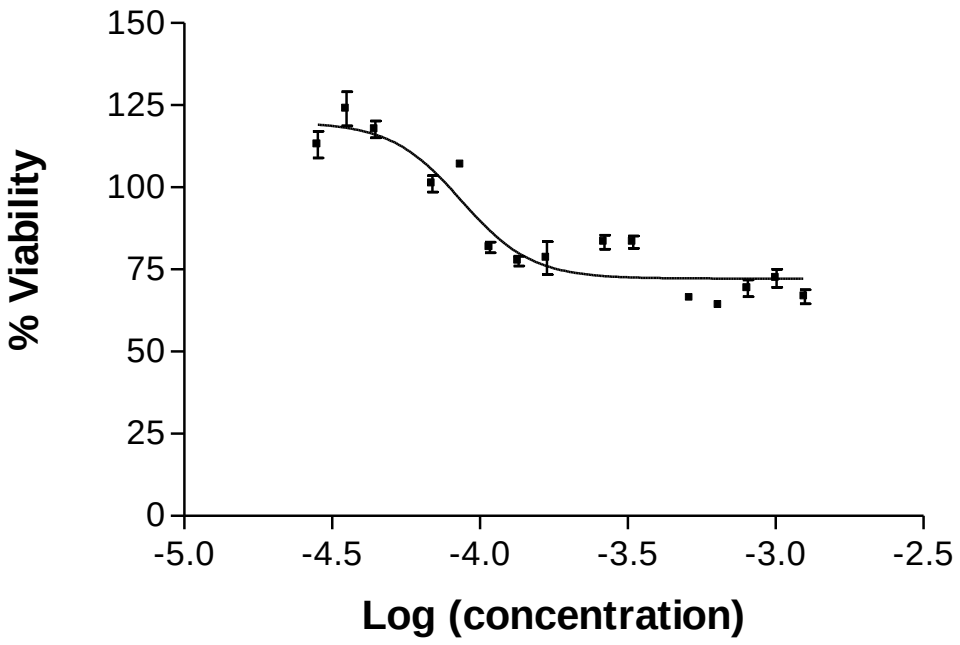

Figure D5: IC_{50} values for ferroceneacetic acid.

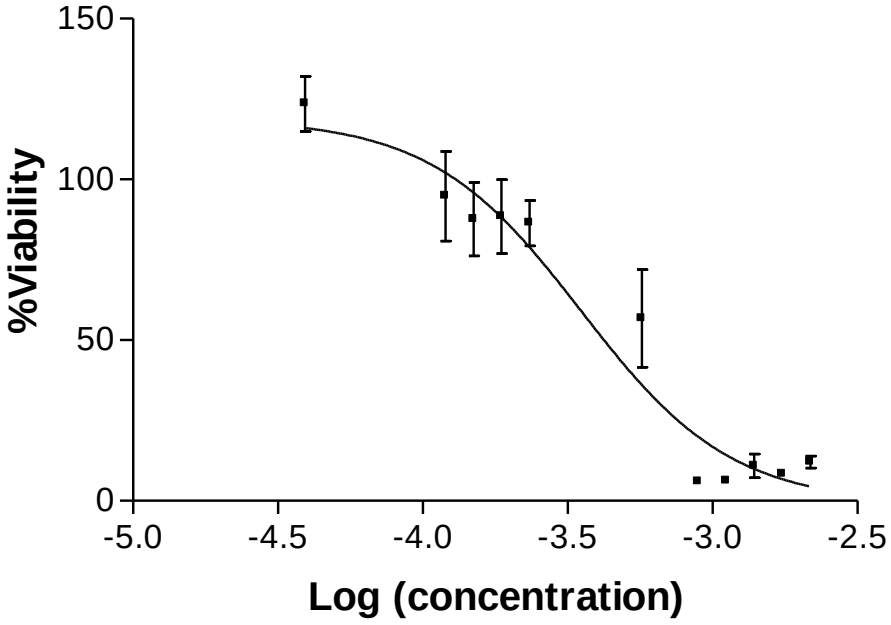

Figure D6: IC_{50} values for 4-(1H-pyrrol-1yl)phenol.

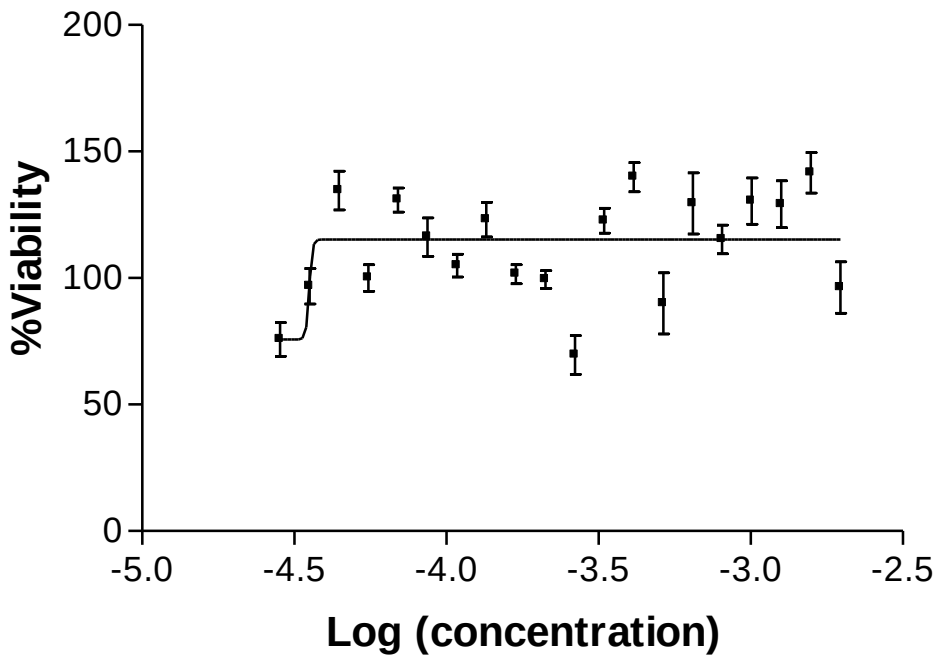

Figure D7: IC_{50} values for 1,1'-ferrocenedicarboxylic acid.

Appendix E: IC_{50} Data of HT-29

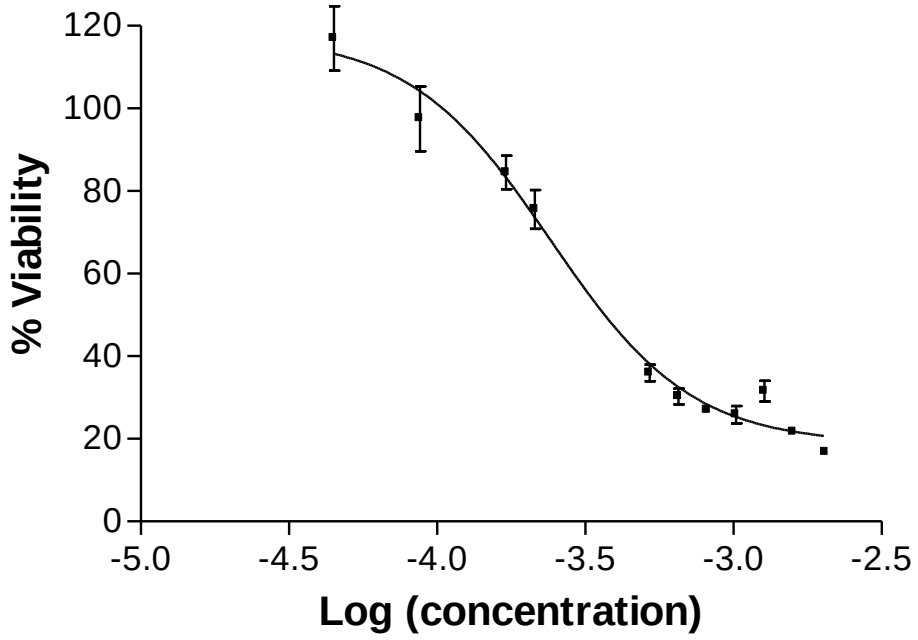

Figure E1: IC_{50} values for 1,1'-4-(1H-pyrrol-1-yl)phenyl ferrocenedicarboxylate ("Fc-$(CO_2$-Ph-4-Py$)_2$").

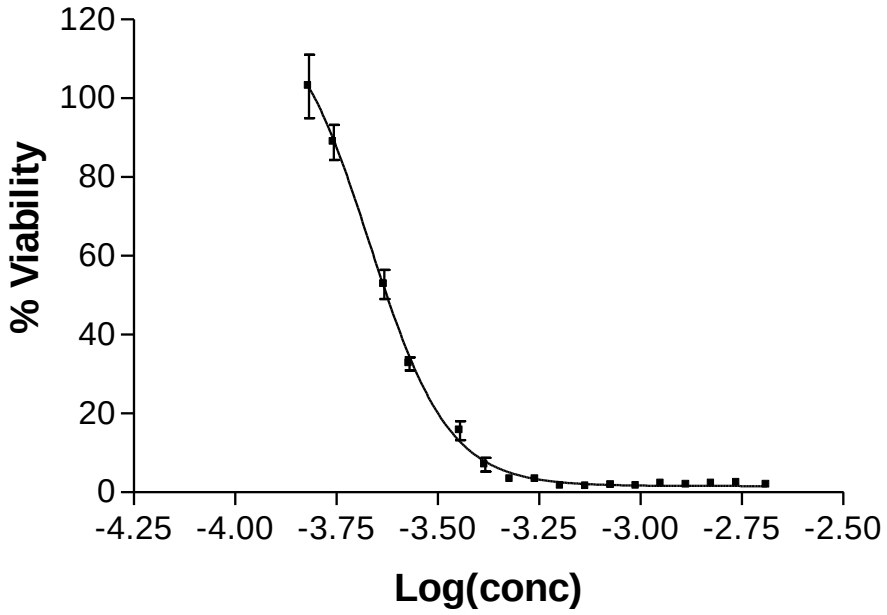

Figure E2: IC_{50} values for 1-4-(1H-pyrrol-1-yl)phenyl, 1'-carboxyl ferrocenecarboxylate ("Fc-$(CO_2$-Ph-4-Py$)CO_2$H").

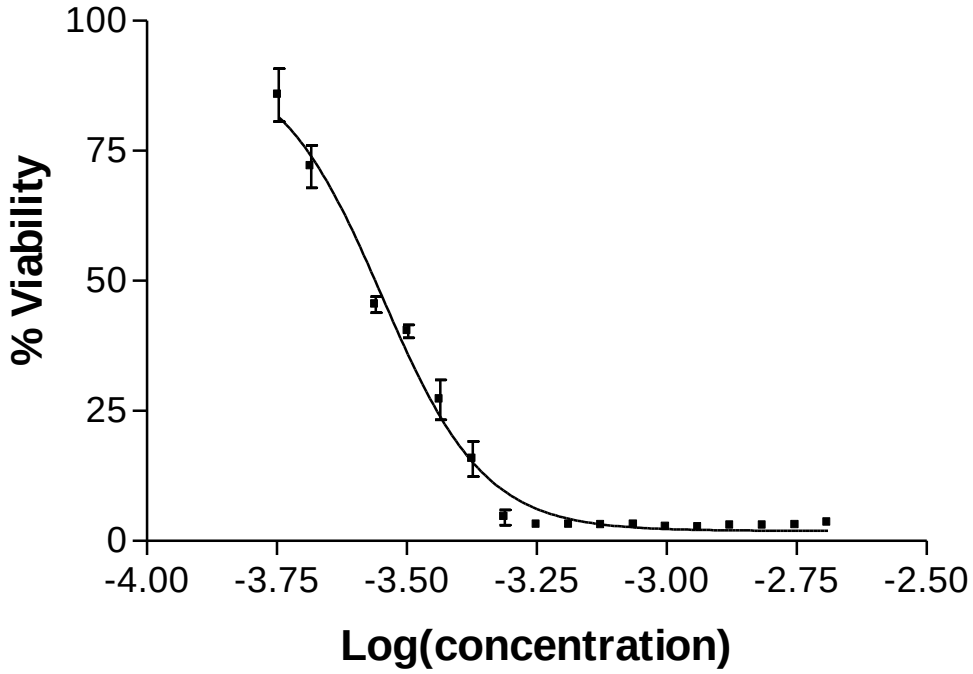

Figure E3: IC_{50} values for 4-(1H-pyrrol-1-yl)phenyl ferroceneacetylate ("Fc-CH_2CO_2-Ph-4-Py").\

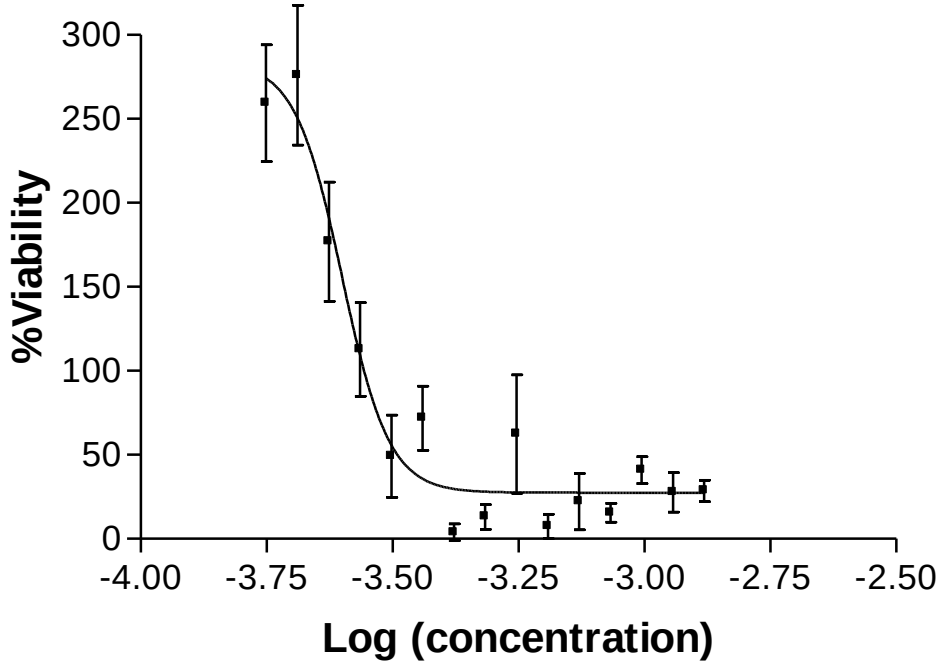

Figure E4: IC_{50} values for ferroceneacetic acid.

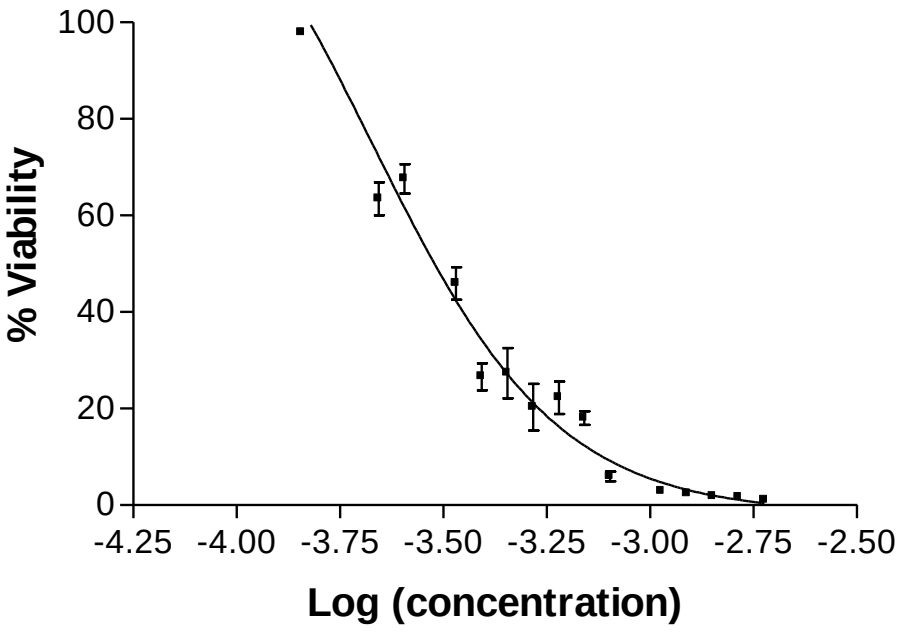

Figure E5: IC_{50} values for 4-(1H-pyrrol-1yl)phenol.

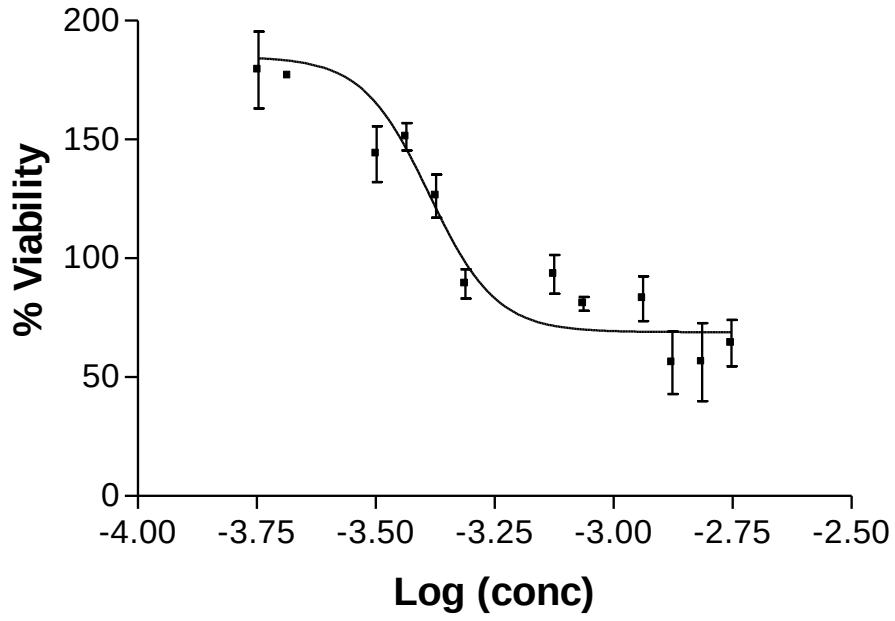

Figure E6:IC_{50} values for 1,1'-ferrocenedicarboxylic acid